TAMPERE UNIVERSITY OF TECHNOLOGY

JOUNI MAHANEN

STEAM-SIDE OXIDATION OF MATERIALS FOR SUPERCRITICAL BOILERS

Master of Science Thesis

Examiner: Professor Toivo Lepistö
Examiner and topic approved in the Automation, Mechanical and Materials Engineering Faculty Council Meeting on 10 March 2010

ABSTRACT

TAMPERE UNIVERSITY OF TECHNOLOGY
Master's Degree Programme in Materials Science
MAHANEN, JOUNI: Steam-side oxidation of materials for supercritical boilers
Master of Science Thesis, 74 pages, 4 Appendix pages
May 2011
Major: Metallic materials
Examiner: Professor Toivo Lepistö
Keywords: oxidation, supercritical steam, austenitic steels

In this work the steam-side oxidation resistance of various austenitic boiler steels was evaluated. The aim was to evaluate applicability of tested steels to over 600 °C live steam temperatures. Experimental work has been performed by exposing various austenitic boiler steels to supercritical steam in autoclave. The mass gains per unit area and oxide scale thicknesses are determined from sample coupons. Compositions of oxide scales are analyzed with energy-dispersive X-ray spectroscopy (EDS) and glow discharge optical emission spectrometry (GDOES).

The efficiency of steam power plant can be increased by increasing the temperature and pressure of live steam. Today's advanced power plants have supercritical steam parameters with live steam temperature approximately 600 °C, and there are several research efforts to increase the temperature even further. High operating temperature sets very demanding requirements to the materials used in hottest components.

The basics of steam boiler technology are introduced in the first part of this thesis. Brief introduction to fluidized bed (FB) combustion is also made. Typically used boiler materials and material degradation mechanisms that are typically occurring in fluidized bed type boilers are also briefly introduced. The main focus is on the steam-side oxidation of boiler steels. Thermodynamic and kinetic considerations affecting the oxidation process are discussed.

The effect of alloy composition, grain size and degree of cold-working in surface layer on steam-side oxidation resistance was recognized from the available literature. Boiler steel must have sufficient chromium content so that protective Cr_2O_3 scale is formed on the surface. Grain size and surface finish affect the diffusivity of Cr in the metal lattice by introducing more diffusion paths for Cr. The effect of cold-working (machining) was observed in the experimental work of this study. However, the detailed analysis of oxide scales revealed that the long term performance of machined alloy may be inadequate. Besides chromium, also other alloying elements were detected from thin oxide scales. This suggests that also other alloying elements (Mn, Si, Al and Ti) have a certain role in the oxidation behaviour of a stainless steel alloy.

The experimental work suggests that advanced austenitic alloys with over 22,5 wt-% Cr will be applicable in final superheaters of advanced supercritical power plants with over 600 ºC live steam temperature. More testing in different temperatures is required in order to determine the actual temperature limits. Shot-peened tube pieces should also be tested in autoclave and compared to the already tested machined sample coupons.

TIIVISTELMÄ

TAMPEREEN TEKNILLINEN YLIOPISTO
Materiaalitekniikan koulutusohjelma
MAHANEN, JOUNI: Steam-side oxidation of materials for supercritical boilers
Diplomityö, 74 sivua, 4 liitesivua
Toukokuu 2011
Pääaine: Metallimateriaalit
Tarkastaja: professori Toivo Lepistö
Avainsanat: hapettuminen, ylikriittinen höyry, austeniittiset teräkset

Kasvava huoli maailmanlaajuista ilmastonmuutosta kohtaan on johtanut pyrkimyksiin rajoittaa kasvihuonekaasupäästöjä. Sähköntuotannon näkökulmasta katsottuna tämä tarkoittaa vaihtoehtoisten tuotantotapojen tutkimusta ja käyttöönottoa, hiilineutraalien polttoaineiden (kuten biomassa) käyttöä, sähköntuotannon hyötysuhteen kasvattamista sekä hiilidioksin talteenottomenetelmien kehittämistä ja käyttöönottoa. Suurin osa mailman sähköenergiasta tuotetaan lauhdevoimaloissa joissa poltetaan fossiilisia polttoaineita, joten näiden voimalaitosten sähköntuotannon hyötysuhteen parantaminen vähentäisi hiilidioksidipäästöjä merkittävästi. Myös hiilidioksidin talteenottojärjestelmien käyttöönotto vaatii sähköntuotannon hyötysuhteen kasvattamista ollakseen taloudellisesti kannattavia, sillä hiilidioksin talteenotossa käytettävät laitteet tarvitsevat sähköenergiaa toimiakseen. Lauhdevoimalan hyötysuhdetta voidaan kasvattaa nostamalla höyryturbiinille syötettävän tuorehöyryn lämpötilaa ja painetta. Kun tuorehöyryn lämpötila ja paine nostetaan yli veden kriittisen pisteen (374 ºC, 221 bar), voidaan puhua ylikriittisestä höyrykattilasta. Uudenaikaisissa lauhdevoimaloissa höyrynlämpötilat ovat tyypillisesti n. 600 ºC. Lämpötilaa pyritään jatkuvasti nostamaan useissa tutkimushankkeissa. Usein tuorehöyryn lämpötilan nostoa rajoittavat putkimateriaalien riittämätön korkean lämpötilan lujuus, tai virumisen kesto, sekä savukaasupuolella tapahtuva korroosio. Lämpötilan noustessa myös putken sisäpinnalla tapahtuvasta hapettumisesta tulee kasvavassa määrin ongelma. Jos oksidikalvo kasvaa liian paksuksi, se voi irrota metallin pinnasta ja kulkeutua höyryvirran mukana putkitaipeisiin, joissa se voi aiheuttaa tukoksia. Jos irronneet oksidipartikkelit kulkeutuvat höyryturbiinille asti, ne aiheuttavat turbiinisiipien eroosiota.

Tämän diplomityön tarkoituksena on tutkia ylikriittisen höyrykattilan lämmönvaihdinputkien sisäpinnalla tapahtuvaa höyryn aiheuttamaa hapettumista, sekä määrittää ylimmät mahdolliset käyttölämpötilat kullekkin testatulle materiaalille. Työssä keskitytään pääosin austeniittisiin kattilateräksiin, sillä ylikriittisen höyrykattilan lopputulistimet valmistetaan pääosin näistä materiaaleista. Työssä esitetyt tulokset pohjautuvat vuosina 2009 ja 2010 suoritettuihin laboratoriokokeisiin, joissa useita austeniittisia kattilateräksiä altistettiin ylikriittiselle höyrylle (650 ºC, 250 bar) autoklaavissa. Koepaloista määriteltiin massankasvu pinta-alayksikköä kohden. Lisäksi koepaloista valmistettiin poikkileikkaushieet, joista määriteltiin oksidikalvon paksuus. Oksidikalvon koostumusta on pyritty selvittämään EDS (energy-dispersive X-ray spectroscopy) ja GDOES (glow discharge optical emission spectrometry) analyysimenetelmillä. Näistä erityisesti GDOES osoittautui hyväksi

analyysimenetelmäksi ohuiden (alle 1 µm) oksidikalvojen koostumuksen määrittämisessä.

Työn alussa on kattava kirjallisuusselvitys, jossa perehdytään höyrykattilatekniikkaan, höyrykattiloissa tavallisesti käytettyihin materiaaleihin, sekä höyrykattilaympäristön materiaaleille asettamiin erikoisvaatimuksiin. Kiertoleijupolttotekniikka ja sen materiaaleille asettamat erikoisvaatimukset ovat myös tarkastelun alla. Höyryn aiheuttaman hapettumisen teoria sekä siihen vaikuttavat termodynaamiset ja kineettiset perusteet on selvitetty. Myös höyryn paineen sekä sen fysikaalisten ja kemiallisten ominaisuuksien merkitystä hapettumisreaktioon on pyritty selvittämään. Kriittisin muuttuja hapettumisen näkökulmasta on höyryn lämpötila.

Kriittisin austeniittisen kattilateräksen pintaan muodostuvan oksidikerroksen paksuuteen vaikuttava tekijä on teräksen kromipitoisuus. Kaikkien tutkittujen terästen kromipitoisuus oli riittävä kromioksidikerroksen muodostumiselle. Oksidikalvot olivat rakenteeltaan joko kaksikerroksisia, joissa ulompi kerros koostuu rautaoksidista ja sisempi kromirikkaasta oksidista, tai yksikerroksisia, joissa oksidi koostuu ainoastaan kromirikkaasta oksidista. Perinteisten 18% kromia sisältävien terästen ja kehittyneiden, yli 22,5% kromia sisältävien terästen suorituskyvyssä havaittiin huomattava ero testauslämpötilassa edellisten hyväksi. Kromipitoisuuden ohella myös kromin diffuusionopeus teräksessä vaikuttaa muodostuvan oksidikalvon paksuuteen ja rakenteeseen. Suurempi diffuusionopeus edesauttaa suojaavan ja ohuen kromioksidikalvon muodostusta. Kromin diffuusionopeutta teräksessä voidaan parantaa hienontamalla teräksen raekokoa sekä pintakerroksen kylmämuokkauksella. Putkentoimittajat hyödyntävät molempia menetelmiä tuotteissaan. Kylmämuokattu pintarakenne saadaan aikaan kuulapuhalluksella, jossa putken sisäpinta puhalletaan teräskuulilla. Tässä työssä testattuihin koepaloihin kylmämuokkaus saatiin aikaan koneistamalla koepalan pinta. Kylmämuokkauksen todettiin vähentävän kaikkien testattujen terästen massankasvua. Erot olivat selkeimpiä teräksillä, joiden nimellinen kromipitoisuus oli 18%. Lähemmässä tarkastelussa paljastui että niiden pintaan muodostunut oksidikalvo ei välttämättä ole suojaava pidemmällä aikavälillä. Kromin lisäksi myös muut seosaineet osallistuvat hapettumiseen. Oksidikalvoista havaittiin kromin lisäksi mangaania, alumiinia, piitä sekä titaania.

Kirjallisuusselvityksen ja kokeellisten tuloksien perusteella soveltuvia materiaaleja yli 600 ºC höyrynlämpötilalle ovat austeniittiset kattilateräkset, joiden kromipitoisuus on vähintään 22,5%. Ylimpien mahdollisten käyttölämpötilojen arviointi vaatisi testejä eri lämpötiloissa. Kuulapuhallettuja teräksiä tulisi testata autoklaavissa ja verrata niistä saatuja tuloksia tässä työssä testattuihin koneistettuihin koepaloihin, jotta niiden todellinen suorituskyky pystyttäisiin määrittelemään.

PREFACE

This Master of Science thesis was done at Foster Wheeler Energia Oy Research & Development department in Varkaus between January 2010 and February 2011. This thesis has been done with the financial support of VYYT-project, which is a venture to improve the knowledge and competitiveness of process and energy industries with the help of universities. The VYYT-project is funded by European regional development fund (ERDF), Finnish government, municipalities and companies. The financing authority is Pohjois-Savon liitto.

I would like to thank all my colleagues at Foster Wheeler for pleasant working environment and support. A special word of thanks must be addressed to Dr. Edgardo Coda Zabetta for professional guidance and support throughout this project.

Professor Toivo Lepistö I would like to thank for supervising this work and giving valuable feedback.

I am much obliged to my family for the love and support you have provided me throughout my life.

Varkaus 13.05.2011

Jouni Mahanen

CONTENTS

ABBREVIATIONS AND NOTATION

A	Arrhenius constant	[gm^2/s, g^2m^4/s]
Cr(eq)	chromium equivalent	[-]
g^*	critical volume fraction	[-]
G^0	standard gibbs free energy	[J/mol]
k	rate constant	[gm^2/s, g^2m^4/s]
M	atomic weight	[-]
N	mole fraction	[-]
N(S)	solubility	[-]
Ni(eq)	nickel equivalent	[-]
p	pressure	[atm, bar, Pa]
q	heat	[J]
Q	activation energy	[J/mol]
R	universal gas constant	[J/K•mol]
T	temperature	[ºC, K]
t	time	[s]
v	velocity	[m/s]
V	molar volume	[m^3/mol]
W	weight gain per unit area	[g/m^2]
Z	valence	[-]

Greek

α	angle	[º]
Δ	difference	[-]
η	efficiency	[-]

Subscripts

1,2,3,..	number, index
crit	critical
l	linear
m	metal
ox	oxide
p	parabolic
	particle

Acronyms

ASME	American Society of Mechanical Engineers
ASTM	American Society for Testing and Materials
AUSC	advanced ultra super critical

BCC	body centered cubic
BFB	bubbling fluidized bed
CCS	carbon capture and storage
CFB	circulating fluidized bed
CTE	coefficient for thermal expansion
EDS	energy dispersive spectroscopy
EDX	energy-dispersive X-ray
FCC	face centered cubic
g	gas
FGC	flue gas condenser
GDOES	glow discharge optical emission spectrometry
HAZ	heat affected zone
LUVO	air preheater
MSW	municipal solid waste
NDT	non destructive testing
PWHT	post weld heat treatment
SEM	scanning electron microscope
SPE	solid particle erosion
USC	ultra super critical
VTT	Technical Research Centre of Finland

1. INTRODUCTION

Increasing the efficiency of energy production is one method to reduce the carbon dioxide emissions generated, and thus contain the global climate change. Increased level of CO_2 in atmosphere derives mostly from combustion of fossil fuels. Since fossil fuels will most probably remain as an important source of energy in the coming decades, increasing the efficiency of energy production will have direct and crucial impact to the green house gas emissions generated. Another method to reduce green house gas emissions generated in combustion of fossil fuels is carbon capture and storage (CCS), which involves capturing the carbon dioxide from the fuel and pumping it to storage where it is not released to the atmosphere. Steam power plants equipped with CCS require considerably more auxiliary power than conventional boilers, so increasing the efficiency is an important step in making CCS economically feasible technology.

Two crucial factors affecting on the efficiency of condensing power plant are the temperature and pressure levels of live steam. With improved steam parameters, higher efficiency is achieved. The maximum operating temperatures of structural alloys limit the achievable steam temperature. The final superheaters are exposed to highest temperatures, so proper material selection for those components is crucial in order to achieve high plant efficiency and availability. The materials must have sufficient mechanical high-temperature strength and adequate resistance against corrosion in both inner and outer tube surface. High-temperature strength and corrosion rate depend on the temperature level. Additionally, corrosion rate is greatly affected by the exposure atmosphere, which in turn is derived from combustion method and fuel on the outer tube surface, and from the water/steam properties on the inner tube surface.

This thesis work focuses on the oxidation process taking place on the inner tube surface, which is also known as steam-side oxidation. Other material degradation mechanisms in steam boilers are discussed superficially in order to introduce the challenges in material selection to the reader. The theory section introduces the theory of high-temperature oxidation and factors affecting the oxidation mechanisms in sub-critical and supercritical steam as they appear in public literature. Additionally, field test results from two extensive campaigns are reported. Some promising austenitic tubular steel grades were exposed to supercritical steam in autoclave. The test pieces were weighed and their mass gains per unit area and time were calculated. Additionally, the cross-sections of samples were analyzed with scanning electron microscope (SEM). The oxide scale depth profile analysis was performed with glow discharge optical emission spectrometry (GDOES).

2. STEAM BOILER TECHNOLOGY

Steam boilers, or steam generators, are an important source of electrical and thermal energy. Steam boiler may be considered to be a heat exchanger which transfers the thermal energy generated by combusting selected fuel in the furnace to the working fluid circulating in the system. The thermal energy carried by the working fluid may be utilized in heating and production of electrical energy. The electrical energy is produced by evaporating the working fluid (water) and using the steam in driving a steam turbine, which in turn drives the electric generator. Majority of electrical energy in the world is produced with this method; see Table 2.1, where sources of electrical energy in the world are listed. Basically, all sources of electricity listed in the table are utilized with steam boilers, except hydroelectric power, wind power and solar power produced with photovoltaic method. Gas and oil may be used in driving a gas turbine, or in a combustion engine which drives electric generator, but also as a fuel in steam boiler. (1)

Table 2.1. Sources of electric energy in the World (2007). (2)

Production from:	**Electricity, GWh**	**Percentage**
Coal	8 227 950	41,440 %
Gas	4 126 912	20,785 %
Hydro	3 162 165	15,926 %
Nuclear	2 719 058	13,695 %
Oil	1 114 455	5,613 %
Biomass	190 468	0,959 %
Wind	173 317	0,873 %
Waste	68 034	0,343 %
Geothermal	61 819	0,311 %
Other sources	5 358	0,027 %
Solar (photovoltaic)	4 104	0,021 %
Solar (thermal)	681	0,003 %
Tide	550	0,003 %

The environmental effect of a steam boiler is defined by the production method of the thermal energy required in heating and evaporating the working fluid. Nuclear power plants are steam boilers too. The thermal energy in a nuclear power plant is produced in fission of atomic nuclei. Also, the solar radiation may be utilized in heating the working fluid. These methods may be considered to have low environmental effect

regarding the emissions. The most common method for producing the thermal energy is combustion of selected fuel in the furnace. The fuels which are combusted may be of various types, and the emissions generated by the combustion are partially derived from the fuel used. Fossil fuels, such as coal, oil and natural gas are most commonly used fuels, but the increased concern of climate change has lead to increasing interest towards renewable fuels, such as biomass. Table 2.1 lists the electrical energy produced different methods, and as may be seen, the combustion of coal is by far the greatest source of energy (2). (3)

Besides broadening the share and variety of renewable fuels for combustion, considerable effort is put in trying to increase boiler efficiency. Modern boilers are able to produce electricity with approximately 35 – 40 % efficiency. Increasing the efficiency will decrease the emissions, since the same amount of energy is produced with less fuel. The current goal is to boost the efficiencies up to 50 % and beyond, which means that the CO_2 emissions are considerably reduced from the current emissions. This would be a remarkable advancement in reducing the emissions of greenhouse gases worldwide, since a majority of energy is produced by combusting fossil fuels. The efficiencies of steam turbines, generators and furnaces are very high in modern power plants, so the largest potential to improve the overall efficiency lies in the water-steam cycle of the boiler. The efficiency of the water-steam cycle depends on the live steam temperature and pressure, so improvement of the efficiency is limited by the maximum operating temperature of heat exchanger materials. There are also process limitations in increasing the live steam temperature, since temperature in the furnace must be considerably higher than the live steam temperature so that heat transfer would be efficient. Increasing the efficiency of water-steam cycle is discussed further in section 2.1. (1) (4)

2.1. Energy production with steam

Water is a cheap and widely available medium to use as a working fluid in boilers. In boilers the heat generated by combustion is transferred to the working fluid circulating in the heat exchangers. The amount of heat transferred from combustion process to the working fluid is equal to the change in its total heat content, if the heat transfer is assumed to take place without any heat losses. The heat transfer process consists of three main steps: i) water preheating to the evaporation temperature, ii) evaporation of saturated steam, followed by iii) superheating of the same steam. The thermal energy transferred to the liquid may be approximated by the change in enthalpy of the working fluid. During preheating and superheating the temperature of the working fluid increases, and the enthalpy is increased linearly as a function of temperature. During evaporation the temperature remains constant, but a great deal of thermal energy is transferred as latent heat to the working fluid. The relationship between enthalpy and temperature is visualized by Figure 2.1, where the evaporation of water under atmospheric pressure is plotted as a temperature-enthalpy graph. (3)

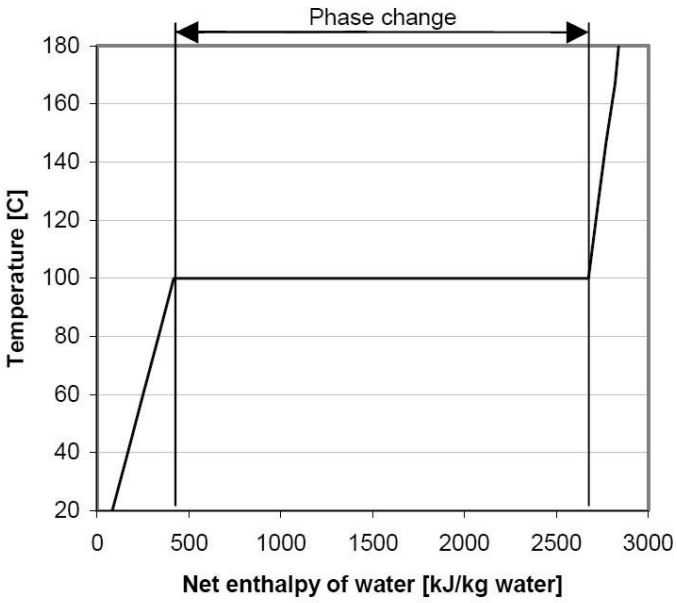

Figure 2.1. Evaporation of water plotted in temperature-enthalpy diagram. (3)

The typical steam boiler process consists of steam generator, steam turbine, condenser and feedwater pump. It is known as Rankine cycle, Figure 2.2. The high pressure steam generated in the boiler is directed to a steam turbine. In the steam turbine, the thermal energy carried by steam is converted to mechanical work, W_{out}, by letting the steam expand in the turbine. The expanding steam drives the turbine, and the mechanical work generated by it may be used, for example, in driving an electric generator which converts the work from the turbine into electricity. The steam used by the turbine is then fully condensed back into water in a condenser and then returned back to boiler as feedwater. The steam may be partially condensed in a turbine, depending on the turbine type (5). The condenser is a heat exchanger that uses water to cool the steam below the condensation temperature. The cooling water is typically taken from a water system nearby, so the condensation heat isn't utilized. One way to make use of the condensation heat is to utilize it as district heating in combined heat and power plant (CHP plant), where the cooling water used in condenser is circulated in district heating distribution pipeline. After expansion in the turbine the pressure level of the working fluid is decreased notably. Since the compression of liquids is considerably easier than compression of gases, the water is pressurized with feedpump (W_{pump}) after the condensator. Usually the ideal Rankine process is described as a four-step process: isentropic compression in pump (1 - 2), heat addition in boiler under constant pressure (2 – 3), isentropic expansion in steam turbine (3 – 4) and heat rejection in a condenser under constant pressure (4 – 1). (1) (3)

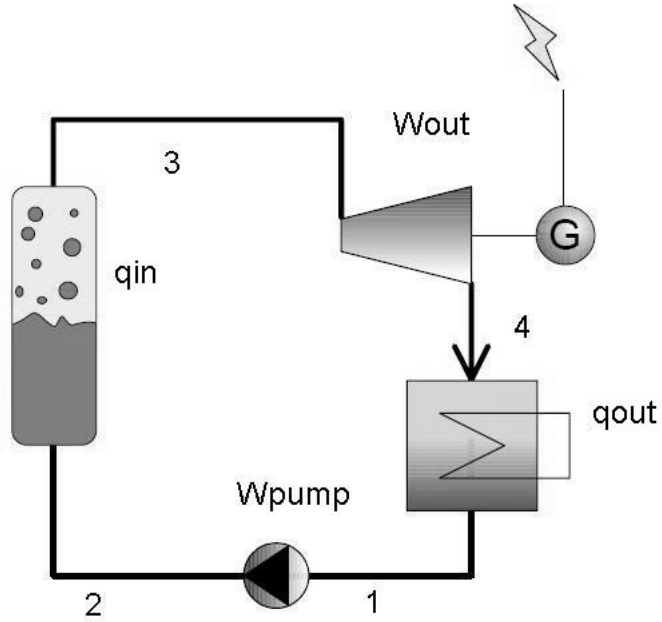

Figure 2.2. A schematic presentation of ideal Rankine cycle. Modified from (3).

The maximum theoretical efficiency of any heat process is related to the heat input q_{in} and heat output q_{out}, defined as in equation (2.1).

$$\eta = 1 - \frac{q_{out}}{q_{in}} \qquad (2.1)$$

The Rankine process is assumed to be fully reversible, which is obviously not the case in real heat processes. Real processes have always some irreversibility, such as pressure losses in evaporation, condensation, and expansion efficiency of steam turbine. However, the thermal efficiency of many heat processes can be calculated accurately enough by approximating them as reversible processes. When calculating the maximum theoretical thermal efficiency of ideal Rankine process, the isobaric heat input (2 – 3) consists of the thermal energy input in the steam boiler. The isobaric heat output on the other hand is equal to heat which leaves the system in condenser to the cooling media. (6)

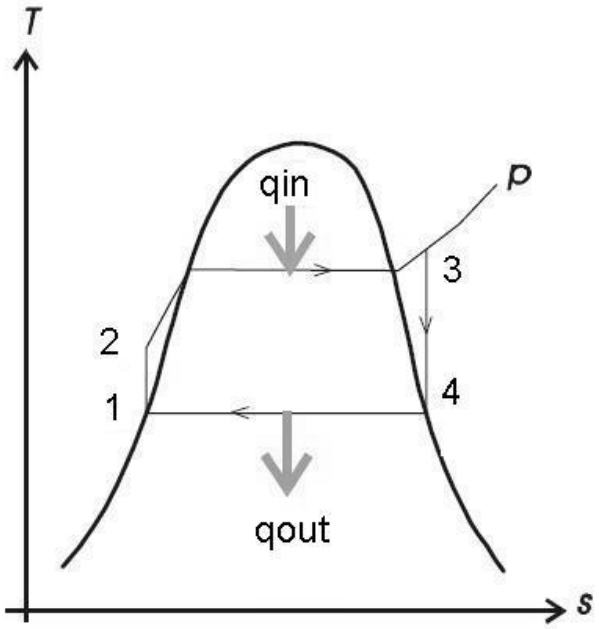

Figure 2.3. An s-T diagram for ideal Rankine cycle. Modified from (7).

Any thermal process can be represented graphically by a temperature-entropy cycle. It can be easily demonstrated that the area inscribed in such graph represents the efficiency of the plotted thermal process. Figure 2.3 shows the ideal Rankine cycle. From the figure and equation (2.1) it is obvious that the efficiency of the water-steam cycle may be increased by decreasing the heat output q_{out} or by increasing the heat input q_{in}. The heat output can be decreased by decreasing the condensation temperature, which in turn decreases the counter-pressure level. Decreasing the temperature is not possible from the current value, because the temperature of the cooling media is fairly fixed value, usually around 20 °C, depending on the climatic conditions of the area. Additionally, when the counter-pressure is decreased, the end part of the turbine must be considerably larger, since the specific volume of the steam increases with decreasing pressure. Typical values for condensing pressure and temperature in Finland are 0,02 bar and 17,5 °C. (6)

Since the heat output cannot be further decreased, the only option to increase the efficiency of a steam-water cycle is to increase the heat input. The most obvious method is to increase the temperature of the superheated steam. Increasing the live steam temperature at constant pressure increases the average heat input temperature, the effect may be visualized by comparing Figure 2.4 a) and b). The limitations of materials for heat exchangers restrict the temperature increase. Such limitations include increase in corrosion and oxidation of materials and decrease in mechanical properties with increasing operating temperature. Another restriction is that if the temperature of the live steam is too high, the steam will be still superheated when leaving the steam turbine and entering the condenser. This leads to increase in q_{out}, and thus, some of the gained efficiency is lost. This is why the condensing steam should be as close to the saturation point as possible. The live steam temperatures in modern power plants are around 600

°C, but there are several research projects going on which intend to increase this value towards 700 °C and above. (4) (6)

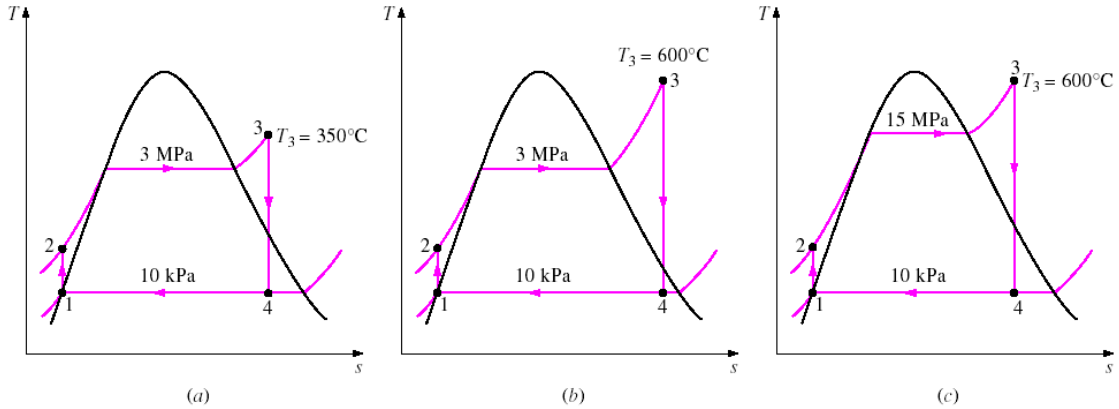

Figure 2.4. Increasing the thermal efficiency of Rankine cycle by a) lowering the condensation pressure, b) increasing the superheated steam temperature and c) increasing the pressure of heat addition. (8)

Another way to improve the efficiency is increasing the pressure of heat addition, Figure 2.4 b) and c). When the pressure is increased, the evaporation temperature is also increased. So, the average heat input temperature is increased leading to higher heat input. On the other hand, the net work output of the steam turbine decreases as the live steam pressure increases. The increase in heat input is nevertheless greater than the decrease in work output, so the overall efficiency is improved. The drawback of increasing the steam pressure is that the moisture content of steam is increased at the end of the turbine. Excessive moisture in steam can erode turbine blades, thus decreasing the estimated life time and efficiency of the turbine. The percentage of moisture inside most steam turbines should not exceed 12 – 14 %. (6)

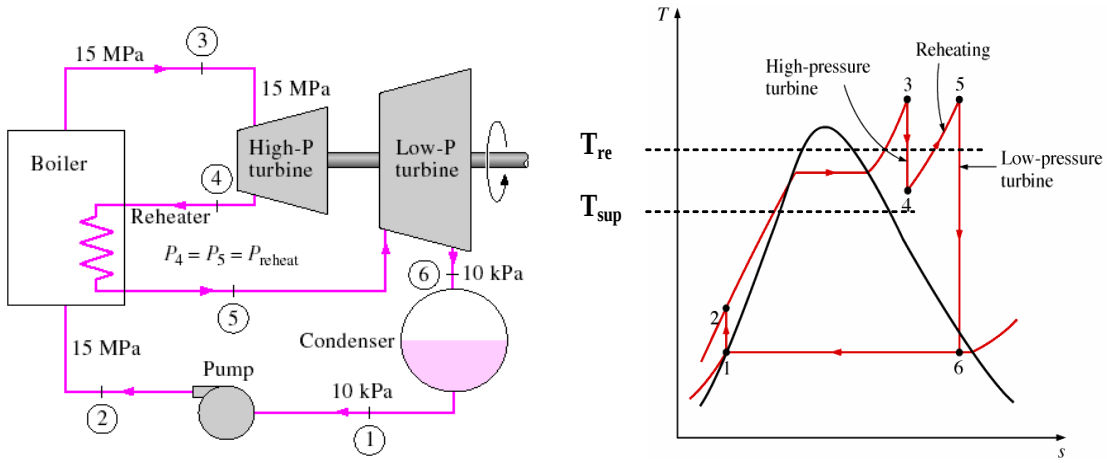

Figure 2.5. a) A schematic presentation and b) s-T diagram of Rankine cycle with reheating. (8)

As discussed above, increasing the live steam pressure leads to certain drawbacks in the process. If live steam pressure is raised to increase efficiency, the moisture content of steam will become increasingly high in the end part of the turbine. This cannot be compensated with increasing the steam temperature, because after certain point the required steam temperature will become too high for superheater materials. Another way to avoid problems caused by increased moisture is to use reheating of the steam. This means that the expansion of the steam is divided in two or more separate turbine sections, and steam is returned to the boiler to reheat between the sections. The reheating process is illustrated in Figure 2.5. Usually the reheat temperature is equal to the temperature of superheated steam, but it can be slightly higher (10 °C), since the pressure level is considerably lower in the reheater section. (6)

2.1.1. Supercritical steam boilers

When temperature and pressure of live steam are increased beyond the critical point of water, the properties of steam will change dramatically. The critical point of water is at 374 °C and 221,2 bar (≡218 atm), Figure 2.6, and it is defined to be the point where gaseous component cannot be liquefied by increasing the pressure applied to it. Beyond this critical point water does not experience a phase change to vapor, but it becomes a supercritical fluid. Supercritical fluid is not a gas or liquid. It is best described to be an intermediate between these two phases. It has similar solvent power as liquid, but its transport properties are similar to gases. (9)

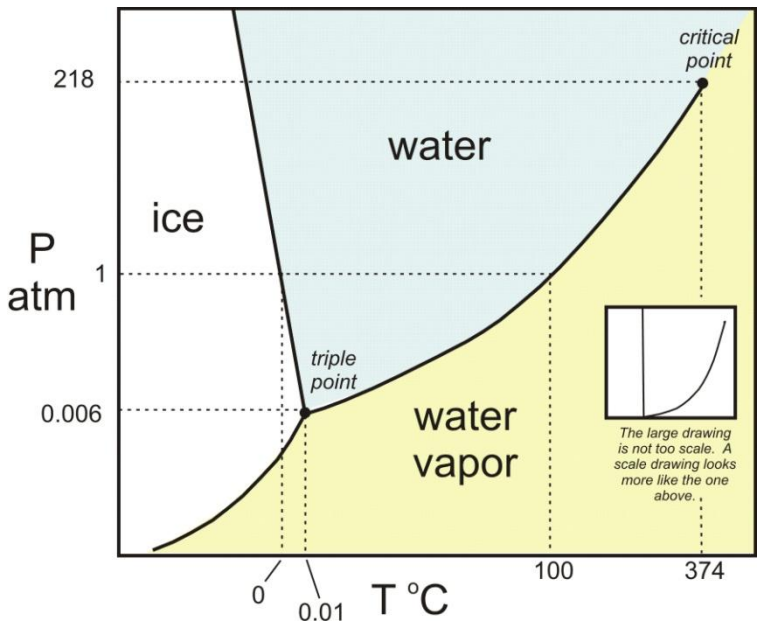

Figure 2.6. Phase diagram of water showing different states of water and critical point. Axes are not in scale. (10)

Supercritical steam sets specific technology requirements. For instance, very important is the issue of proper material selection, since higher pressure and temperature require more advanced materials. Additionally, there are some restrictions

to the boiler design too. Since there is no distinguishable boiling point, the de-watering of the steam is no longer possible, since there is no difference in densities. For this reason the supercritical boilers are always designed as once-through boilers, and have no steam drum. Supercritical boilers may be further classified by the live steam temperature. The classification varies a bit depending on source, but according to (11), if the live steam temperature is over 593 °C, the boiler may be classified as ultra-supercritical (USC) boiler. Boilers operating below this temperature are referred to as supercritical boilers. Boilers which have live steam temperature above 720 °C are often referred to as advanced ultra-supercritical (AUSC) boilers. (1)

2.2. Steam boiler types

Steam boiler types may be distinguished by the way in which fuel is burned, the type of fuel combusted or the design of the steam cycle. This thesis concerns the oxidation of steam-touched surfaces, so in this context it is more useful to distinguish boiler types according to the steam cycle, since the steam-side oxidation is not directly affected by the fuel combusted or the combustion method.

Accordingly, steam boilers may be roughly divided to two groups: boilers which have steam drum and boilers that don't. Boilers without steam drum are referred to as once-through boilers. These two groups may be further divided: boilers equipped with steam drum may have natural or assisted water circulation. Once-through boilers may have either fixed or variable evaporation point, often referred to as Sulzer and Benson boilers, respectively. Boilers with steam drum and once-through boilers are introduced briefly in the following sections. (1)

2.2.1. Boilers with steam drum

Figure 2.7 represents a typical design of a steam boiler with drum. Water circulation can be natural or assisted, but the design of the water-steam circulation is pretty similar in both cases. At first the feed water is preheated with flue gases in an economizer. This improves the boiler efficiency, since thermal energy of the flue gases is utilized more efficiently. After that, preheated feed water is directed to the steam drum. From the steam drum water flows to the evaporating tubes via a downcomer and then back to the steam drum. This is the location where the difference between natural and assisted circulation is. The water-steam circulation is natural if the water flows between steam drum and evaporator tubes without pumping. The circulation is based on the density differences between water and steam: when the water evaporates, its density decreases and thus the mixture of water and steam flows upwards to the steam drum via the evaporating tubes. At the same time, water is flown from the steam drum via the downcomer to replace the evaporated water. The circulation is assisted if the water is pumped from the steam drum to the evaporator section. With assisted circulation the evaporation tubes do not necessarily have to be vertical, since now the circulation is not

based on the density differences. Also, the live steam pressure may be slightly higher with assisted circulation, but still below supercritical level. (1)

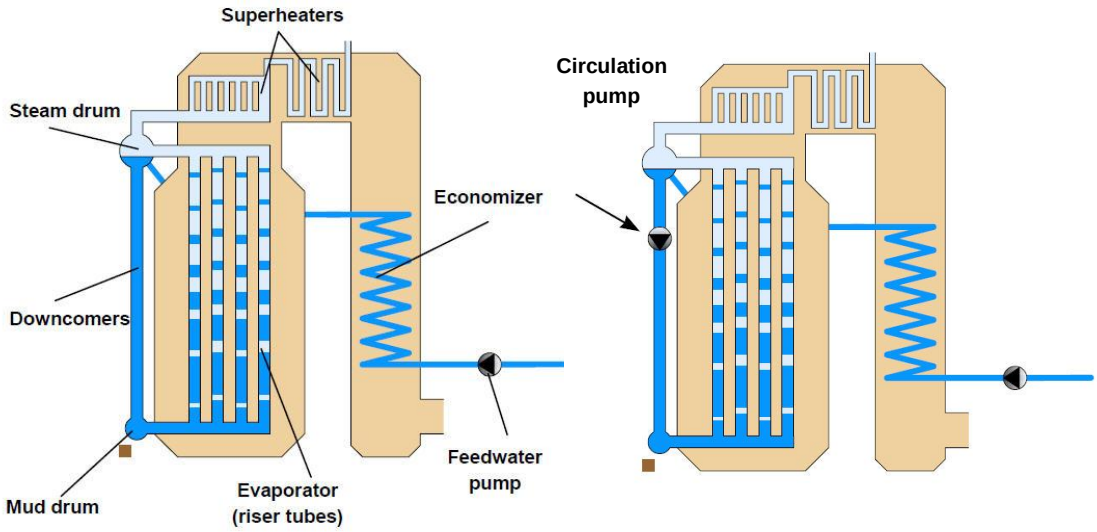

Figure 2.7 Steam boiler equipped with steam drum with a) natural circulation and b) assisted circulation. (3)

Saturated steam is separated from saturated water in the steam drum before the steam is introduced to the superheaters. The steam entering the superheater section should not contain water vapor, since the water contains dissolved salts. If the steam contains water, it will evaporate in the superheater and the dissolved salts may form deposits on the steam-touched surfaces of superheater tubes and turbine blades. Instead, the dissolved salts become enriched in the steam drum, where they can be easily removed from the water-steam circulation. The de-watering of steam is based on the density differences between water and steam. Additionally, modern steam drums contain also cyclones and droplet separators, which separate the water more efficiently. (1)

2.2.2. Once-through boilers

Once-through boiler may be considered to be a long bundle of tubes, which is heated externally. The feedwater is fed from one end of the bundle and it exits as superheated steam from the other end. The water-steam cycle (Figure 2.8) is somewhat different than in boilers with natural or assisted steam circulation, since there is no steam drum. Since there is no need for de-watering, live steam pressure may be at supercritical level. The absence of de-watering under supercritical pressures means also that the scale-forming salts cannot be removed from the water-steam circulation. Because of this, the feedwater must be very pure. (1)

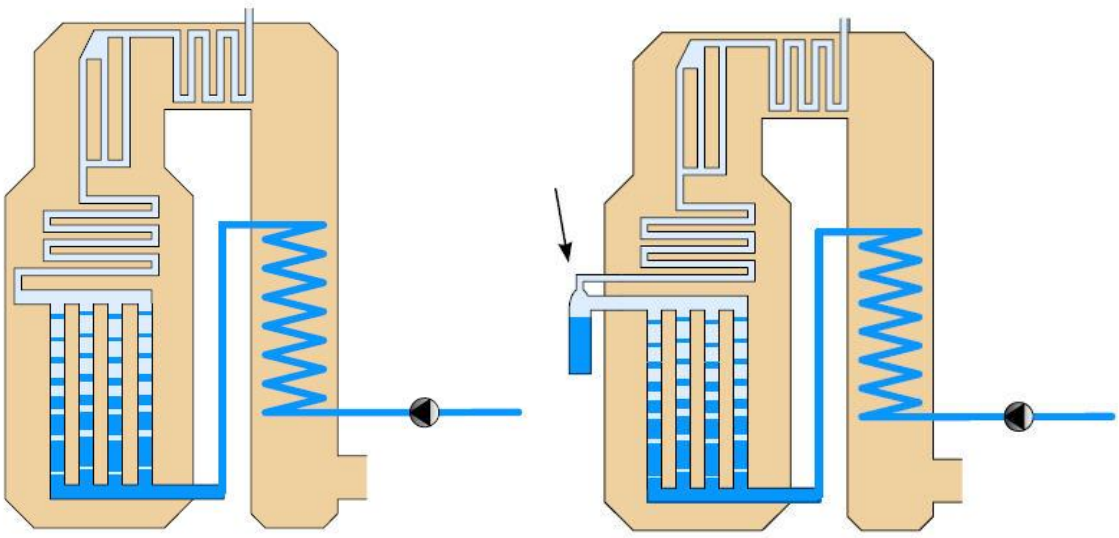

a) b)

Figure 2.8. Once-through boiler with a) Benson and b) Sulzer design. (3)

Once-through boilers have usually variable point of evaporation (Benson boiler), but there are also boilers with fixed point of evaporation. If the point of evaporation is fixed (Sulzer boiler), the water-steam circulation is similar to boilers with steam drum, with only exception that the steam drum is replaced with a water separation bottle. The evaporation stops in the water separation bottle, and after that the superheater section begins. Usually Sulzer boilers are subcritical, but it is possible to design a Sulzer boiler with supercritical live steam parameters. Naturally, the water separation bottle does not work under supercritical pressure. (1)

The Benson boiler has a floating pressure control: the pressure of live steam decreases as the load of the boiler decreases. This has certain advantages compared to Sulzer boilers. First, the overall process efficiency increases, since the feedwater pump requires less power on a partial load. Additionally, when the boiler load is varied, the temperatures in the boiler and turbine blades remain practically constant, so there are no thermal stresses induced as the load is varied. The main idea in designing boilers of Benson-type is to reach the desired live steam temperature by adjusting the feedwater and fuel flows appropriately. Because of this, the relative effectiveness of each heat exchanger varies with varying boiler load. In other words, the designed final point of evaporating and the starting point of superheating vary with varying boiler load. (1)

2.3. Heat exchangers

Heat exchangers transfer the thermal energy generated in combustion of fuel to the water/steam circulation of the boiler. In order to achieve high thermal efficiency, the thermal energy of flue gases must be exploited as efficiently as possible. However, the risk for acid dew point corrosion, see chapter 3.2., limits the lowest achievable temperature of the flue gases to roughly 150 – 200 °C when steel is used as heat exchanging material. Heat exchanging surfaces refer to all surfaces which are heated up

with flue gases and cooled down with heat transferring mass flows, which are: water, water-steam mixture, pure steam, supercritical steam and air. The heat exchanging surfaces are divided by their purposes of use:

- evaporators
- superheaters and reheaters
- feedwater preheater, economizer
- air preheater, LUVO (luftvorwärmer).
- flue gas condenser (FGC).

An example of arrangement of heat exchanging surfaces and mass flow types circulating inside them is represented in Figure 2.9. If the boiler design includes flue gas condenser, it is the final heat exchanger. The proper arrangement of heat exchanging surfaces will affect the durability and fouling of heat exchanger materials, live steam temperature and to the exit temperature of flue gases. (1) (3)

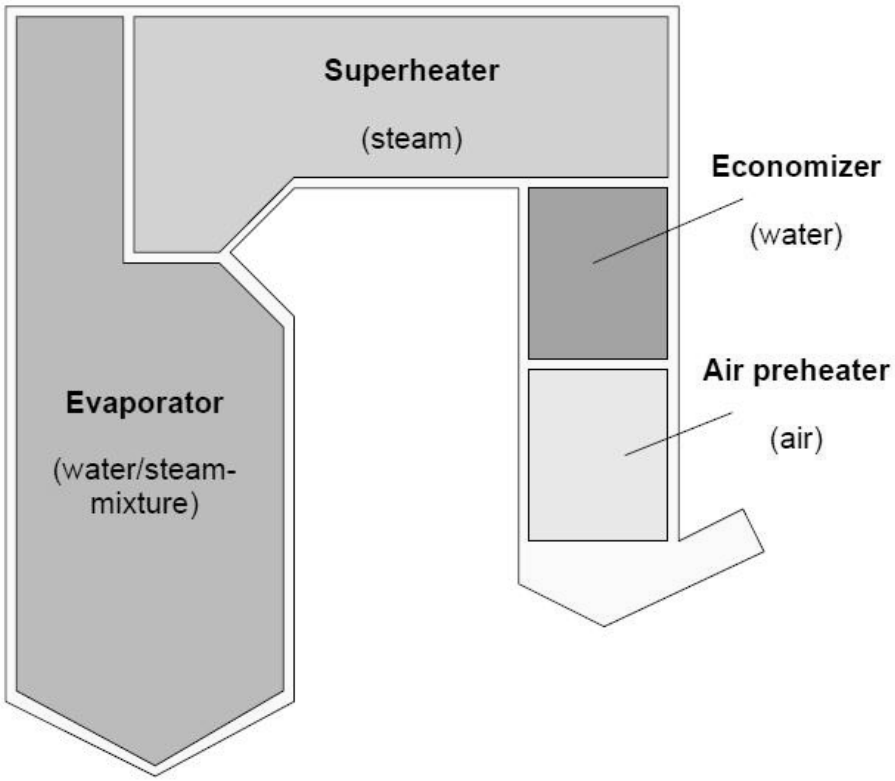

Figure 2.9. Physical locations of heat exchanging surfaces in a boiler with two-pass layout. (3)

Different types of boilers may have very different heat exchanger constructions and designs, but the principle of arrangement in the flue gas path is more or less similar in all boiler types. The second law of thermodynamics states that heat transfer can only occur from a higher temperature to a lower temperature. In other words, the flue gas temperature must be higher than the temperature of the heat transferring working fluid. An example of arrangement of heat exchanging surfaces is presented in Figure 2.9. The evaporation of water requires the highest amount of energy in the water/steam cycle, and this is one reason why evaporators are located in the furnace. Since the evaporator

tubes are effectively cooled, the requirements for furnace materials are not as high as in superheater section. Superheaters are exposed to the most severe conditions in a boiler, since they are exposed to the highest working fluid temperatures and thus will have the highest metal temperatures. Superheater and reheater materials must have sufficient high temperature strength and creep strength. Corrosion resistance of candidate materials must be considered too, since corrosion processes are usually temperature dependant. (1) (3)

After the superheater section flue gases will still have moderately high temperature. They are further cooled down by transferring the heat to the feedwater in economizers and to the combustion air in air preheaters. Some boilers have flue gas condenser, which utilizes the latent heat of moist flue gas e.g. in heating the water circulating in the district heating network (12). Economizers can be either evaporating or non-evaporating. In evaporating economizers the feedwater will be partially evaporated at the economizer outlet. The outlet feedwater temperature in non-evaporating economizers is roughly 20 °C lower than the boiling point of water. In many cases the feedwater is also preheated with steam bled from the steam turbine. With combustion air preheating the ignition of the fuel particle becomes easier and the combustion process takes place more rapidly. Also, the combustion of moister fuels becomes easier if combustion air is preheated. Combustion air can be preheated to temperatures between 100 – 400 °C, depending on the design. As mentioned earlier, the risk for acid dew point corrosion increases when flue gases are cooled down. Because of this, the designed flue gas temperature after LUVO is controlled by the flue gas composition and material selection. (1)

2.4. Fluidized bed combustion

Fluidized bed combustion is a relatively new combustion technology, and it is discussed here briefly. Fluidized beds were first applied in energy production in the 1970s, although fluidized beds were commonly used in various other industrial applications before that. In recent decades it has become a relatively common combustion technology. Fluidized bed combustion has certain advantages when compared to other combustion technologies. The most important advantage is that it is possible to burn a wide variety of fuels, even low-grade fuels, with good combustion efficiency. Additionally, the control of emissions is easier. Since the combustion temperature is relatively low, considerably under 1000 °C, the emissions of nitrogen oxides (NOx) are low. Moreover, desulphurization of flue gases can be done by feeding limestone in the furnace. (1)

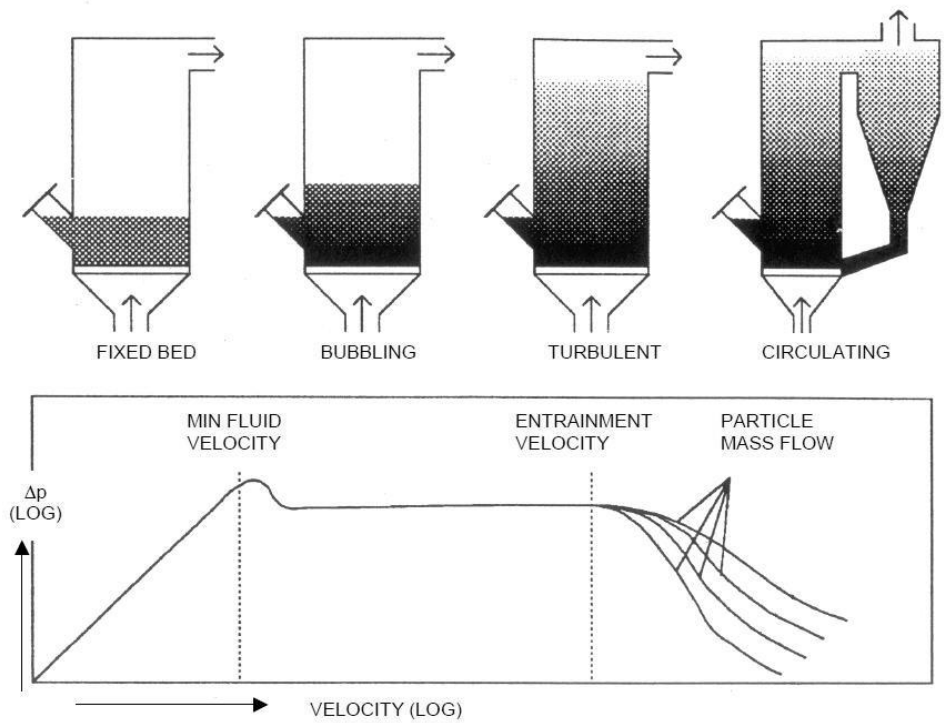

Figure 2.10. Different regimes of fluidized bed systems. (3)

In fluidized bed the combustion of fuel takes place in a bed, which usually consists of fuel ash, sand and/or limestone. Since the bed material has high heat capacity, fluidized bed boilers are not very sensitive to variations in fuel quality. The bed material is fluidized with primary air blown from the bottom of the furnace. The minimum air flow velocity required for bed fluidization is called minimum fluidization velocity, and it depends on the particle size of bed material. Fluidized bed boilers can be classified in two types, depending on the air flow velocity, Figure 2.10: bubbling fluidized bed (BFB) boilers which operate with moderate fluidization velocities resulting in a bed bursting of air bubbles (chapter 2.4.1), and circulating fluidized bed (CFB) boilers which operate with higher fluidization velocities and with finer bed material resulting in solids material circulation (chapter 2.4.2). (1)

The bed temperature in fluidized bed boilers must be kept within the designed range in order to avoid problems during boiler operation. If the bed temperature becomes too high, the risk for ash sintering and bed agglomeration increases. This in turn may cause uneven fluidization, or even defluidization of the bed, which will lead to unexpected boiler shutdown or, in some circumstances, substantial damage to the boiler. Additionally, sintered or agglomerated bed material cannot be removed from the furnace during boiler operation. The agglomeration of bed material is strongly dependent on the temperature, but compositions of fuel ash, bed material and additives have also an effect. Agglomeration of bed material owes mostly to the formation of low-temperature melting compounds and eutectics. It has been identified that the reactions between alkali from the fuel and quartz particles from the bed material are key events in formation of sticky alkali-silicate coating layers that lead to agglomeration.

Commonly used countermeasures for bed agglomeration are increasing the bottom ash removal, maintaining the local bed temperatures below the level at which the agglomeration takes place, selecting alternative bed material, and introducing suitable additives to the furnace. (13) (14)

2.4.1. Bubbling fluidized bed

Bubbling fluidized bed boilers are perhaps the most common application of fluidized beds. Their operating principle is represented in Figure 2.11. The furnace consists of a bed section and the area above it, which is called freeboard. The superheaters are usually located in the freeboard section or in the beginning of the convective pass. Economizers and air preheaters are commonly located in the convective pass. The fuel is fed on top of the bed material, which is fluidized with primary air flow on the bubbling velocity region (Figure 2.10). The large heat capacity of the bed material allows for relatively high moisture content of fuel and changes in the fuel quality. The primary air flow should be sufficient to fluidize most of the bed particles, but less than the terminal velocity of the smaller bed particles. The particle size distribution of bed material affects also to this. Secondary and tertiary air are usually introduced above the bed level, possibly in different levels. (1) (15)

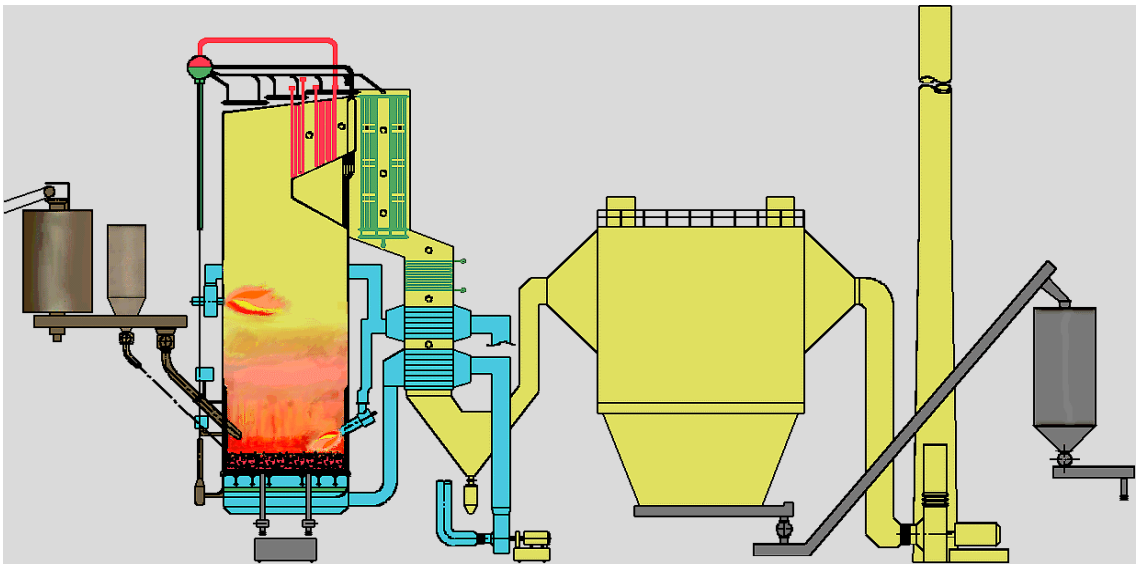

Figure 2.11. A schematic presentation of a typical bubbling fluidized bed boiler. (16)

Bubbling fluidized bed type boilers have some shortcomings which limit their applicability. Since the bubbling fluidized bed has solids flowing in the furnace, the heat exchanging surfaces that are immersed in bed material are exposed to solid particle erosion. They also have a limited ability to part-load operation. Also the fuel flexibility is limited, and it is not always possible to change designed fuel to fuel with considerably lower or higher heating value than the designed fuel. The capacity of BFB boilers is limited to small and medium scale, because of a relatively large amount of fuel feed points required. (15)

2.4.2. Circulating fluidized bed

Circulating fluidized bed boilers, Figure 2.12, have bed material with smaller particle size and faster primary air flow velocity than BFBs. This results in better mixing of bed material and fuel. There is no distinctive bed surface as in BFB boiler, but the density of the bed will decrease as a function of furnace height. The bed particles are separated from flue gases in the solid separators (cyclone) and returned back to the bottom of the furnace via a return leg. Different manufacturers have different cyclone designs; Figure 2.12 illustrates the Compact design commonly used by Foster Wheeler Energia Oy. After the solids separator the flue gases are directed to the convective pass, where superheaters/reheaters, economizers and air preheaters are usually located. In some cases the final superheater is immersed in bed material. An example of this design is Foster Wheeler's INTREX superheater, which is located below the solids return leg. With this kind of arrangement the corrosion caused by fly ash deposits will be eliminated from the final superheater, since now it is not exposed to flue gases. Also, the erosion will not be a significant problem, because the fluidizing air flow velocity is relatively low in the INTREX chambers. (1) (17)

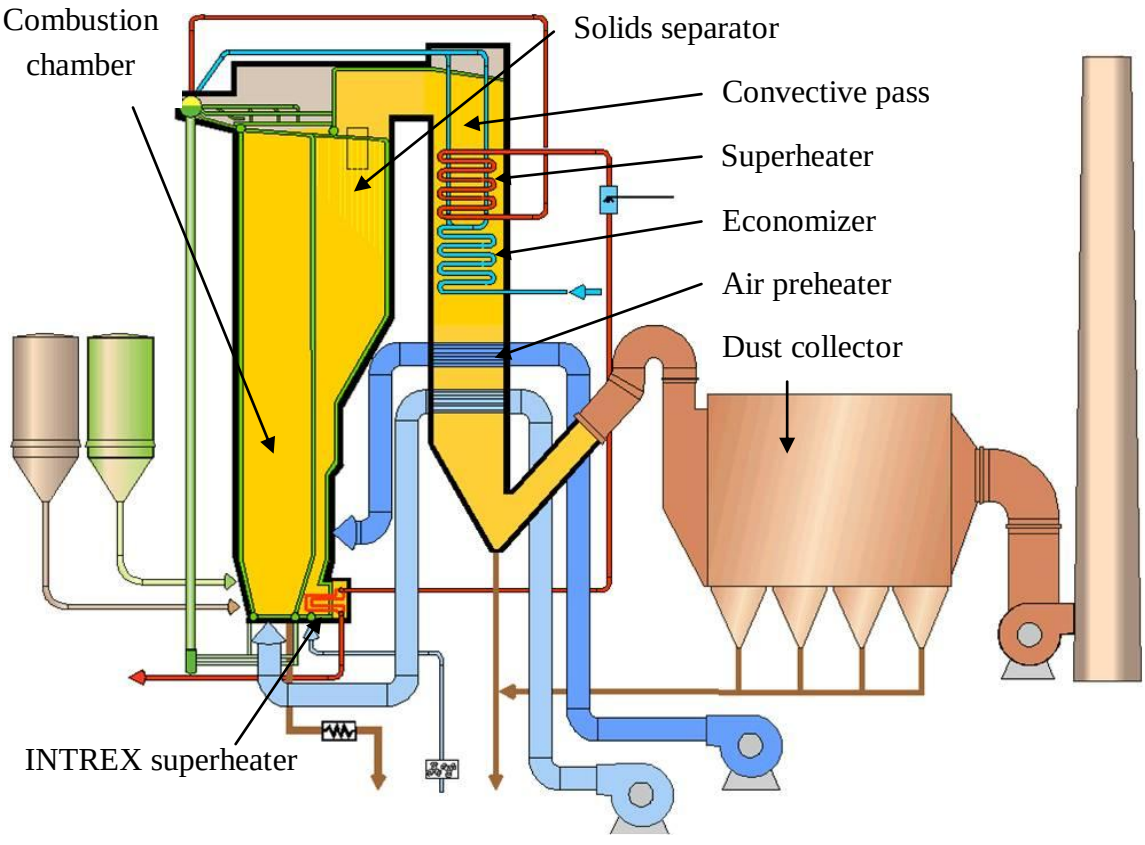

Figure 2.12. A schematic presentation of a typical circulating fluidized bed boiler. (17).

3. MATERIAL DEGRADATION IN BOILERS

Degradation of heat exchanger materials in steam boilers may be roughly divided to three different types or modes: steam-side oxidation, fire-side corrosion and erosion. Steam-side oxidation takes place on the steam-touched inner surfaces of superheater and reheater tubes. Fire-side corrosion and erosion take place on the outer side of the heat exchanging surface. It is reasonable to divide material degradation types by above-mentioned manner, as the mechanisms for each degradation type are distinctive. Steam-side oxidation behavior is controlled by steam temperature, pressure and alloy composition. Impurity levels of steam are strictly limited, so there are little impurity deposits formed on the steam-side of a superheater tube. The scale formed on the steam-side consists of different oxides of metal, depending on alloy composition. Fire-side corrosion is a substantially different process, as most frequently it involves some impurity deposit contributing to the corrosion process. The deposit is derived from the fuel burned and additives used. In case of fluidized bed process the deposits may derive from residues of bed material also. Erosion is a process of wear in which material is removed from solid surface through impingement of solid particles on it. The impinging solids are fly ash and, in case of fluidized bed type boilers, residues of bed material and additives. (15)

3.1. Steam-side oxidation

The steam-side oxidation of superheater and reheater materials is one of the major limiting factors in materials selection for supercritical boilers. Steam-side oxidation occurs usually in the superheater and reheater section, where the materials are exposed to highest steam temperatures. The oxide scales formed on the steam-side may lead to major failures and thereby reduced plant availability. There are three different failure types which may be recognized due to steam-side oxidation. First, the wall loss of the tubes caused by oxidation may increase the hoop stresses and cause premature creep failures in the heat exchanging tubes. Second, the insulating oxide scale may lower the thermal conductivity, resulting in increased metal temperature and thereby accelerated creep and corrosion processes. The third concern is that if the oxide scale on the steam-side becomes increasingly thick, it will spall more easily. The spalled oxide scale particles may lodge in the steam circulation and cause tube blockages, or if they enter the steam turbine, cause erosion in turbine blades and nozzles. Steam-side oxidation is discussed more extensively in chapter 5. (18)

3.2. Fire-side corrosion

The corrosion process taking place in the surface exposed to the flue gases is called fire-side corrosion. The conditions are different in different locations in the boiler, and thus the expected corrosion modes are different. The boiler may be divided to roughly three different sections with different conditions regarding the corrosion process. In the furnace metal temperatures are relatively low since the evaporating water cools the water wall tubes quite efficiently. Corrosion in the furnace section is caused mostly by locally reducing atmosphere. In superheaters and reheaters the metal temperature is highest due to high steam temperature and lower heat transfer coefficient of steam. The reasons for corrosion in this section are high metal temperatures and formation of deposits due to fly ash particles. The deposits will also hinder the flue gas flow in the boiler which in turn will increase the internal energy consumption of the boiler and reduce the boiler efficiency. After superheater section the flue gas temperature is lower and the risk for hot corrosion is notably lower. However, if the flue gas temperature becomes lower than acid dew point before the flue gases pass the last heat exchangers, there is a risk for cold corrosion. The sulfur trioxide in the flue gas may react with water vapor forming sulfuric acid via

$$SO_3(g) + H_2O(g) \leftrightarrow H_2SO_4(g) \qquad (3.1)$$

The sulfuric acid may condensate on the heat exchanging surface, if the condensation point is exceeded. The condensation point depends on the SO_3 and H_2O contents of the flue gases, and typical values are between 150 – 250 °C. The most effective ways to eliminate cold corrosion is maintaining the flue gas temperature above the acid dew point, or selecting corrosion-resistant materials for the last heat exchanging section. Corrosion resistant materials against sulfuric acid are, for example, glass and some plastic grades. (19) (20)

The heat exchanging surfaces may corrode, slag and foul from the outer surface. Slagging and fouling refer to different contamination mechanisms of heat exchanging surfaces: slagging takes place in the combustion chamber while fouling takes place in the convective pass. The most problematic ash components regarding corrosion of heat exchanging surfaces are considered to be sulfur, vanadium, chlorine and alkali and heavy metals. They may form molten deposits on the metal surfaces, which will favor corrosion. In the molten deposits the ion transportation is much faster than in solid deposits, and thus the corrosion reaction takes place at a higher rate. If the atmosphere is locally reducing and the partial pressures of oxygen and sulfur are favorable, the sulfur may diffuse through the oxide layer and form metallic sulfides with the base metal. This accelerates the corrosion since metallic sulfides are not protective against further corrosion. Alkali and earth alkali metals and chlorine are found especially from biomasses. Alkali and earth alkali metals in the fuel ash may increase fouling as they may form sticky deposits that are difficult to soot-blow. (13) (19) (20)

Chlorine contributes to corrosion by mechanism often referred to as active oxidation. The process has following steps: i) inward penetration of chlorine into the scale, ii) formation of metallic chlorides at the oxide/metal interface, iii) evaporation of the chlorides and iv) conversion of evaporating metallic chlorides into oxides. In other words, in active oxidation the chlorine plays a catalyzing role. The resulting oxide scale is loose, fragile and multilayered, i.e. not protective. At reducing gas conditions, i.e. when the oxygen partial pressure is low, chlorine may also form hydrochloric acid (HCl), which may react with the base metal and form gaseous metallic chlorides. In boilers, reducing gas conditions may exist near burners. Typical chlorine contents in biomasses range from 100 to 10 000 $(mg/kg)_{dry}$ (13) (20) (21)

Table 3.1. Ash compositions of selected fuels. The ash was produced at 815 °C, except for municipal solid waste (MSW) where temperature was 550 °C. (22)

Fuel	Bituminous Coal (Polish)	Peat	Wood (pine)	Bark	Wheat Straw (Danish)	Sewage Sludge	MSW
SiO_2	42,4	43,0	39,0	14,8	59,9	22,4	34,7
Al_2O_3	21,7	13,4	14,0	3,7	0,8	9,0	20,2
CaO	7,0	17,2	25,5	34,8	7,3	12,5	13,1
MgO	4,2	3,0	6,5	3,6	1,8	2,8	1,6
Fe_2O_3	11,3	14,7	3,0	5,2	0,54	24,6	4,4
Na_2O	0,8	0,9	1,3	-	0,4	4,6	2,7
K_2O	1,7	1,3	6,0	-	16,9	0,8	2,5

The formation of ash deposits on the heat exchanging surfaces depends most notably on the fuel combusted and additives used. Different fuels can form different amounts of ash, and the ash composition can vary greatly between different types of fuels. Thus, different corrosion problems are encountered with different fuels, and some fuels produce fewer deposits than others. The ash compositions of some typically combusted fuels are represented in Table 3.1. It must be noted that the values represented in the Table 3.1 are just nominal values, and the ash composition does not necessarily correspond with the composition of the deposits formed. The actual values may vary significantly, especially in the case of biomass and waste derived fuels. The ash composition of biomass fuels may vary with the habitat, fertilization and harvest time and method. Other factors affecting the ash formation chemistry and formation of deposits are flue gas composition, temperature and velocity and ash particle size, which depend on the combustion technique. (19)

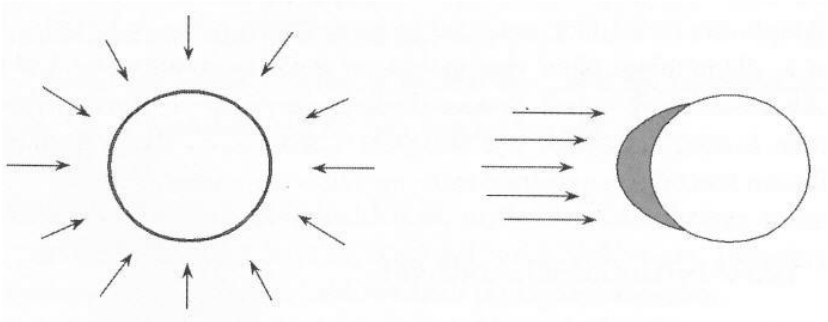

Figure 3.1. Migration of ash particles to the tube surfaces. Picture on the left (a) represents the diffusion process of small ash particles. Picture on the right (b) represents the impaction of larger particles to the heat exchanging surfaces. Arrows indicate the flow of fly ash particles. (19)

The formation of ash deposits require that the ash particles reach the heat exchanging surface and adhere to it. The ash particles may reach the metal surface by two different ways, depending on the particle size. Small particles (< 0,5 – 5 µm) reach the metal surface by diffusion, and form relatively uniform deposits regardless of flue gas flow direction, Figure 3.1(a). Larger particles (> 0,5 – 5 µm) reach the surface by impacting it. As a result, the deposits are formed on the flue gas entry-side, Figure 3.1(b). The adherence of ash particles takes place by sintering of a fluffy ash deposit or with partially molten ash phase. The sintering of a fluffy deposit can happen if time is allowed. It results from reactions of deposit with flue gases, and does not involve molten phase. Partially melted ash particles adhere very efficiently on the heat exchanging surface. Because the ash consists of variety of silicates, sulfates and chlorides of alkali, alkali earth and heavy metals, they may form eutectic compounds which have relatively low melting temperatures, even as low as under 500 °C. These types of ash deposits do not have a certain melting temperature, but the melting takes place on a wide temperature range, which in many cases is several hundreds of degrees Celsius. The critical parameter for determining the adherence of the ash is, according to (19), the temperature range where the ash particles are 15-70 % melted, also known as T_{15} and T_{70} temperatures. If ash particles are solid enough, they are rebounded back to flue gas flow when they reach the metal surface. On the other hand, if the ash particles are too molten they flow away from the surface and do not increase the thickness of the deposit. (19)

The corrosion caused by deposits may be hindered by selecting suitable materials for heat exchangers and keeping the heat exchanging surfaces clean by using sootblowers. The sootblowers may use pressurized air, water or steam from the boiler steam circulation in the cleaning process, or they may be based on mechanical or ultrasonic vibrations. If sootblowers are insufficient in keeping the heat exchanging surfaces clean, the formation of harmful ash components can be eliminated by, for example, choosing suitable fuel mixture or by introducing additives in the fuel. (1) (13)

3.3. Erosion

Erosion of heat exchanger surfaces may be a larger problem in fluidized bed type boilers, which have much higher solid concentration in furnace than other boiler types. Erosion is affected by three major factors: gas flow and environmental conditions, properties of erosive particles and nature of the eroding target material. The erosion process is explained in Figure 3.2. The process is similar to metal cutting: the eroding particle acts as a cutting tool. (15)

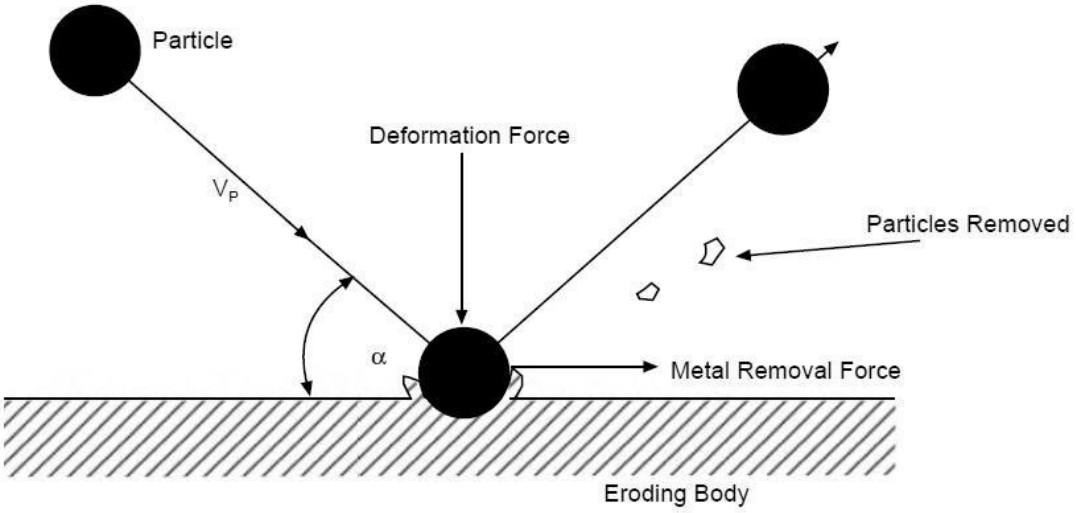

Figure 3.2. An eroding particle hits metal surface causing deformation and removes the deformed piece. (15)

The environmental factors affecting erosion rate are angle of impingement, α and the particle velocity or momentum v_p,. The angle of impingement is the most important factor influencing erosion. Erosion is minimal when the particle flow is parallel with eroding body surface, i.e. $\alpha = 0$. The maximum value is reached when the angle is 45°. Beyond this value the erosion decreases on ductile materials, reaching another minimum value at 90°. Brittle materials, e.g. refractory linings, behave differently than ductile steels. The erosion rate of brittle materials increases when the angle of impingement increases over 45°. The increasing particle velocity increases the erosion rate since the momentum of eroding particles increases. The particle properties affecting the erosion potential are hardness, abrasiveness and shape of the particle. Hard, more abrasive and angular particles erode the surface material more rapidly than soft and rounded particles. The denser particles have greater momentum, so the erosion rate increases when the eroding particles are denser. (15)

In CFB boilers, erosion is commonly detected on locations where the eroding particles are forced to change direction, resulting in a lateral change in momentum. Erosion of hemispherical butt welds of furnace waterwall tubes and the interface between the waterwall tubes and refractory lined lower furnace are locations where erosion is most commonly detected. The best way to avoid erosion is designing the boiler so that the solids flow is undisturbed, i.e. that the change in horizontal momentum

of the solids is avoided near the tube wall. Erosion is also detected on the superheater tubes located in the backpass. This occurs due to the impingement of small fly ash particles, which have passed through the solids separator. Often the erosiveness of ash is correlated to its quartz content. The size and shape of fly ash particles also affect to erosion rate. The erosion of the backpass tubes may be reduced by reducing the local flue gas velocity and leveling the gas flow across the boiler section in order to remove localized turbulent regions. Another method is to reduce the fly ash loading and to spread it out across the whole boiler section. (15)

4. SUPERHEATER MATERIALS

Superheaters and reheaters are exposed to highest temperature and pressure levels in boiler steam circulation systems. Therefore the proper material selection is very crucial. The most important criteria for material selection are high-temperature mechanical strength and creep resistance as well as corrosion and erosion resistance of material (1). The designed operating temperature has a great effect on the material selection since higher temperatures generally lower the creep strength of material and accelerate the corrosion processes on both the inner and outer surfaces of tubes. Because of relatively high steam-side heat transfer coefficient, the metal temperature in superheater loops is close to the steam temperature, and less dependent on the furnace temperature. According to Basu (15), the metal temperature T_{metal} in superheater and reheater tubes may be roughly approximated by the following equation:

$$T_{metal} = T_{steam} + 50\ ℃. \tag{4.1}$$

Sometimes the oxide scale formed on the steam-side can act as an insulator and thus reduce the heat transfer coefficient. In this case the metal temperatures may be locally much higher than expressed in equation (4.1), and superheater tubes may experience local overheating, which may cause accelerated corrosion and creep. (18)

Most common materials for superheater and reheater tubes are heat-resistant ferritic and ferritic/martensitic steels, which contain typically 2 – 13 wt-% chromium. When combusting regular fossil fuels, the temperature limit for steels containing 2-3% Cr is roughly 580 – 600 °C and for steels containing 10-13% Cr roughly 620 °C (23). If steam data is increased beyond this point, alloys with improved high temperature mechanical properties and corrosion resistance must be employed. In practice this means selecting alloys which have higher Cr content. This is when austenitic stainless steels and superalloys are considered. Austenitic stainless steels and iron- or nickel-based superalloys may be used, depending on the alloy composition, in temperatures up to 816 °C, which is the ASME Boiler and Pressure Vessel Code creep rupture base limit for these materials. Naturally, the alloys which have practical significance will have remarkably lower temperature limits, since alloys for extremely high temperatures will be extremely expensive. However, it is evident that low chromium steels are out of question when the superheater and reheater materials for advanced supercritical steam power plants are considered. (23)

The classification of steels to ferritic, martensitic, and austenitic and their variations is made based on their microstructure and alloying elements. The classification can be roughly done by calculating the chromium equivalent

$$Cr\,(eq) = Cr + 2Si + 1{,}5Mo + 5V + 5{,}5Al + 1{,}75\,Nb + 1{,}5\,Ti + 0{,}75W, \quad (4.2)$$

and nickel equivalent,

$$Ni(eq) = Ni + Co + 0{,}5Mn + 0{,}3Cu + 25N + 30C. \quad (4.3)$$

The alloying element contents in equations (4.2) and (4.3) are all expressed in weight percents. The alloying elements in Cr(eq) stabilize the ferritic microstructure, and the elements in Ni(eq) favor the austenitic phase. The alloy microstructure at room temperature may be evaluated by comparing the values of Cr(eq) and Ni(eq) to Schaeffler diagram, Figure 4.1. The Schaeffler diagram is very useful indetermining the microstructure of the weld seam and possible tendencies for undesired phase transformations, embrittlement or cracking developed in the weld seam. (24) (25)

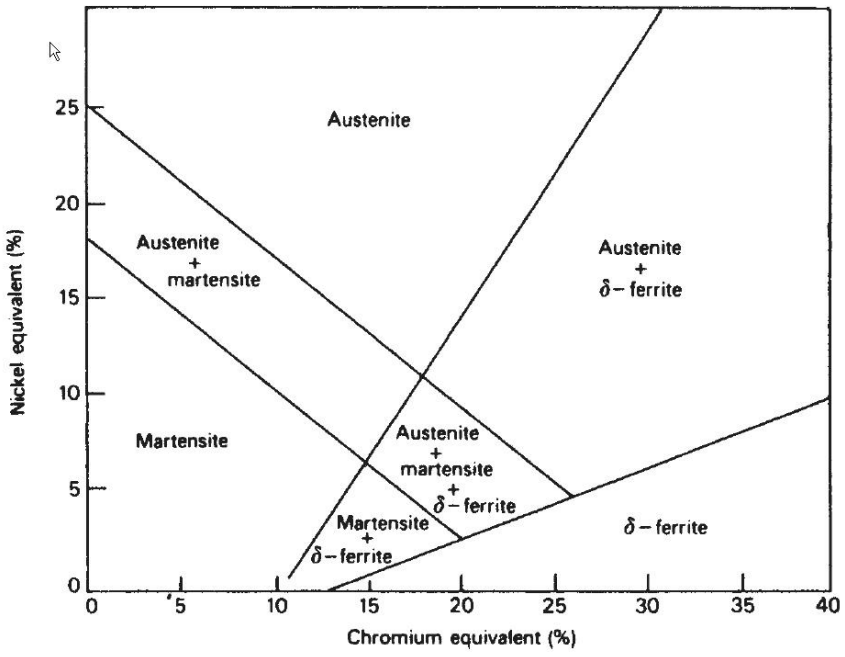

Figure 4.1. Schaeffler diagram. Effect of chromium and nickel equivalents on the basic structure of chromium containing steels. (25)

Corrosion resistance is improved by alloying the steel with elements which are able to form protective oxide layers on the steel surface. There are not many metals which can form protective oxide layers at elevated temperatures. While many metal oxides may be stable at elevated temperatures, their growth rates are too high, and therefore are not sufficiently dense and adherent to protect the alloy underneath. There are only three known oxides, which are protective at high temperature, and can be

grown on commercial metal alloys. These are chromia (Cr_2O_3), alumina (Al_2O_3) and silica (SiO_2). There is a minimum proportion for each of these alloying elements required to form a scale of the desired oxide. Additionally, the effect of these alloying elements must be considered in the light of desired physical and mechanical properties of the alloy too. The effect of alloying elements on the steam-side oxidation behavior of material is discussed more thoroughly in section5.5.5. (26)

Superheater and reheater sections of steam boilers are manufactured of seamless tubes. The tubes are first butt welded to provide desired tube length and then bent according to heat-exchanger panel design. The quality of the weld seams must fulfill the demands set by standards, so the selection of welding consumables and welding process must be made very carefully and according to standards and regulations. Some materials require post weld heat treatment (PWHT) in order to relief residual stresses and to provide tempering action on the microstructure produced by thermal cycles during the welding process. Sometimes NDT (nondestructive testing) monitoring must be used to confirm the quality of the weld seam. The bending is arranged so that the weld seam is not at the section which experiences the greatest deformation in the bending process. All of these matters must be considered during material selection process for superheaters and reheaters. (24)

4.1. Ferritic steels

Ferritic steels have body-centered cubic (BCC) microstructure. Heat-resistant ferritic steels are preferred as superheater material mainly because of their relatively low price. The most important alloying elements for these types of steels are molybdenum and chromium. Molybdenum improves the creep strength even in relatively small amounts of 0,5 – 1 wt-% (1). Chromium enhances the corrosion resistance, and has some beneficial effect on creep strength too. Additionally, ferritic steels have better heat transfer coefficient and smaller coefficient for thermal expansion when compared to austenitic steels. This makes the ferritic steels a good choice in applications where thermal cycling is present, e.g. when the boiler load is varied. While combusting fossil fuels, ferritic steels have limited resistance against corrosion and oxidation when steam temperature is raised above 600 °C mostly because of their insufficient chromium content. Corrosion and oxidation rates become unacceptably rapid even for higher-chromium (10-13 wt-%) ferritic steels roughly at 620 °C, so other materials than ferritic steels must be used in final superheaters and reheaters when the steam temperature at the superheater outlet is raised. When more challenging fuels, e.g. biomasses of various types, are combusted, the maximum operating temperatures are considerably lower due to increased risk for corrosion. The ferritic steel grades 91 (X10CrMoVNb9-1) (27) and 92 (X10CrWMoVNb9-2) (28) were developed for high-temperature steam tubes in the 1970s and 1990s, respectively. These steels offer improved high-temperature mechanical strength and creep resistance, but their corrosion and oxidation rates are similar to traditional ferritic steels that contain 9 wt-% chromium. The maximum steam

parameters recommended by the manufacturer (Vallourec & Mannesmann) for grades 91 and 92 are 560 °C and 600 °C respectively. The 12 wt-% chromium containing steel T122 is a duplex ferritic-martensitic steel, which has similar mechanical strength properties than T92, with slightly increased steam-side oxidation resistance due to higher Cr content. Some advanced ferritic superheater steels and their chemical compositions are introduced in Table 4.1. (23) (29) (30)

Table 4.1. Selected high-chromium ferritic steel grades and their nominal chemical compositions. (30)

Steel grade	Chemical composition, wt-%										
	C	Si	Mn	Cr	Mo	W	V	Nb	B	N	Other
T91	0,1	0,4	0,45	9	1	-	0,2	0,08	-	0,05	
T92	0,07	0,03	0,45	9	0,5	1,8	0,2	0,05	0,004	0,06	
T122	0,11	0,1	0,6	12	0,4	2	0,2	0,05	0,003	0,03	Cu 1

4.2. Austenitic stainless steels

Austenitic stainless steels, often referred to as 300-series stainless steels, are highly alloyed steels with austenitic, face-centered cubic (FCC) microstructure, which provides good high-temperature mechanical properties by high phase stability and good formability. The main alloying elements are chromium and nickel. Chromium provides good corrosion resistance properties, and nickel stabilizes the austenitic phase. Nickel can be replaced by manganese, which is another element that can stabilize the austenitic phase. It is roughly half as effective as nickel, but it is used because of it's low price compared to nickel. Most familiar austenitic stainless steels are 18-10 and 18-8 steels, which contain nominally 18 wt-% Cr and 8-10 wt-% Ni. Examples of this type of steels are TP304H, Super304H, Tempaloy A-1, TP347H and TP347HFG. These steels have the minimum composition of alloying elements which is required to maintain an austenitic microstructure at room temperature. If the temperature is lowered, the microstructure of these steels will transform substantially to martensite. TP304H and TP347H are widely used instead of T91 in superheater applications. More advanced austenitic steels Super304H, Tempaloy A-1 and TP347HFG are developed based on the conservative 18-8 austenitic steels by minor alloying element additions and/or heat treatments. With proper additions of Nb and Ti the austenitic steel may be stabilized against intergranular corrosion (sensitization). Addition of copper and employment of proper heat treatment increases precipitation strengthening by fine precipitation of Cu-rich phase. When higher chromium content is required for better corrosion resistance, more nickel or manganese is needed to stabilize the austenitic phase, Figure 4.1. HR3C, Tempaloy A-3 and NF709 are examples of alloys with higher Cr content. These steels are especially developed for advanced steam boiler applications. High price due to high Ni content limits the usability of these steels. Some austenitic stainless steels used in

superheaters and reheaters and their chemical compositions are introduced inTable 4.2. (25) (29) (30)

Table 4.2. Some austenitic steel grades used for boiler applications and their nominal chemical compositions. (30)

Steel grade	Chemical composition, wt-%								
	C	Si	Mn	Ni	Cr	Mo	Nb	Ti	Other
TP304H	0,08	0,6	1,6	8	18	-	-	-	
Super304H	0,1	0,2	0,8	9	18	-	0,4		Cu 3 N 0,1
Tempaloy A-1	0,12	0,6	1,6	10	18	-	0,1	0,08	
TP347H TP347HFG(1	0,08	0,6	1,6	10	18	-	0,8	-	
HR3C	0,06	0,4	1,2	20	25	-	0,45	-	N 0,2
Tempaloy A-3	0,05	0,4	1,5	15	22	-	0,7	-	B 0,002 N 0,15
NF709	0,15	0,5	1	25	20	1,5	0,2	0,1	

1) TP347HFG is a fine grained version of TP347H

Austenitic steels usually possess good high-temperature strength and creep resistance due to austenitic microstructure, and good corrosion resistance due to high chromium content. Maximum creep-based operating metal temperatures are up to 675 °C (18). Austenitic steels are nonmagnetic, and they can be hardened only by cold working. Because of their good high-temperature properties they are good materials for final superheaters and reheaters when steam temperature is raised above the maximum operating temperature of ferritic steels. On the downside, austenitic steels have higher thermal expansion coefficient and lower thermal conductivity than ferritic steels. This must be taken into account in the design of superheaters and reheaters, when the alloy class is changed. When the boiler is constructed of materials which have differencet thermal expansion coefficients, thermal stresses will be imposed in the boiler structure when the temperature varies i.e. boiler load is varied. Due to lower thermal conductivity the heat exchanger surfaces must be designed larger. Austenitic stainless steels are more expensive than ferritic steels mostly because of their high nickel content. On the other hand, the excess cost may be contained as the material consumption may decrease when ferritic steel is switched to austenitic stainless steel because the wall-thickness may be decreased due to better high-temperature strength and creep resistance of austenitics. (29)

Austenitic stainless steels are susceptible to sensitization when they are cooled slowly after welding or when reheating within the temperature range of approximately 550 – 800 °C. This is because the austenitic microstructure is supersaturated with carbon in room temperature. When the temperature is raised, the carbon will be rejected

from the solution, usually as a chromium rich carbide. Sensitization is a mode of intergranular corrosion. It is a consequence of precipitation of chromium carbides $Cr_{23}C_6$ in the grain boundaries at the above mentioned temperature range. If the chromium carbides precipitate in the grain boundaries, the areas near the grain boundaries become depleted from chromium. As a consequence the grain boundaries become suspectible to corrosion. The sensitization effect can be prevented by lowering the carbon content of steel or stabilizing the steel with elements which form more stable carbides than chromium carbide, such as niobium and titanium. Carbon is then bound with other carbide formers forming e.g. TiC and NbC, and less carbon remains dissolved in the metallic matrix. If there is less carbon available in the matrix, the formation of chromium carbides in the grain boundaries is limited, and thus sensitization does not occur. Most austenitic steels which are used in superheater tubing contain niobium and/or titanium. (20) (25) (29)

4.3. Superalloys

Superalloys that may be used in superheaters and reheaters are iron- or nickel-based alloys. They could be used when the corrosion resistance and high-temperature strength of austenitic stainless steels is inadequate. Iron-based superalloys are developed from high-alloyed austenitic stainless steels, so their main alloying elements are nickel and chromium, and they have austenitic, FCC microstructure. Nickel-based superalloys are advanced heat-resistant materials, which are usually based on nickel-chromium system.. The microstructure of nickel-based superalloys is also FCC. Chromium is used to improve oxidation resistance. Typical chromium contents are 15 wt-% and above. Sometimes also aluminum is used to improve the oxidation resistance, but it is not as efficient as chromium in sulfidizing conditions. Usually the nickel-based alloys that may be used in superheaters and reheaters contain iron, molybdenum and cobalt besides of nickel and chromium. Iron reduces the susceptibility of nickel to internal oxidation. Cobalt and molybdenum improve the mechanical properties of alloys. Some of the superalloys used in boiler tubing and their chemical compositions are represented in Table 4.3. (29) (30) (31)

Table 4.3. Selected nickel- and iron-based superalloys for boiler applications and their nominal chemical compositions. (30)

Alloy	Chemical composition, wt-%										
	Ni	Cr	Mo	Co	Fe	Mn	Si	C	Al	Ti	Other
INCO740	48	25	0,5	20	0,7	0,3	0,5	0,06	0,9	2	Nb 2,0
HR230	Bal	22	2	5	3	-	0,4	0,1	0,3	-	W 14 La 0,2
IN625	61	21,5	9	-	2,5	0,2	0,2	0,05	0,2	0,2	Nb 3,6
IN617	54	22	9	12,5	-	-	-	0,07	1	-	
HR6W	43	23	-	-	Bal	1,2	0,4	0,008		0,08	B 0,003
CR30A	50	30	2	-	Bal	0,2	0,3	0,06		0,2	Zr 0,03
800HT	30/35	19/23	-	-	40	1,5	1	0,08	0,5	0,5	
HR120	37	25	2,5	3	33	0,7	0,6	0,05	0,1	-	N 0,2 W 2,5 Nb 0,7

High-Ni superalloys are also susceptible to sensitization. Same methods can be used to contain sensitization, i.e. reducing the carbon content or adding alloying elements that stabilize the carbides. Molybdenum and tungsten are considered to be the two most deleterious solutes in terms of hot corrosion resistance. Some Ni-Cr alloys containing molybdenum have experienced catastrophic oxidation at 900 °C static air, probably due to formation of liquid MoO_3 which melts at 801 °C and is able to form relatively low-melting eutectics with several oxides. Tungsten additions have been observed to induce some scale breakdown on Ni-Cr alloys. Still, one or both of these elements are required to provide sufficient mechanical strength. (29) (31) (32)

4.4. Composite tubes

Composite tubes are tubes which are manufactured from two or more separate materials. Tubes may be manufactured by weld overlaying or co-extruding the tube from billet which consists of two different materials. By using composite tubes it is possible to select the best performing material for both surfaces of the heat exchanger. Because the requirements set by conditions in the steam-side and fire-side of the heat exchanging surfaces are different, the material selection is made based on the most demanding condition. Additionally, the material must have sufficient high-temperature mechanical strength and creep resistance too. Thus, the material selection is always compromising on fulfilling the requirements set by the operating conditions. For example, the material may have outstanding corrosion resistance, but the strength is in sufficient, or vice versa. Usually the fire-side of the boiler is the more demanding environment, especially when biomass or waste derived fuels are combusted. The fire-side corrosion resistance can be improved by cladding the tubes with corrosion resistant weld overlay. The base material must have sufficient resistance to steam-side oxidation and sufficient high-temperature strength.

5. STEAM-SIDE OXIDATION

The oxidation behavior of superheater materials in steam may become the limiting factor in material selection. When the steam temperature is increased, oxide films grow more quickly, leading to three potential concerns. First, the wall loss of the tubes caused by oxidation may increase the stress in tube walls and cause creep ruptures. Second, the oxide layer may act as an insulating layer because of lower thermal conductivity. This may lead to local overheating of a superheater tube. The third concern is the spallation of the oxide scale. Usually the thicker oxide scales spall more easily, especially when the boiler is cooled down and restarted. This is due to differences in coefficients of thermal expansion between the oxide and base metal. The spalled oxide particles may lodge somewhere in the steam circle, particularly in tube bends, and cause reduced flow or even tube blockages. The spalled particles may also enter the steam turbine with steam flow. This causes erosion damage to turbine components which are in touch with steam. Overheating due to thick oxide scales or tube blockages and solid particle erosion (SPE) caused by spalled oxide particles have been reported for nearly 30 years, so the problem is recognized. Viswanathan et al. (18) have suggested that overheating failures due to flow restriction caused by exfoliated oxide scale is the second most important cause for boiler tube failures and reduced plant availability worldwide. (18)

Due to global climate issues there are demands on increasing boiler efficiencies in order to produce same amount of energy with less fuel, i.e. lower emissions. This is done by increasing the steam temperature and pressure, so the steam-side oxidation becomes more important issue when selecting boiler materials. Besides the general trend toward higher steam parameters, the extended running of steam boiler near to full load, longer periods between scheduled maintenances and plant cycling may lead to increase of steam-side oxide scale thicknesses. (18)

5.1. Oxidation mechanisms and thermodynamics

Metal surface will always oxidize when it is exposed to an environment which contains oxygen. Oxidation of pure, divalent metal may be expressed by the following equation:

$$M(s) + \frac{1}{2}\, O_2(g) \rightarrow MO(s), \qquad (5.1)$$

where M represents metal atom. Equation (5.1) may be further divided to oxidation and reduction step reactions. Oxidation reaction,

$$M \rightarrow M^{2+} + 2\, e^{-}, \qquad (5.2)$$

produces metal ions and takes place at the scale-gas interface. The reduction step reaction,

$$\frac{1}{2}\, O_2 + 2\, e^- \rightarrow O^{2-}, \qquad (5.3)$$

takes place on the scale-gas interface, and it produces oxygen ions. Figure 5.1 represents schematically metal-scale-gas system and oxidation and reduction step reactions. (33)

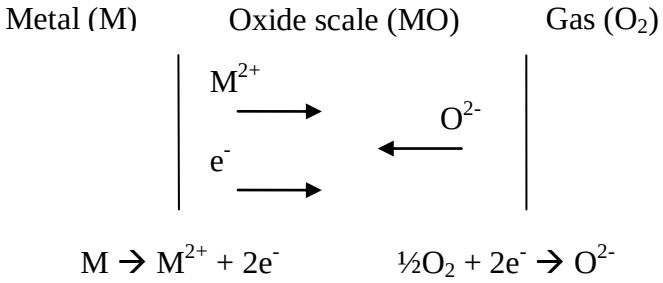

Figure 5.1. Schematic representation of the metal-scale-gas system. Adapted from (33).

The initial stage of oxidation reaction may be rapid, but the rate will slow down when the metal surface is separated from the gas phase by oxide layer. As can be seen from the Figure 5.1, one or both of the reactants must be able to penetrate the oxide scale in order for the reaction to proceed further. This means that the oxide layer may grow outwards or inwards. If the scale grows outwards, metal ions are migrated through the oxide scale to the scale-gas interface. When oxygen ions are migrated to metal-scale interface, the scale grows inwards (internal oxidation). These oxidation mechanisms are called cation mobile and anion mobile, respectively, and are presented in Figure 5.2. (32)

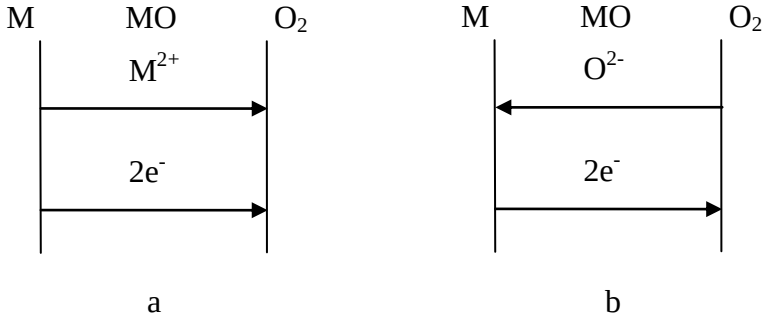

Figure 5.2. Possible ion transfer mechanisms on high temperature oxidation. Cation mobile (a) and anion mobile (b). (32).

If the oxide layer grown on metal surface is thermodynamically stable, solid and forms continuous, complete and dense layer along the surface, it can protect the metal against further corrosion and oxidation. Protective layers must also be good insulators, because oxidation reactions involve transfer of electrons through the oxide scale, as can be seen from reactions (5.2) and (5.3). Additionally, the ionic and crystallographic

structure of the oxide determines the diffusion rate of the reacting species. Diffusion rate affects greatly on the protectiveness of the oxide layer: lower diffusion rates mean lower oxide growth rates and thus better oxide scale adherence and protection against corrosion or further oxidation. (32)

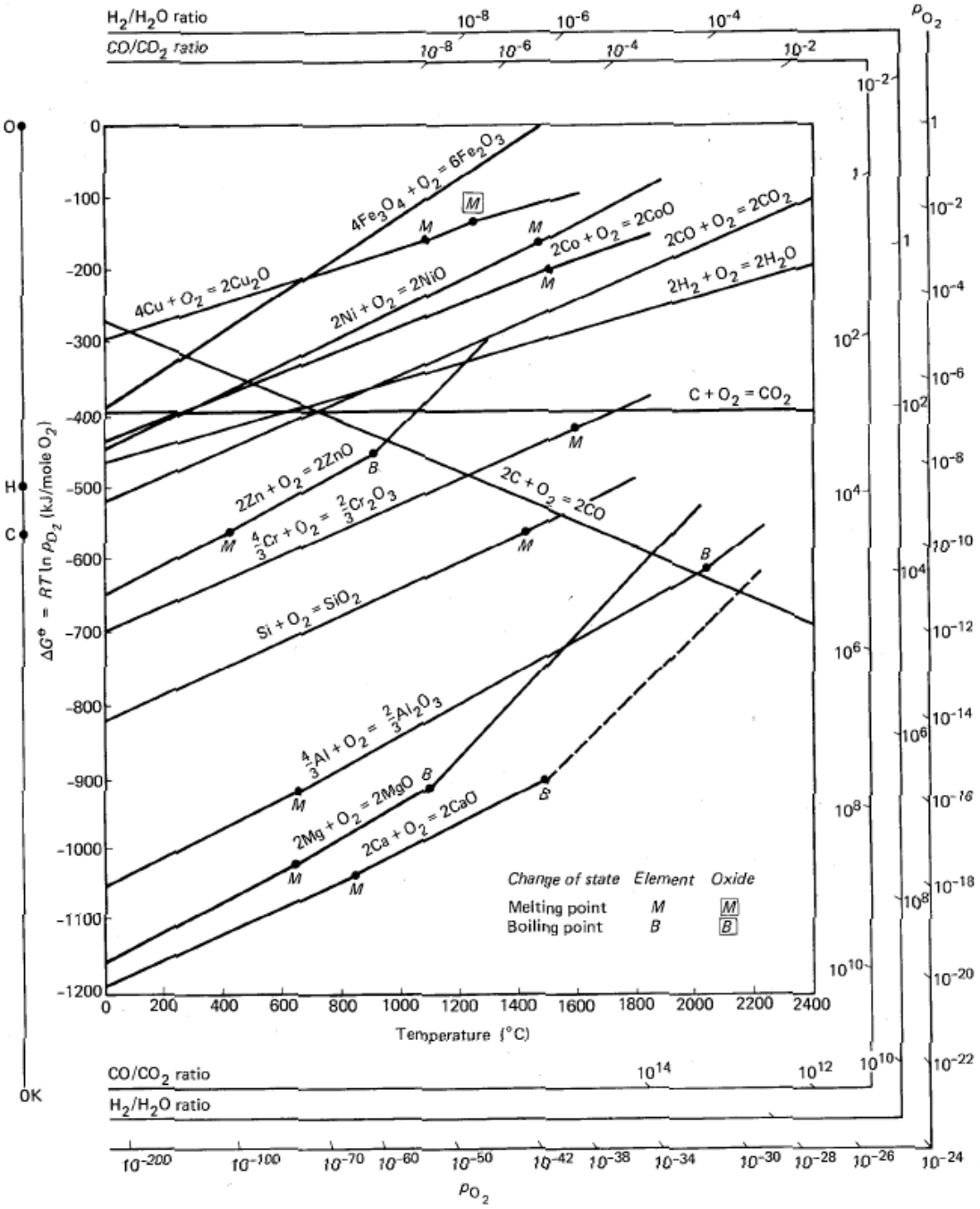

Figure 5.3. Standard free energy of formation of selected oxides as a function of temperature. (32)

The thermodynamic stability of various metallic oxides may be approximated by using Ellingham diagram, Figure 5.3. The Ellingham diagram plots the change in standard free energy as a function of temperature. The values in Figure 5.3 are expressed in kilojoule per mole O_2, so the stabilities of various oxides can be compared

directly: the lower the position of the line on the diagram, the more stable the oxide is. (32)

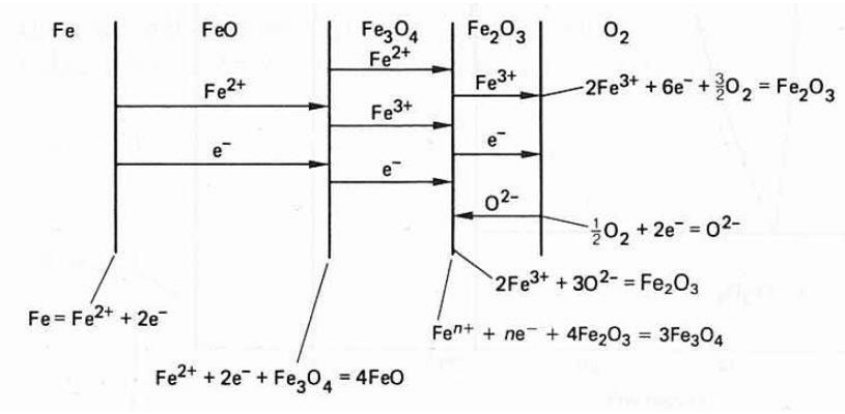

Figure 5.4. Oxidation mechanisms for pure iron to form a three-layered scale at temperatures above 570 °C. Diffusion steps and interfacial reactions are also included. (32)

Iron has three different oxides, which are magnetite (Fe_3O_4), hematite (Fe_2O_3) and wüstite (FeO). The layer morphology presented in Figure 5.4 is valid only for pure iron at temperatures over 570 °C, because FeO is not formed in temperatures below 570 °C. This temperature is somewhat critical temperature for oxidation of pure iron, because wüstite has actually non-stoichiometric composition varying between $Fe_{0,95}O$ and $Fe_{0,85}O$. High cation vacancy concentration makes the mobility of cations and electrons extremely high, and thus the wüstite scale will grow fast and does not offer protection against oxidation. Oxidation mechanisms of steels are more complicated, because the oxidation of alloying elements must be taken into account too. After Birks & Meier (32), alloy oxidation is much more complex as a result of some, or all, of the following factors:

- Metals in the alloy will have different affinities for oxygen reflected by the different free energies of formation of the oxides.
- Ternary and higher oxides are formed.
- A degree of solid solubility between the oxides may exist.
- The various metal ions will have different mobilities in the oxide phases.
- The various metals will have different diffusivities in the alloy.
- Dissolution of oxygen into the alloy may result in sub-surface precipitation of oxides of one or more alloying elements (internal oxidation).

As a consequence, the composition of oxide layer formed on a metal alloy may differ greatly from the alloy composition: oxides of all alloying elements are not necessarily found from the oxide scale. Usually some of the oxides becomes dominant, even when it’s composition in the alloy is relatively low. (20) (32)

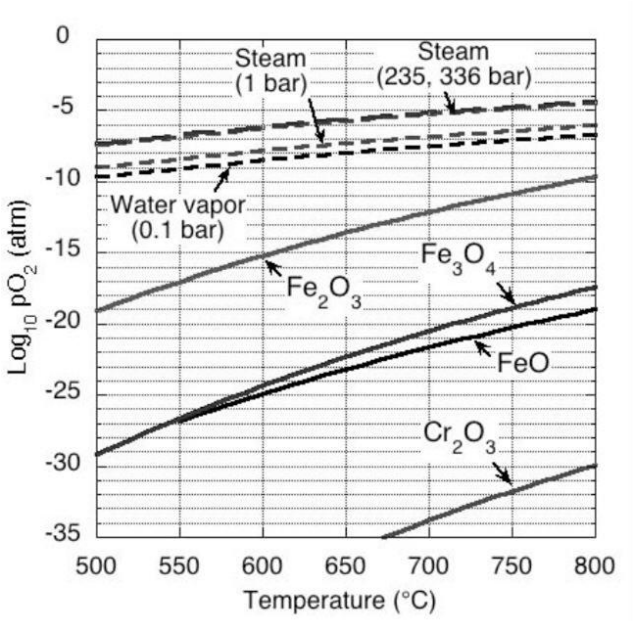

Figure 5.5. Effective oxygen partial pressures in steam under three different pressure conditions and the stability of some metal oxides as a function of dissociation oxygen partial pressure. (26)

The stabilities of different oxides depend on their standard Gibbs free energies of formation (ΔG^0_{MO}), oxygen partial pressure (pO_2) and temperature. It is possible to evaluate the stabilities of different oxides in different atmospheres by calculating the oxygen partial pressure where the oxide dissociates, i.e. equation 5.1 proceeds from right to left. If the oxygen partial pressure in atmosphere is greater than dissociation oxygen partial pressure, the oxide is thermodynamically stable. Dissociation oxygen partial pressure $(pO_2)_{dissoc}$ for the oxide MO is calculated by equation

$$\log(pO_2)_{dissoc} = 2\Delta G^0_{MO} / (2{,}303RT) \qquad (5.4)$$

where ΔG^0_{MO} is the standard Gibbs free energy of formation for oxide MO, R is the universal gas constant and T is the absolute temperature. Dissociation oxygen partial pressures for chromium and iron oxides are plotted in Figure 5.5 together with oxygen partial pressures of steam in different pressures. It is assumed that steam is pure, i.e. all of the oxygen is generated by dissociation of steam via:

$$H_2O(g) \rightarrow H_2(g) + 1/2O_2(g) \qquad (5.5)$$

Lower value of $(pO_2)_{dissoc}$ means more stable oxide. Figure 5.5 indicates that all oxides are stable in supercritical steam, and the most stable oxide is chromium oxide. It must be noted that thermodynamics do not take into account kinetics of the oxidation reaction, so a high stability does not necessarily mean good protection against oxidation. A good example of this is wüstite, which appears to be the most stable oxide of iron, but

it does not offer protection against oxidation because the formation reaction of wüstite is too fast. (26) (20)

Because alloys that contain chromium have a big role in modern boilers with advanced steam data, oxidation theory of iron-chromium and nickel-chromium alloys are discussed here briefly. The high temperature oxidation resistance of these alloys is based on the formation of stable chromium-rich oxide film on the alloy surface. This oxide is slowly growing and stable, and it prevents oxidation of the parent material. Both alloy systems experience selective oxidation of chromium, if the alloy chromium content and the diffusivity of chromium to the oxidation front are sufficient. The critical chromium content is approximately 20wt-% for iron-based alloys and approximately 10wt-% for nickel-based alloys. If the chromium content is lower than the critical value, the outer layer consists of base metal oxides, i.e. Fe_2O_3 or NiO and the chromium will oxidize by internal oxidation, illustrated in Figure 5.2(b). Oxygen dissolves either at the external surface of the specimen or at the alloy-scale interface and diffuses inward through the metal matrix, so the chromium oxide is formed inside the metal matrix. The outer oxide layer grows simultaneously by rate which is controlled by outward diffusion of base metal ions, e.g. Fe and Ni ions. This outward diffusion is hindered by Cr_2O_3, which may be detected as precipitates in the metallic matrix or in solid solutions with base metal oxides, i.e. $FeCr_2O_4$ or $NiCr_2O_4$. The amount of Cr_2O_3 precipitates and/or solid solutions increases as the chromium content of the alloy is increased. In iron-based alloys, a scale of mixed spinel $Fe(Fe,Cr)_2O_4$ is produced when the alloy chromium content is increased. This is somewhat protective scale, as the oxidation rates are noticed to be lower when the spinel layer is formed. However, it does not offer protection equal to continuous Cr_2O_3 scale. Nickel-based alloys designed against high-temperature oxidation usually contain excess amount of chromium, so usually a continuous Cr_2O_3 is formed. Meanwhile, for chromium containing steels the internal oxidation is remarkable. Critical Cr-content for steels is approximately 20 wt-%, so a variety of oxide scale morphologies are detected on steels exposed to steam. (32)

A chromium containing alloy experiences transition from internal to external oxidation when the chromium content exceeds certain boundary value. Critical mole fraction (N_{Bcrit}) for alloy AB where, for example, A = Fe and B = Cr may be approximated by:

$$N_{Bcrit} = V(\pi k_p / D_B)^{0,5} / Z_B M_O, \qquad (5.6)$$

where V is the molar volume of the alloy, k_p is the parabolic rate constant for exclusive formation of BO (i.e. Cr_2O_3), D_B is the interdiffusion coefficient of B in alloy, Z_B is the valence of B atoms and M_O is the atomic weight of oxygen. Birks & Meier (32) have expressed equation (5.6) in the form where the effects of changing exposure conditions may be assessed:

$$N_B^{(0)} > \left(\frac{\pi g^*}{2Z_B} N_O^{(S)} \frac{D_O V_m}{D_B V_{ox}}\right), \quad (5.7)$$

where $N_B^{(0)}$ is the initial concentration of B, g^* is the critical volume fraction of oxide for transition from internal to external oxidation corresponding to N_{Bcrit}, $N_O^{(S)}$ is the oxygen solubility in A, D_O is the diffusivity of oxygen in A and V_m and V_{ox} are the molar volumes of metal A and oxide BO, respectively. It can be seen from equation (5.7) that variables promoting the formation of external, more protective scale (i.e. factors that decrease the initial concentration of B required), are improved outward diffusivity of B and decreased inward diffusivity of oxygen and oxygen solubility in A. The diffusivity of chromium may be improved by cold working the alloy surface or decreasing the alloy grain size (34) (35) (36). Oxygen diffusivity and solubility may be decreased by lowering the pO_2 in the atmosphere or by certain alloying elements, see section 5.5.5. (26) (32)

5.2. Steam quality and pressure

The quality of steam flowing in the steam boiler is directly determined by the quality of water circulating in the boiler tubes. The water supplied to the boiler inlet, i.e. feed water, consists of returned condensate water and make-up water, which is supplied to compensate the losses of water and steam in the system. Since feed water is usually taken from natural water resources, it is highly important to control the water quality and apply appropriate water treating processes. The quality of boiler feed water is controlled by European standard EN-12952-12. The requirements set by the European standard are different for natural or assisted circulation boilers and for once-through boilers. The standard defines the allowable levels for dissolved solids and certain physical and chemical properties which the feed water must fulfill. It also defines the allowable chemical agents used for feed water conditioning and their optimum levels. The conditioning agents can contribute to supporting the formation of protective oxide layer, stabilizing the protective layer and minimizing the corrosion by optimizing pH value. The optimum pH value of feed water is slightly alkali, pH > 9,2 for natural or assisted circulation and 7-10 for once-through boilers, because the magnetite layer formed on the tube wall will be destroyed in acidic solution. On the other hand, when the pH is increased, the risk to stress corrosion increases. The pH level is usually controlled by additions of ammonia. (26) (37) (38)

The following substances are known to be most problematic to steam boilers and turbines: calcium, magnesium, silica (SiO_2), sodium, chlorides of calcium, magnesium and sodium, iron, oil, oxygen and carbon dioxide. Substances Ca, Mg, SiO_2 and oil may form deposits and scales on the tube wall surface or turbine components. These scales may act as an insulating layer and increase the tube metal temperature, or reduce the steam flow in turbine so that its energy output is decreased. Sodium may form NaOH, which may cause stress-corrosion cracking to occur. Chlorides are usually found from

deposits formed in steam turbine, as it has a very good solubility in steam. Chlorides may cause corrosion on 300 series stainless steels and pitting on 12-Cr steels. Iron found from feed water originates from boiler tubes, as the magnetite layer is exfoliated. Iron particles cause solid particle erosion (SPE) of turbine blades and steam tubes and pipes. Oxygen and carbon dioxide can accelerate the corrosion process. Increasing oxygen content in steam means higher oxygen content available for oxidation reaction (5.1) and thus more rapid oxidation process. The dissolved oxygen is limited to 0,02 mg/l in boilers with natural or assisted steam circulation and to 0,25 mg/l in once-through boilers. These are the limits suggested by European standard. The turbine supplier may require considerably lower values of dissolved oxygen. The carbon dioxide may react with water to form carbonic acid (H_2CO_3), which will cause corrosion in steam and return lines. (39)

Water treatment methods for removing impurities include softening, demineralization, decarburization and filtration. Oxygen and other gases are removed by deaeration and oxygen scavenging. Hydrazine N_2H_4 is commonly used oxygen scavenger. It is applicable since it meets all high pressure chemistry requirements, because it does not decompose into troublesome by-products. Hydrazine is a reducing agent, which may affect to oxygen stabilities in steam, Figure 5.5. It may transfer the oxygen partial pressure in steam to the extent where haematite is unstable and magnetite becomes the most stable iron oxide. (26) (38)

According to Viswanathan et al. (18) the steam pressure seems to have only little effect to oxidation kinetics in subcritical region. It has been suggested that the oxidation rate for ferritic steels is proportional to $P^{1/5}$. This relationship has been derived from different oxide scale thicknesses developed on superheater and reheater, as the scales developed on superheater tubes were 45% thicker than scales developed on reheater tubes. The steam temperature was the same, but the steam pressure on reheater tube was lower. The reason for this pressure effect was speculated to be differences in oxygen partial pressures. In conclusion, the steam pressure seems to have smaller effect on the rate of oxidation process than steam temperature. (18)

5.3. Oxidation kinetics

Whether the oxidation takes place on the scale-gas interface or metal-scale interface, ion diffusion through the oxide scale is a very important rate controlling factor. If the oxide layer acts as a diffusion barrier for oxygen or metal ions or as an insulating layer, the rate of oxidation slows down when the oxide scale becomes thicker. That is, of course, if the oxide layer is presumed to be compact and adherent. In this case, the oxidation rate can be described by a *parabolic* relationship,

$$W^2 = 2k_p t, \tag{5.8}$$

where W is weight gain per unit area, t is time and k_p is the parabolic rate constant, which is a time-independent constant at a given temperature. Equation (5.8) represents an idealized case, because the protective scale is assumed to grow by parabolic rate from the beginning of the exposure. In practice, when a "fresh" metal surface is exposed to oxygen atmosphere, there is always an initial stage where the overall oxidation rate is usually much faster. This initial oxidation stage is also called transient oxidation stage, and it is usually very short. During transient oxidation stage the oxide layer starts to form and becomes continuous and protective, so after initial stage the oxidation rate will become controlled by diffusion through the completed oxide layer. If this transient oxidation were taken into account, a constant, off-setting parameter should be added to equation (5.8). Usually the effect of transient oxidation is ignored for simplicity because it has only little practical purpose. This leads to fact that the calculated oxide scale thicknesses or mass gains have always slightly lower values than actual values. (33) (26)

If the oxide scale does not prevent diffusion, the oxidation rate follows *linear* relationship,

$$W = k_l t, \tag{5.9}$$

where k_l is the linear rate constant. The third possible relationship is *logarithmic*, but it will not be discussed here since it is only detected on very thin oxide layers which form at relatively low temperatures. Figure 5.6 illustrates the above mentioned oxidation rate expressions. Oxidation rate may also be expressed in the form of scale thickness instead of weight gain per unit area. Scale thickness can be calculated mathematically, assuming that the oxide layer is homogenous and compact. Another method is to section the sample and measure scale thickness from the cross-section. (33)

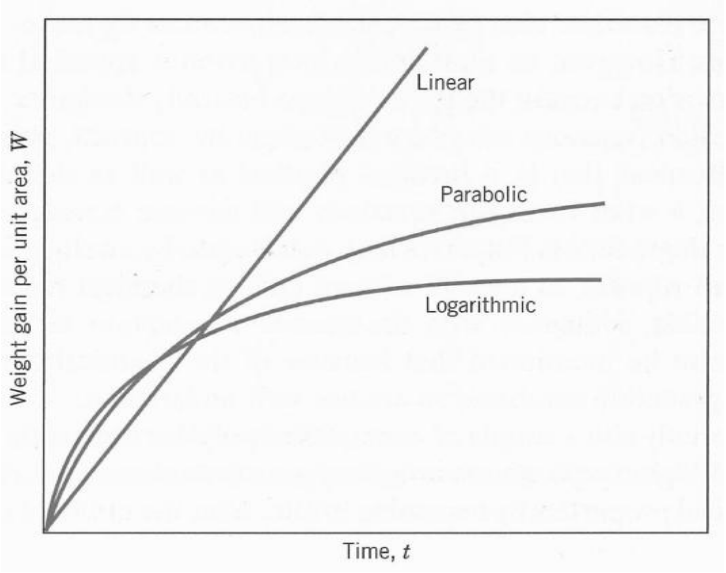

Figure 5.6. Oxide scale growth curves as a function of time for linear, parabolic and logarithmic rate laws. (33)

In oxidation studies reviewed by Viswanathan et al. (18) it was noticed that the oxidation rate in steam actually follows exponential rate law, where the rate exponent varies from 1/2 to 1/3. In other words, the oxidation kinetics fall between *parabolic* (n = 2) and *cubic* (n = 3) relationships. The exponential rate law is expressed by equation

$$W^n = k\,t, \tag{5.10}$$

where W is weight gain per unit area, k is proportionality coefficient and n is the rate exponent. However, many studies which Viswanathan et al. (18) have reviewed use the parabolic expression, so it is reasonable to assume that it describes oxidation kinetics with adequate accuracy.

The oxidation kinetics will follow parabolic relationship if the scale grown on the alloy surface is protective. This is usually expected to occur on superheater tubing, so if the oxide scale comes partially loose, the regrowth rate of new oxide layer depends on the thickness of the remaining oxide scale. However, the oxidation kinetics may change from parabolic towards linear when steam data is improved or alloy composition changes, e.g. alloy becomes partially depleted from chromium. It has been noticed that the oxidation kinetics observed on ferritic steels may vary as a function of alloy chromium content and exposure temperature. This trend is showed in Figure 5.7. Austenitic alloys are expected to follow parabolic kinetics, but if the alloy becomes locally depleted from chromium or the temperature is increased, linear kinetics may be observed on austenitic Fe-Cr-Ni alloys too. (18)

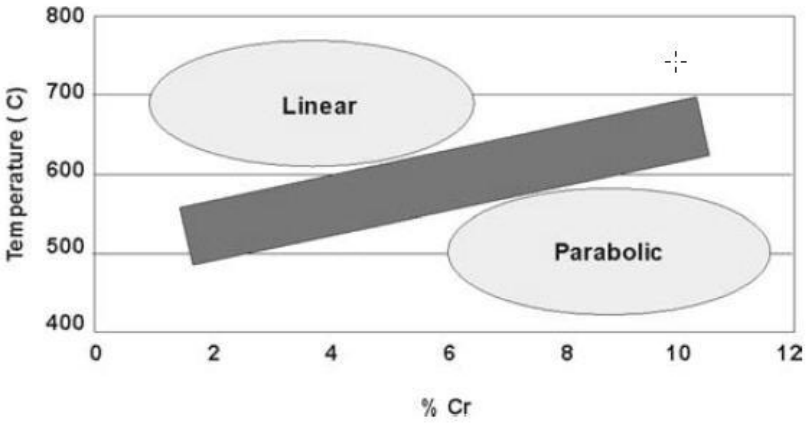

Figure 5.7. General trend of oxidation kinetics observed on ferritic steels as a function of chromium content and temperature. (18)

All rate constants from above mentioned equations (5.8, 5.9 and 5.10) are dependent on temperature. The rate constant k may be calculated by Arrhenius equation:

$$k = A\,e^{-Q/RT} \tag{5.11}$$

where A is the Arrhenius constant, Q is the activation energy for the rate controlling process, R is the universal gas constant and T is the absolute (metal) temperature. The activation energy does not vary with temperature, so it is considered to be an important constant value when determining the oxidation kinetics of an alloy. Now equation (5.10) becomes

$$W^n = A\, e^{-Q/RT} t \qquad (5.12)$$

Equation (5.12) is used when determining the activation energy for oxidation from measured data. Measured data must include weight gain per unit area (or oxide thickness), exposure time and metal temperature. These data are represented in Arrhenius-type plots where y-axis has values of natural logarithm of k, i.e. W^n/t, and x-axis has values of inverse T. The data points should form a linear function which has a slope equal to activation energy. (26) (18)

5.4. Chromium volatilization

When chromium-containing alloys are exposed to steam, there is a possibility that Cr forms volatile species. This may lead to reduced service life through a loss of scale protectiveness (26). The chromium oxide Cr_2O_3 may react with oxygen and water vapor and form volatile chromium oxy-hydroxide $CrO_2(OH)_2$ via:

$$\frac{1}{2} Cr_2O_3(s) + \frac{3}{4} O_2(g) + H_2O(g) \rightarrow CrO_2(OH)_2(g) \qquad (5.13)$$

In steam boilers, where the steam is relatively pure, the oxygen partial pressure in steam will be controlled by equation (5.5). The oxygen partial pressure in steam will be the rate controlling factor in equation (5.13), as other reactants will be excessively available. Young and Pint (40) have studied the chromium volatilization of austenitic Fe-Cr-Ni steel in flowing air containing 10% H_2O. The steel contained sufficient amount of chromium so that continuous Cr_2O_3 scale was formed on the alloy surface. They measured the Cr-loss from foil specimens at temperature range 650 – 800 °C up to 10 000 hours, and compared the measured data to theoretically calculated values. The calculations showed to predict correctly the Cr-loss. Based on these results they calculated the Cr loss rates in pure steam. The calculated values in pure steam were notably lower than in water vapor because of decreased partial pressure of $CrO_2(OH)_2$ resulting from the low oxygen partial pressure of pure steam. Additionally, the mass-transfer properties of pure steam differ from the properties of water vapor. The values of $pCrO_2(OH)_2$ are plotted for different system steam pressures in Figure 5.8, and calculated chromium losses in supercritical steam (P = 241 bar) are represented in Table 5.1. (40)

Table 5.1. Calculated Cr loss by volatilization in supercritical (p = 241 bar) steam. (26)

Temperature (°C)	$pCrO_2(OH)_2$ (atm)	Cr-loss, mass versus area and time	
650	$5{,}0 \times 10^{-8}$	$1{,}4 \times 10^{-12}$ g/cm^{2}s	0,04 mg/cm^{2}year
700	$1{,}6 \times 10^{-7}$	$4{,}2 \times 10^{-12}$ g/cm^{2}s	0,13 mg/cm^{2}year
800	$1{,}2 \times 10^{-6}$	$3{,}0 \times 10^{-11}$ g/cm^{2}s	0,95 mg/cm^{2}year

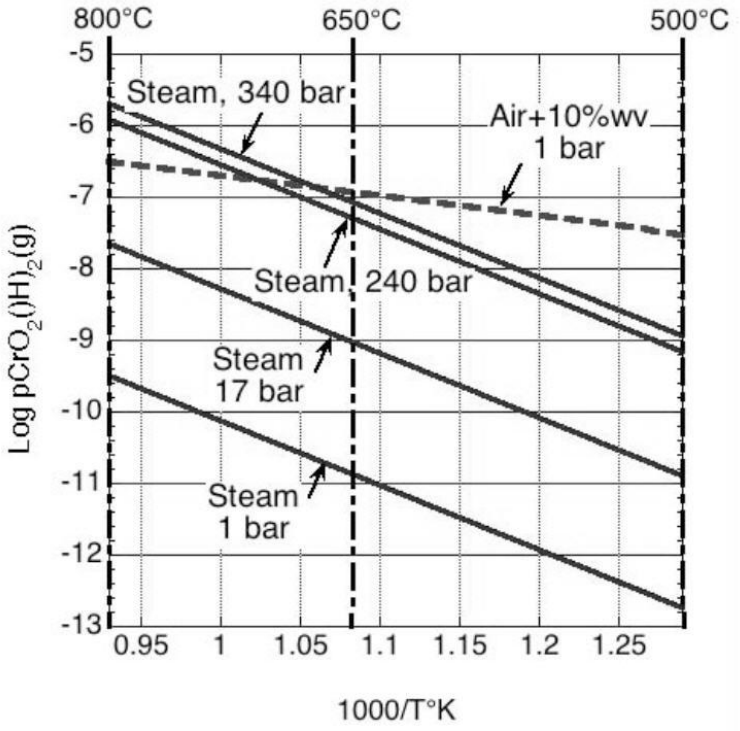

Figure 5.8. Calculated $CrO_2(OH)_2$ partial pressures as a function of inverse temperature for various total system steam pressures. (26)

The rate of chromium volatilization will accelerate when steam pressure and temperature are increased. This may be concluded from Figure 5.8, as the partial pressure of chromium oxy-hydroxide increases when steam pressure and temperature increase. Chromium volatilization is a long-term problem. As the chromium is evaporated from the oxide surface, the alloy adjacent the oxide scale becomes depleted from chromium. When alloy becomes critically depleted in Cr, the oxidation process will become accelerated, and thus the service life of the tube is reduced. (40)

5.5. Evolution of oxide scale morphologies

As noted in previous chapters, the morphology of the oxide scale formed in steam depends on thermodynamic stabilities of different oxides and oxidation kinetics. Meanwhile, these parameters are affected by the alloy composition and microstructure.

The most important alloy derived variables for steels are considered to be chromium content, grain size and surface condition. (26) (18)

Different oxide scale morphologies are detected as the chromium content of the alloy is varied. Typically the oxide scale formed on steel containing chromium at elevated temperatures consists of multiple layers of different iron and chromium oxides and their spinels, as indicated in Figure 5.9. All three oxides of iron are stable at temperatures above 570 °C (32), and thus all of these oxides may be detected from oxide layer. Chromium oxide Cr_2O_3 is detected as a solid solution with magnetite and in a mixed spinel $Fe(Fe,Cr)_2O_4$. Additionally, if the chromium content of the alloy is sufficient, a continuous layer of pure Cr_2O_3 may be detected. However, in elevated temparatures the chromium content required to form a continuous scale of Cr_2O_3 is relatively high, approximately 25 wt% as seen from Figure 5.9. On lower chromium contents the Cr_2O_3 can be detected, but it does not form a continuous layer and thus does not provide sufficient protection at elevated temperature and pressure levels. Thus, the typical austenitic 18Cr-8Ni steels grades will keep oxidizing if exposed to supercritical steam. (32) (18)

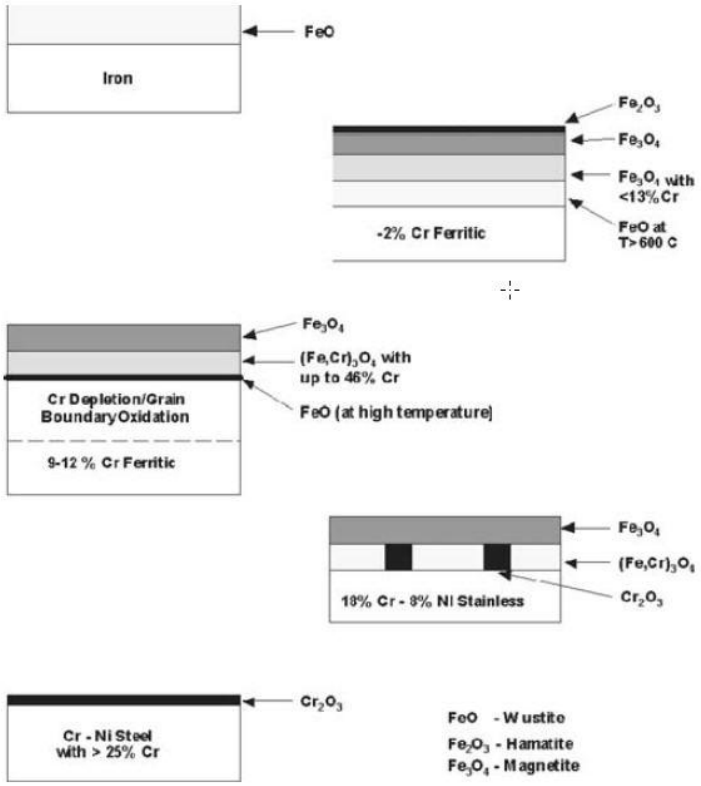

Figure 5.9. Summary of oxide scale morphologies formed on chromium containing steels in high temperature steam. (18)

When the oxide layer starts to grow on the alloy surface, the most stabile oxide will grow preferentially, see chapter 5.1. Thus, the most stabile oxide will be grown on the alloy surface, and so the growth rate of the other layers depends on the diffusivity of reacting species (i.e. metallic ions) to the scale-gas interface. The stabilities of the relevant oxides are represented in Figure 5.5, and by comparing the plots to Figure 5.9,

it is confirmed that typically the most stable oxide is formed on the alloy surface, and the least stabile oxide is found on the outermost surface.

In the following chapters the factors affecting the oxide scale evolution and morphology are discussed. Ferritic (low chromium content) steels, austenitic (high chromium content) steels and nickel-based alloys are discussed separately, as their oxide scale morphologies are different. Relevant laboratory test results available in public literature are included. Additionally, the effect of grain size, surface finish and other alloying elements (besides chromium) are discussed in their own chapters.

5.5.1. Oxidation of ferritic steels

The oxidation behavior of ferritic steels in steam is a relatively well documented subject. The oxide scale formed on ferritic steel in steam is typically double-layered magnetite (Fe_3O_4) scale, layers being approximately equal in thickness. The outer layer is characterized by columnar grain structure with pores often at grain boundary triple points. The outer layer consists of essentially pure magnetite. The inner layer has an equiaxed grain structure, i.e. the grains don't have any preferred orientation and finer, irregular porosity. The inner layer contains chromium with respect to the alloy chromium content, i.e. more chromium containing alloys will have higher chromium content in the inner oxide layer. With higher chromium contents (approximately 9-12 wt-%) the inner scale consists actually of mixed $Fe(Fe,Cr)_2O_4$ spinel with chromium content up to 46 %, as indicated in Figure 5.9. Although haematite (Fe_2O_3) would be expected to be found on the outermost layer by thermodynamic considerations (see Figure 5.5), it is not always present. Usually there are only discontinuous patches of haematite, and sometimes it is completely absent. A schematic presentation of a typical scale structure formed on ferritic steel is showed in Figure 5.10. (26) (18)

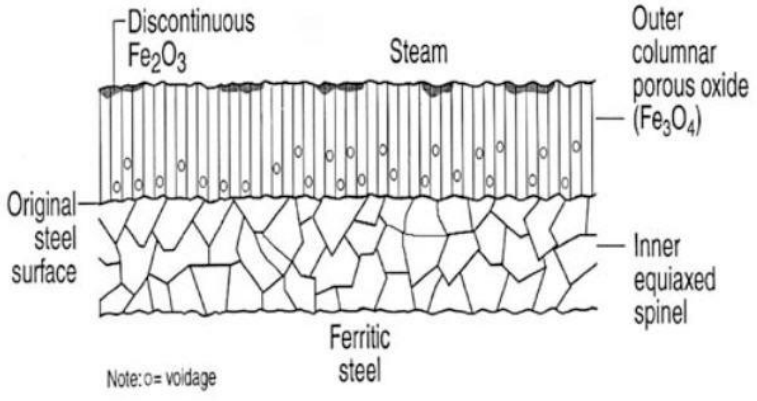

Figure 5.10. A schematic presentation of typical cross section of oxide scale formed on ferritic steel in steam. (26)

Studies performed for ferritic steels in steam show that double-layered oxide structures grow simultaneously at scale-oxide-gas and metal-scale interfaces. As a consequence, the interface between two layers corresponds roughly the original metal

surface. The layers are roughly equal in thickness, and the ratio of the thicknesses of inner and outer layer is usually reported to be independent of time, but it is increased with increasing Cr content. (26)

According to laboratory studies reviewed by Wright & Dooley (26) and Viswanathan et al. (18), short-term oxidation rates up to 570 – 620 °C for ferritic steels containing 1-12 wt-% Cr are not very different. These results reflect the fact that chromium does not bring great improvement to oxidation resistance until the Cr content is sufficient to provide at least partial layers of Cr_2O_3 or Cr-rich Fe-Cr spinel at the inner scale. In some cases the 9-12 Cr alloys exhibited some degree of initial, very protective behavior. (26)

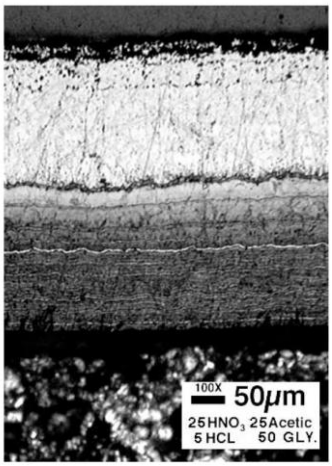

Figure 5.11. Heavily etched cross section view of oxide scale formed on T22 after nominally 263 000 hours in service as a superheater tube at 588 °C. The multi-layered structure of the inner layer is evident. (26)

Lower-Cr ferritic steels (e.g. T22) show typically transformation of the inner oxide layer into multi-layered structure, which consist of repeating series of double layers of relatively large-grained magnetite and fine-grained Fe-Cr spinel, Figure 5.11. It has been suggested that this type of scale morphology is a result of periodic scale failure or cracking and subsequent re-oxidation at the alloy-oxide interface. (26)

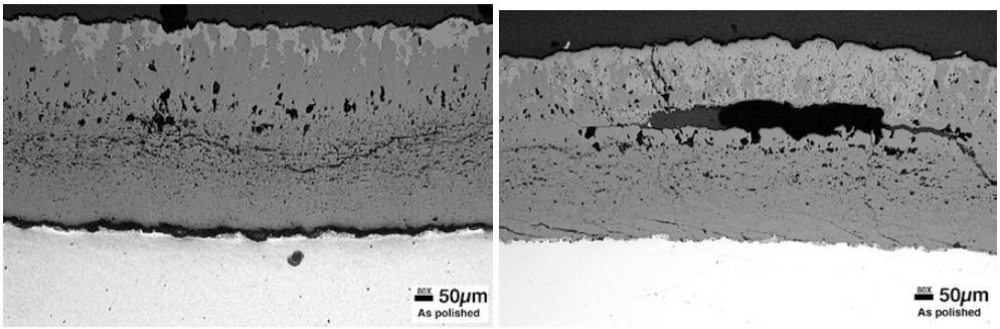

Figure 5.12. Cross sections of oxide scale formed on T91 in steam after nominally 63000 hours service at 566 °C showing morphological features associated with crack development (left picture) and separation of the main outer layer (right picture). (26)

With longer exposure times and higher chromium contents the inner oxide layer becomes enriched in Cr and an increasing number of voids start to form along the

interface between the outer magnetite and inner Fe-Cr spinel layers. These voids may inflict a separation of the outer scale, Figure 5.12. If the separated scale remains attached, there is a risk of local overheating, as the heat transfer rate is reduced. At sufficiently high Cr levels, the Cr content in the inner spinel layer increases, and eventually slowly growing islands of Cr_2O_3 are formed. Increasing chromium content in the inner layer leads to reduced scale growth rate, as the diffusion of iron to the scale-gas interface is impeded. When the availability of iron ions on the scale-gas interface becomes limited, the magnetite layer starts to oxidize to haematite. The lighter gray phase seen in Figure 5.12 is haematite. The amount of haematite phase detected in the left picture is relatively small when compared to the right picture, where the outer magnetite layer is separated. (26) (18)

Table 5.2. Summary of laboratory-derived mass-based oxidation rates and calculated mass gains in steam for ferritic steels. (26)

Alloy type / wt-% chromium	Temperature °C	A ($g^2cm^{-4}s^{-1}$)	Q (kJ/mol)	Calculated mass gain after 40kh (mg/cm^2)	
				550 °C	650 °C
0 – 2 Cr	< 500	$2{,}29 \times 10^{-5}$	109	-	-
0 – 2 Cr	500 – 700	$5{,}87 \times 10^{3}$	230	66	405
T91 (9 Cr)	500 – 700	$4{,}92 \times 10^{-5}$	115	27	66
T92 (9 Cr)	600 – 800	10,6	203	20	100
9 Cr	360 – 800	$3{,}12 \times 10^{-2}$	160	25	89
12 Cr	360 – 800	$2{,}86 \times 10^{-3}$	146	21	67

Wright & Dooley (26) have derived oxidation parameters (Arrhenius constant A and activation energy Q) for ferritic steels from a compilation of laboratory tests, Table 5.2. All results were reported in terms of mass change as a function of time, because it is the most accurate and reproducible measurement that can be performed in laboratory studies. Based on the defined oxidation parameters they calculated mass gains and total oxide thicknesses according to equations (5.7) and (5.4) after 40000 hours exposure at 550 °C steam and assuming parabolic kinetics, i.e. n = 2. Additionally, the mass gain values are calculated for oxidation at 650 °C to get a better understanding on oxidation in supercritical steam. The mass gains increase notably when the temperature is increased to 650 °C. The calculated values presume that oxidation follows parabolic kinetics and oxide scale is not lost during oxidation. In reality, however, it is expected that at certain temperature level (Figure 5.7) oxidation rate will begin transforming from parabolic towards linear, and thus the oxide scales grow at notably faster rate. Oxide scale loss also accelerates the overall kinetics, because the oxidation process will start from a “fresh” surface. (26)

5.5.2. Oxidation of austenitic steels

According to Wright & Dooley (26), the oxidation behavior of austenitic steels may be roughly divided to two distinct classes:

- Alloys with approximately < 20 wt-% Cr and < 20 wt-% Ni and coarse microstructure (ASTM 6 or coarser). These alloys do not form uniform chromium-rich oxide layer because of insufficient Cr content and Cr diffusivity
- Alloys with approximately > 22 wt-% Cr and >20 wt-% Ni, or fine-grained microstructure (ASTM 7 or finer). Alloys belonging to this class form a dense chromium-rich oxide layer, and oxidize at a slower rate than the coarse-grained and lower Cr and Ni alloys.

Figure 5.13 and Figure 5.14 show typical cross-sections of both oxide scale morphologies detected on austenitic steels exposed to steam. (26)

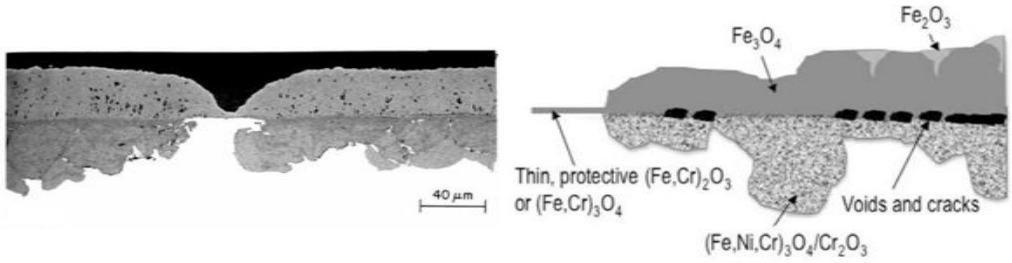

Figure 5.13. Typical oxide morphology formed on coarse-grained, 300-series (18Cr-12Ni) austenitic steels in steam. Cross section of scale formed on TP304H after 28000 hours at 538 °C and 5bar steam (left) and a schematic representation of oxide types (right). (26)

The oxide layer formed on lower Cr and Ni steels consist predominantly of two layers: an outer layer of magnetite and inner layer of Fe-Cr spinel, Figure 5.13. As in ferritic steels, sometimes an outer zone of haematite may be detected. Both layers become thicker with time. The inner layer becomes increasingly non-uniform, and the outer magnetite layer becomes more porous with time. Oxidation studies reviewed by Wright & Dooley (26) indicate that initially the scale consist of uniform layer of M_3O_4 or M_2O_3 oxides, where M represents Fe and Cr. Typically the layer is enriched in Cr. After some time, a local breakdown of these initial scales begins through formation of nodules, which grow simultaneously inward an outward, Figure 5.13. The outward growing layer is essentially pure magnetite, while the inward growing layer is a mixture of magnetite, Fe-Cr spinel and elements of other alloying elements, e.g. Ni, Mn and Mo, having same crystal structure as magnetite. The inner Cr-rich layer grows by penetration of Fe-Cr spinel along alloy grain boundaries. Eventually the whole grain is encircled by Fe-Cr spinel, and the grain body becomes depleted from chromium. When a grain becomes completely encircled by Fe-Cr spinel, further penetration of the inner layer into the alloy is slowed. The chromium-depleted grain bodies oxidize to form essentially magnetite. The resulting inner oxide layer consists of magnetite and Fe-Cr spinel, with Cr-rich spinel on the oxidation front next to the base metal. (26)

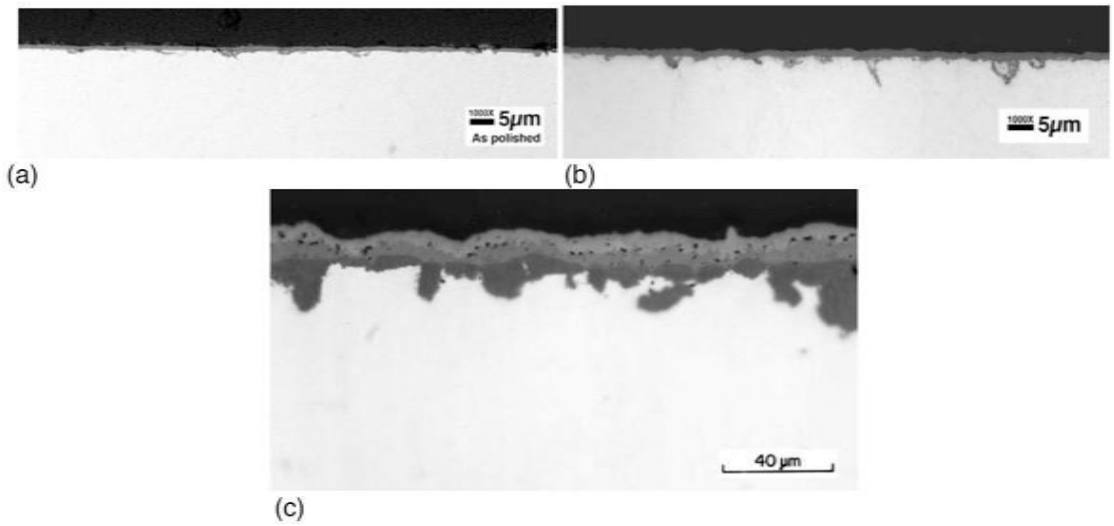

Figure 5.14. Typical scale morphologies formed on highly-alloyed and fine-grained austenitic steel HR3C in steam. Figures (a) and (b) are from laboratory tests after 4000 hours exposure at 650 °C and 700 °C, respectively. The pressure was 17 bars. Figure (c) is from actual boiler after 21000 hours at 552 °C. (26)

Higher Cr and Ni austenitic steels and fine-grained steels with lower Cr and Ni contents develop similar scale structures, except that the scales on higher Cr and Ni steels develop at considerably slower rate. The scale is double-layered with outer magnetite layer and inner, homogenous Cr_2O_3 layer. With lower chromium contents there may be a layer of chromium rich Fe-Cr spinel between the magnetite and Cr_2O_3 layers. Figure 5.14 shows a cross-section of typical scale structures formed on fine-grained steel and high Cr and Ni steels. These steels have a sufficient chromium content and improved diffusivity of chromium so that the chromium rich oxide layer is formed to the alloy-scale interface. In some cases the oxide layer may be very thin, so that it is difficult to distinguish the scale morphology. The scales should however become thicker with increasing exposure time, as Figure 5.14 (c) suggests. (26)

Otsuka et al. (34) have studied extensively the effect of alloy chromium content and grain-size on the oxidation behavior of austenitic stainless steels in steam at the range of 500 – 900 °C. They concluded that there are three distinguishable oxidation behaviors on austenitic stainless steels in steam. These are, in order of descending oxide scale protectiveness, formation of external Cr_2O_3 scale, formation of a band of compact oxides (spinel) which function as a healing layer and the formation of stratified inner scale, which results from an alternative internal-external oxidation. The scale structure is similar to the structure presented in Figure 5.11. The formation of external Cr_2O_3 scale showed little temperature dependence. External oxidation was detected when the Cr content exceeded 21wt-% for both fine- and coarse-grained steels. The formation of healing oxide layer was detected on fine-grained steels only. It showed apparent temperature dependence. Types of oxide scales and their schematic representations observed by Otsuka et al. (34) are represented in terms of chromium content and temperature in appendices 1 and 2 for coarse-grained and fine-grained austenitic stainless steels, respectively. (34)

Table 5.3. Summary of laboratory-derived mass-based oxidation rates and calculated mass gains in steam for austenitic steels. (26)

Alloy type	Temperature °C	A ($g^2cm^{-4}s^{-1}$)	Q (kJ/mole)	Calculated mass gain after 40kh (mg/cm^2)	
				550 °C	650 °C
300 series coarse-grained	538 – 760	20	215	11	63
High Cr, high Ni	650 – 800	$6{,}1 \times 10^{-4}$	213	0,07	0,4

Wright & Dooley (26) have derived oxidation parameters for austenitic steels based on laboratory derived mass-change data. The alloys are divided to two classes, which are 300-series coarse-grained alloys with nominally less than 20 wt-% Cr and 12 wt-% Ni and high Cr and high Ni alloys which have higher Cr and Ni contents than 300-series and/or fine-grained structure. Based on these values, the mass gains are calculated with same parameters as for ferritic steels (Table 5.2) so that the results are comparable. The alloys with high Cr and Ni contents or fine-grained microstructure show notably lower mass-gains compared to coarse-grained 300-series austenitic steels. The calculated mass gain for 300-series steels in 650 °C is roughly same as for higher Cr ferritic steels. (26)

5.5.3. Oxidation of nickel-based alloys

The oxide scales grown on nickel-based alloys containing >16wt-% chromium in steam up to 700 °C are usually very thin and uniform in thickness. The layer consists of an outer layer, which is essentially Cr_2O_3 with some $MnCr_2O_4$ and Ni, depending on the alloying. In some cases there may be some internal penetration beneath the external oxide scale. Internal penetration may range from few discrete precipitates to high population of internal precipitates and penetration along alloy grain boundaries, again depending on alloy composition. Internal penetration is particularly detected on alloys containing Al and Ti. A schematic presentation of oxide layer formed on nickel-based alloys in steam is presented in Figure 5.15. (26)

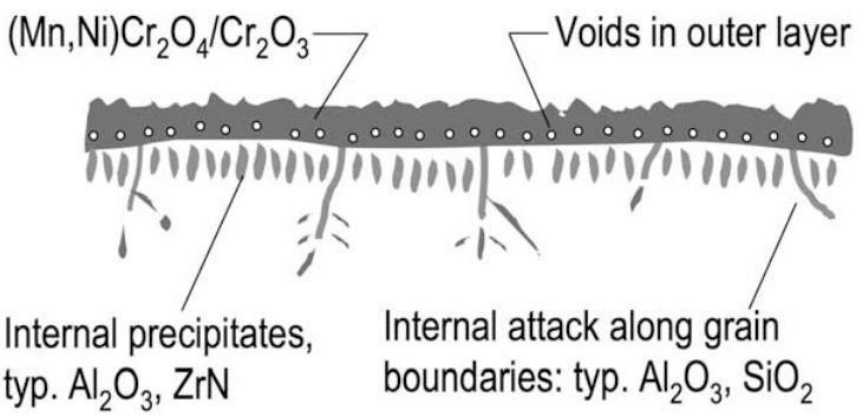

Figure 5.15. A schematic presentation of a typical scale morphology developed on Cr-alloyed nickel-based alloys exposed to steam. (26)

5.5.4. Effect of grain size and surface condition

Equation (5.7) suggests that the critical chromium content required to form external oxide scale can be reduced by improving interdiffusivity coefficient of chromium in the alloy (D_B). The interdiffusivity may be improved by selecting fine-grained version of steel or by cold-working the surface exposed to steam. Both of these methods improve the interdiffiusivity coefficient of chromium by introducing short-circuit diffusion paths to the crystal structure of alloy. (35) (41)

Because the fine-grained steel has more grain boundaries than coarse-grained, the grain boundary diffusion of chromium becomes dominant in fine-grained steels (34). Figure 5.16 is a schematic presentation of oxide scale structures formed on coarse- and fine grained steels in steam. The faster diffusion rate through grain boundaries is evident. (35)

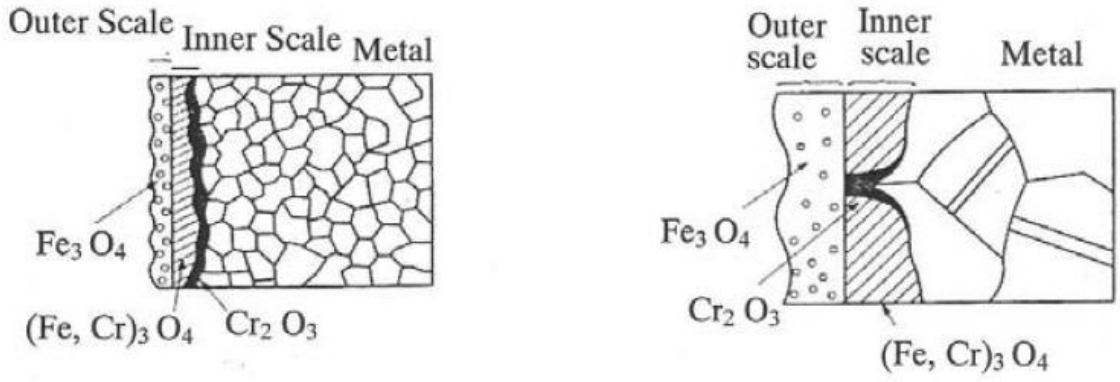

Figure 5.16. A schematic presentation of oxide scales formed on fine-grained (left) and coarse-grained (right) type 347H steel in steam. (35)

Cold-working the alloy surface increases its dislocation density (33). With higher dislocation density, the dislocation diffusion of chromium becomes promoted. The mechanism is similar to grain boundary diffusion. (41) Matsuo et al. (35) have reported improvements in both coarse- and fine-grained steels by cold-working the alloy

surface. In temperatures below 700 °C fine- and coarse-grained steels showed similar oxidation resistances in laboratory tests. When temperature was raised above this, the oxidation resistance of coarse-grained and shot-peened steels deteriorated and the Cr_2O_3 layer almost disappeared completely. The reason for this was speculated to be the disappearance of cold-worked layer due to recovery of deformation or re-crystallization. The fine-grained and shot-peened steels showed superior oxidation resistance and formation of continuous Cr_2O_3 layer even at temperatures up to 750 °C. The effect of grain-size diffusion was still maintained, and so fine-grained steel showed better oxidation resistance compared to coarse-grained steel, even when the effect of cold-work was lost. The effect of cold-work is also lost in the tube manufacturing process in proximity of heat affected zones (HAZ) and tube bends. The oxidation in these locations may be unexpectedly fast when coarse-grained and shot-peened tube material is selected. (35)

5.5.5. Effect of other alloying elements

Besides chromium, there are some other alloying elements which can improve the steam-side oxidation resistance of an alloy. The effect of other alloying elements has been studied particularly on ferritic and martensitic steels because their chromium content is notably lower than in austenitic stainless steels. Alloying elements which have confirmed beneficial effect on steam-side oxidation resistance are Si, S, Mn, Pd and B. Mo and W have been reported to improve the oxidation resistance in some circumstances, but they may have a detrimental effect too because both form volatile oxides. Additions of Nb and N stabilize the strengthening particles such as carbides ($M_{23}C_6$), carbo-nitrides [Nb(C, N)] and nitrides (NbCrN) at higher temperatures. Besides this, they contribute to availability of chromium at the oxidizing surface by improving the distribution of chromium. The good distribution of chromium is important particularly on alloys which have Cr level close to the critical level of scale formation. (23) (26)

Silicon improves the oxidation resistance by developing protective oxide scales. Silica (SiO_2) has lower standard free energy of formation than Cr_2O_3, so it is expected to form more stable and slower growing oxide layer than chromium. Si has been ranked four to five times as effective as Cr in decreasing the oxidation rate of ferritic (up to 12% Cr) steels (26). However, excess additions of Si may lead to embrittlement of the steels and deterioration of high-temperature creep strength (23). The Si level should be maintained between 0,2 and 1 wt-% to achieve improved oxidation resistance. The silicon has been found to segregate beneath the Cr-rich layer, where it impedes the outward diffusion of Cr. (26)

In steelmaking process sulfur is considered to be an impurity element, and every effort has been made to lower sulfur content of the steel. Sulfur lowers the fracture toughness and ductility of the steel after long exposures to high temperatures. However, it has been noted that small amounts of sulfur bring dramatic improvement to oxidation resistance of ferritic steels. For best performance, the sulfur content should be

maintained between 0,005 to 0,01 wt-% in high-Cr ferritic steels. In this range the oxidation resistance is improved and there is no harmful effect on mechanical properties. The mechanism of the sulfur effect remains unclear, but it has been suggested that S slows the chemisorption of oxygen and retards its access to the metal surface. Other suggestion is that sulfur reacts with chromium and forms chromium sulfide precipitates which are responsible for the observed effects. (23) (26)

Manganese has been reported to improve the oxidation resistance due to its participation in formation of protective chromium rich scale and its suppression of chromium volatilization. Palladium has been reported to promote the formation of thin and protective Cr-rich oxide layer on ferritic steels. Boron has been noted to bring some improvements in oxidation resistance probably by stabilizing carbides. The stabilized carbides act as a Cr-reservoir if they are distributed uniformly. (26)

5.6. Oxide scale exfoliation

If the oxide scale on the steam-side of superheater or reheater tubes becomes increasingly thick, it is more likely that it will exfoliate. The exfoliated oxides may cause unscheduled boiler shutdown due to tube blockages caused by lodged oxide particles, or tube failures caused by reduced tube wall thickness. If the exfoliated oxide particles enter the steam turbine, they cause accelerated wear of turbine components and reduced service life of the steam turbine. If the protective scale is exfoliated from alloy-oxide interface, the oxidation rate in these areas will be more rapid, as the oxidation process starts from fresh metal surface. This accelerates the thinning of tube walls. The general discovery is that exfoliation occurs only after several thousands of hours of service unless the material selection is wrong. This suggests that the criterion for scale exfoliation is related to scale thickness. Exfoliation is common phenomenon in both ferritic and austenitic stainless steels, although the mechanisms differ because of different scale morphologies developed. (18) (42)

Exfoliation of oxide scale is greatly affected by the oxide scale morphology. The exfoliation may occur near the metal-scale interface or at the interface between outer and inner part of the scale, depending on the distribution of pores and internal stresses present in the scale. The pores and voids create planes of weakness within the oxide scale or at the alloy-scale interface. They may act as initiation points to the cracks because the stresses developed are amplified in the proximity of internal flaws. It has been noted that the oxides which form isothermally, i.e. in laboratory conditions, contain fewer voids than scales grown in actual boiler service, where heat flux exists. Generally speaking, the scales formed in service are more susceptible to spalling than the scales formed isothermally. (18) (33)

According to Mohammed & Sarver (23) various researches have concluded that the exfoliation of steam-side oxide scale is associated with stresses generated in the scale. The major sources of stresses in the oxide scale are growth stresses and thermal stresses. Growth stresses are generated during the isothermal formation of the scale,

whereas thermal stresses develop during change of temperature due to different coefficients for thermal expansion between the metal and the oxide scale. Additional source for stresses is deformation of the base alloy, typically by creep. This may transmit strains to adherent oxide. (42) In some cases the stresses generated in oxide scale and scale-alloy interface may be relieved by plastic deformation (creep) of the oxide or the alloy. If the stress relieving through plastic deformation is insufficient, the stress will be relieved by cracking or spalling of the oxide. (32)

Growth stresses are basically developed during the oxidation process because of change in the volume as metal transforms to oxide as the oxide scale becomes thicker. Thicker scales mean greater growth stresses (42). Stresses induced by volume change are tensile if the volume decreases and compressive if the volume increases. Most metals experience increase in volume during oxidation, so the oxide scales are in compression. This kind of principle is valid for scales growing inward. For outward growing scales the mechanisms for developing scale growth stresses are different, but still follow the same principles. (18) (32)

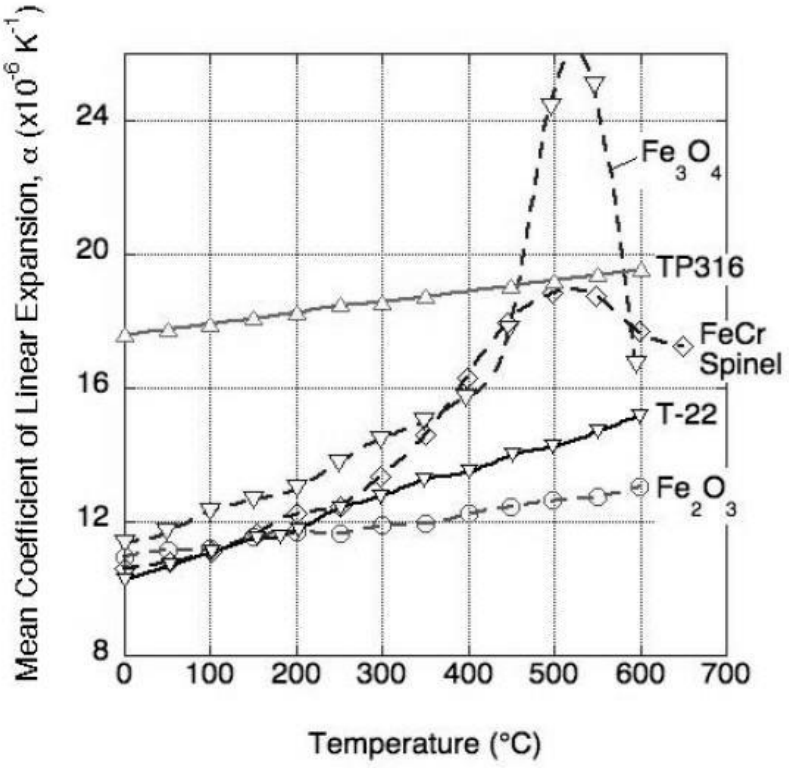

Figure 5.17. Coefficients of thermal expansion for selected oxides and alloys. TP316 is austenitic steel and T-22 is ferritic steel. (42)

Thermal stresses are induced in the oxide layer when the operating temperature is changed, i.e. during start-up or shutdown of the steam boiler, or even during load changes. Thermal stresses are particularly significant during cooling, because there is a limited time available to accommodate them by stress-relieving through creep or other mechanisms. Thermal stresses are induced by differences in thermal expansion coefficients (CTE) of the metal and oxides. The magnitude of thermal stress generated may be approximated with the ratio of CTEs. If the oxide coefficient / metal coefficient

is near unity, the scale is expected to remain adherent as the thermal stress generated is small. The CTEs of certain oxides and alloys, and their dependence on temperature are represented in Figure 5.17. Generally speaking the thermal stresses developed in scales formed on ferritic steels are tensile, and stresses developed on scales formed on austenitic steels are compressive. Therefore oxide scales formed on ferritic steels commonly experience through-scale cracking, so that the double-layered oxide scale is completely lost. If the oxide scale is multilayered, Figure 5.11, the outmost double-layer is lost and the inner laminated structure is prevailed. Because oxide scale in austenitic steel is usually in compression, the oxide layer experiences delamination so that only the outer layer of the scale is lost. The fact that oxide particles spalled from ferritic steels are usually double-layered and the ones spalled from austenitic steels are single-layered supports this assumption. (32) (42)

The complete scale loss will accelerate the oxidation process because the oxidation process starts again from fresh metal surface. The oxidation will be further accelerated if the new alloy surface has been depleted from chromium, as is the case in some ferritic steels, Figure 5.9. Austenitic steels experience accelerated oxidation to a lesser amount, because the protective Fe-Cr spinel will be usually adherent and only the outer magnetite/haematite scale is lost. (42)

The presence of haematite, Fe_2O_3 has also some effect on the exfoliation behavior. Haematite will form on the outmost layer and, because of relatively low CTE compared to magnetite, develops compressive stresses during cooling. On ferritic steels the formation of haematite promotes transition in the failure mode from through-scale cracking to delamination of scale along variety of planes. On austenitic steels the increasing Fe_2O_3 / Fe_3O_4 ratio in the outer scale increases the compressive stress in the outer layer during cooling. This can be a major cause for exfoliation from standard austenitic 300-series superheater and reheater tubes. (42)

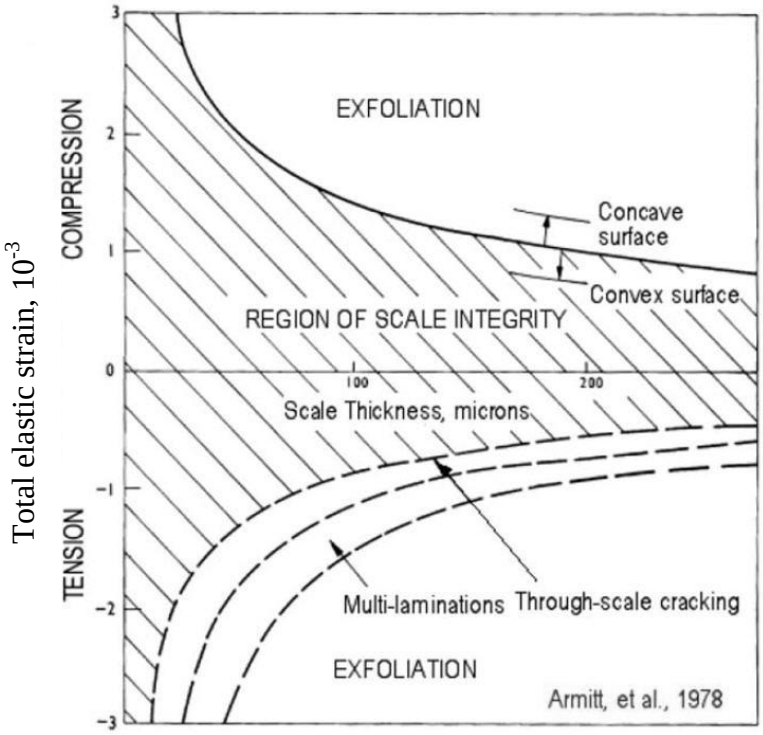

Figure 5.18. The "Armitt" diagram. (43)

The exfoliation may be roughly estimated by Armitt-diagram, if the scale thickness data and stresses acting in the scale are known. The diagram includes scales grown on both ferritic (tension) and austenitic (compression) steels, although their failure mechanisms differ. It is evident that the amount of elastic strain that can be accommodated decreases rapidly as the oxide scale becomes thicker. This concept of predicting the scale exfoliation in terms of oxide thickness and total elastic strain in the scale has proved to be a very useful for rationalizing the exfoliation behavior. Post-exposure examination of tubes removed from service has showed very good agreement with the condition predicted by the Armitt diagram. Reliable prediction is, however, impossible because it is difficult to approximate the elastic strains in the oxide scale. Simplified formulas to estimate the strains generated while cooling have been suggested by Wright et al. (42), Table 5.4. Based on these formulas and the Armitt diagram, the critical scale thicknesses can be evaluated. If the final superheater manufactured from austenitic stainless steel is cooled down from 650 ºC to room temperature (20 ºC), it will generate 1.96×10^{-3} % - 2.17×10^{-3} elastic strain to the oxide scale, depending on the amount of haematite on the scale. This type of cooling corresponds quite well a shutdown of a supercritical steam boiler. According to Armitt diagram, this type of strain will increase the risk for scale exfoliation when the oxide layer is more than 50 µm thick, so it can be considered as a maximum scale thickness that can be allowed on austenitic boiler steels. However, this is only a very rough estimate: the true critical value may be considerably lower, depending on the scale structure and adherence. (42) (43)

Table 5.4. Formulas to estimate the cooling strains generated in the steam-side oxide scale. (42)

Oxide	300-series austenitic steel	T22 Ferritic steel
0% Fe_2O_3	$1.8 \times 10^{-3} (T_s - T_a) / (600\ ^oC - T_a)$	$-1 \times 10^{-3} (T_s - T_a) / (600\ ^oC - T_a)$
20% Fe_2O_3	$2.0 \times 10^{-3} (T_s - T_a) / (600\ ^oC - T_a)$	$-0.5 \times 10^{-3} (T_s - T_a) / (600\ ^oC - T_a)$

T_s = Service temperature, °C

T_a = Temperature to which the component is cooled

5.7. Field test results

Solid particle erosion and tube blockages caused by exfoliation of steam-side oxide scale are detected in numerous steam power plants. Typically steam-side oxidation has been a problem in pulverized coal fired power plants, where steam parameters are more advanced than in typical CFB boilers. However, CFB boiler manufacturers are going to face this problem as well when steam parameters are raised above supercritical level. Available plant data can be applied quite well to CFB boiler technology, because steam is practically similar in a CFB boiler and in a pulverized coal fired boiler. There is, however, one difference when considering INTREX superheater which is immersed in bed material. Heat exchange in immersed superheater happens by solid-to-solid heat exchange, which is much more efficient than gas-to-solid heat exchange. This leads to much higher temperature gradient in immersed superheaters, and may affect on the kinetics of oxidation and oxide scale morphology. There are some field test experiments where the effect of temperature gradient is studied, but currently none test results are available.

In this work, the results from two different field testing campaigns are introduced. Both test campaigns were completed in the 2000s and studied materials which are potential candidates for supercritical boilers with advanced steam data. Majority of the studied alloys were austenitic stainless steels, which are the most promising candidate materials for supercritical boilers. These results will give a good idea about the suitability of materials for the target steam parameters.

5.7.1. KOMET 650

KOMET 650 (Power station options: developments in materials and measurement techniques and tests under operating conditions at 650 °C) was a German joint research programme launched in 1998. The goal of this project was to create a technical basis for construction and design for coal-fired power plant with steam temperature 650 °C and efficiency level of 47 % or above. A major part of the programme was to evaluate the performance of different materials in superheaters, steam pipe lines, turbines and control valves. The test sections were installed in unit B of the RWE's Westfalen power station. The superheater tube test section consisted of four identical test loops which were removed after 5890, 12000, 17770 and 23215 hours of operation at full load, i.e.

steam temperature was above 640 °C at the test loop outlet. The test loop section was composed of ten different materials including martensitic and austenitic steels and nickel-based alloy. The tested materials and their nominal chromium contents, exposure temperatures and observed scale thicknesses are reported in Table 5.5. E911 and NF 616 are ferritic/martensitic steels with approximately 9wt-% Cr, Inconel 617 is nickel-based alloy and all the rest are austenitic steels with variable chromium content. When superheater tube test sections were removed, they were investigated by the following methods: metallographic assessment of the steam-side oxide layers on unetched cross micro-sections under scanning electron microscope (SEM), structural assessment of etched cross micro-sections under light optical microscope, Vickers hardness tests and energy-dispersive X-ray (EDX) analyzes which were performed with SEM. (44) (45)

Table 5.5. Tube materials and their chromium contents, operating temperatures and observed scale thicknesses. (45)

Material	Cr content, wt-%	Temperature range, °C	Scale thickness after 23215 hours, µm
E 911	8,95	514 – 562	90 – 230
NF 616 / T92	9,04	535 – 566	240 – 280
Esshete 1250	14,85	574	< 95
X3CrNiMoN 17 13 (1.4910)	16,95	514 – 605	< 125
X8CrNiTi 18 10 (1.4941)	17,30	522 – 568	< 100
TP 347 HFG	18,20	568 – 601	40 – 60
Super 304 H	18,65	581 – 632	90 – 140
NF 709	20,19	612 – 643	70 – 110
Inconel 617 (Ni-based)	22,35	639 – 647	< 10
AC 66	27,10	539 – 630	3 – 8

Table 5.5 shows the general trend of exposure temperature and chromium content on the steam-side oxidation behavior of pipe material. When the chromium content is increased, the oxide scales are generally thinner. The remarkably thin oxide layers detected on high-Cr alloys Inconel 617 and AC 66 indicate the formation of a continuous chromium oxide layer. The positive effect of grain-refinement is observed on the fine-grained austenitic steel TP 347 HFG, which shows considerably thinner oxide scales when compared to e.g. X8 CrNiTi 18 10 which has similar Cr content and exposure temperature. On the other hand, Super 304 H, which is also a fine-grained steel, did not show any enhancement in steam-side oxidation resistance when compared to X8 CrNiTi 18 10. The reason for this remains unclear. (45)

Based on the extensive investigations, practical temperature limits were derived for all tested alloys. Ferritic/martensitic materials E 911 and NF 616 are suitable for heat exchanging surfaces when the steam temperature is below 550 °C because of the

rapid growth of oxide layer in temperatures above this limit. Austenitic steels Esshete 1250, X3 CrNiMoN 17 13, X8 CrNiTi 18 10 and Super 304 H have acceptable scale thicknesses in temperatures below 570 °C. Fine-grained austenitic steel TP 347 HFG is applicable up to 600 °C steam. It was noted that the scale thickness on TP 347 HFG didn't remarkably increase after 5890 hours at full load, which suggests the formation of protective and adherent inner chromium-rich oxide scale, Figure 5.16. Austenitic steel NF 709 is applicable up to 620 °C. There was some intercrystalline breakdown of the grains detected after only 5890 hours, but this was suggested to occur because of problems in heat treatment or pickling process. Austenitic steel AC 66 showed excellent oxidation behavior in whole temperature range, so it may be applicable in temperatures well above 630 °C. However, a tendency towards carbonization and formation of nickel sulphides was detected in the flue gas atmosphere. These factors may limit the maximum exposure temperature of this material. The carbonization was detected at temperatures above 600 °C. The nickel-based alloy Inconel 617 is expected to perform well in temperatures up to 650 °C and beyond. The carbonization was detected in temperatures above 630 °C. These may be somewhat conservative limits. At least austenitic steel TP 347 HFG would be expected to perform satisfactory in temperatures above 600 °C, but since it was not exposed to hotter steam during the testing period, Uerlings et al. (45) have limited the practical steam temperature to 600 °C. (45)

5.7.2. Eddystone Power Station

Eddystone Unit 1 was designed and built in the 1950s. It was designed for steam temperature of 654 °C and pressure of 365 bar, but these parameters had to be downgraded in the 1960s to roughly 613 °C and 345 bar because of wall loss in superheater and reheater tubing due to coal ash corrosion. (46) Still, these steam parameters are considered to be very advanced even in nowadays. A material testing campaign was initiated in the Eddystone Unit 1 in 1991. The purpose of the campaign was to determine the suitability of newly developed austenitic stainless steels in superheaters and reheaters of supercritical boiler. Six austenitic stainless steels were selected to replace originally designed superheater material 17-14 CuMo. Experimental tubing section was installed in final superheater section. Test tubes were removed for examination after 75075 service hours. Reported steam temperature and pressure were 615 °C and 351 bar at the superheater outlet. The steam-side oxide scales were generally two-layered. To avoid any error in results generated by possible scale exfoliation, only thickness of the inner scale was measured. This gives pretty reliable results since the inner, chromium rich oxide scale is usually remained when the scale exfoliation occurs. Fireside corrosion behavior was evaluated by measuring the tube outside diameter before and after service. Additionally, the changes in microstructure and mechanical properties were evaluated after service. All six tested materials and the original superheater material, their measured chromium contents and maximum scale thicknesses are represented in Table 5.6. (47)

Table 5.6. Tube materials and their chromium contents and observed maximum oxide scale thicknesses. (47)

Material	Cr content, wt-%	Maximum inner scale thickness after 75075 hours, µm
17-14 CuMo	16,01	205
Super 304 H	18,13	110
TP 347 HFG	18,25	40
NF 709	19,71	90
Tempaloy A-3	21,54	45
HR3C	24,68	35
Tempaloy CR30A	30,65	0-5

The steam-side scales were examined with optical microscope. Generally the scale was observed to have two-layered structure consisting of outer iron oxide layer and inner chromium rich oxide layer, as expected according to oxidation theory. The EPMA (electron probe microanalyser) analysis of the scale revealed that the outer layer was partly exfoliated from materials 17-14 CuMo and Super 304 H. The exfoliation of other materials was hard to distinguish because the scale thicknesses were too small for reliable analysis. (47)

The reported results in Table 5.5 and Table 5.6 are not directly comparable because of different operating parameters and measuring methods, but the same trend can be observed in both results: the alloys with higher chromium content show better resistance against steam-side oxidation. This behavior is evident particularly in austenitic stainless steels. The improvement of fine-grained microstructure in type 347 HFG steel is obvious as it performed similarly in both test campaigns, KOMET 650 and Eddystone. However, it remains unclear why fine-grained microstructure does not seem to improve the oxidation resistance of material Super 304 H. It has similar fine-grained microstructure and chromium content than TP 347 HFG, but has roughly twice as thick oxide scales when compared to TP 347 HFG. It was noted that in Eddystone samples, the microstructure of TP 347 HFG was slightly finer near the inner surface. It is, however, questionable if this small difference affects so dramatically on the oxidation behavior. (47)

6. LABORATORY TEST SETUP

6.1. Description of test equipment

Laboratory testing of candidate materials is an important step in determining whether the material is suitable for boiler applications or not. Steam-side oxidation of materials may be tested by exposing the samples to superheated steam in desired temperature and pressure. The steam properties may be adjusted so that they are similar than in the water-steam circulation of a steam boiler. When studying the oxidation in supercritical steam, the high pressure and temperature levels set very demanding requirements for the test equipment. The tests must be conducted in a pressure vessel, which is able to contain temperatures above 600 °C and pressure level above 221 bar. No leakages should occur during the exposure time, which may be up to thousands of hours.

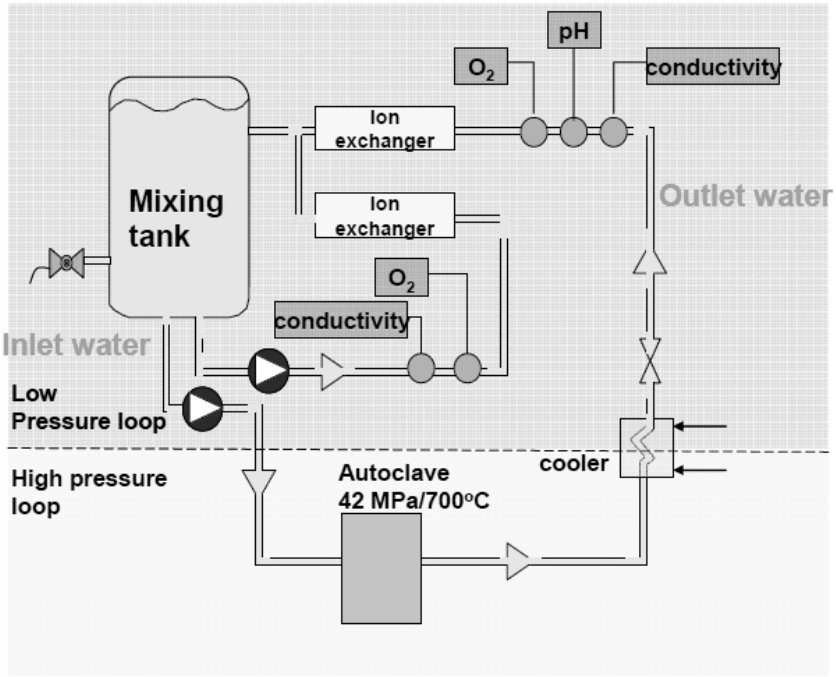

Figure 6.1. A schematic presentation of the test equipment. (48)

The test setup used at VTT is represented in Figure 6.1. The main components are mixing tank, feed water pump, high pressure heat exchanger, autoclave chamber and cooler. Temperature, pressure, pH level, inlet and outlet conductivities and inlet dissolved O_2 values of the circulating water/steam are monitored continuously.

Sample coupons are mounted to the specimen rack. The specimen rack and the sample coupons are electrically insulated from each other by using ZrO_2 washers. The specimen rack is also electrically insulated from the body of the autoclave chamber.

6.2. Sample preparation, testing and analyzes

Totally six different candidate austenitic alloys were selected for ultra super critical (USC) autoclave testing. The nominal chromium contents of the candidate alloys varied between 18 and 27 weight percent. Additionally, one reference austenitic material with nominally 16 wt-% chromium was placed in the autoclave chamber. The purpose of this reference sample is to validate if results from different test campaigns are comparable. The test program consisted of two distinctive test campaigns performed during years 2009 and 2010. Chemical compositions, surface finishes and testing periods of the tested alloys are introduced in Table 6.1.

Table 6.1. Chemical compositions of tested alloys, their surface finishes and testing periods.

Steel	C	Si	Mn	S	Cr	Ni	Mo	Nb	Surface finish [1] and test period
Alloy A [2]	<0,11	<0,45	<0,63	<0,018	22,5	25,0	-	0,45	g (09)
Alloy B	0,015	0,41	1,73	0,001	26,7	30,6	3,34	-	g (10)
Alloy C	0,062	0,36	1,12	0,002	25,1	20,0	0,10	0,42	g (10) m (10)
Alloy D	0,048	0,29	1,84	0,013	17,6	10,7	-	0,56	g (09) m (10)
Alloy E (FG) [3]	0,070	0,42	1,65	0,002	18,1	11,8	-	0,8[4]	g (09) m (10)
Alloy F (FG) [2,3]	<0,14	<0,35	<1,04	<0,015	18,0	9,0	-	0,45	g (09)
Alloy G (ref.)	0,014	0,42	0,8	0,001	16,6	11,3	2,11	0,01	g (09) m (09&10)

1) Surface finishes are marked by coding, g = ground state, m = machined state.
2) Nominal chemical composition according to VdTÜV Werkstoffblatt
3) FG stands for fine grained (ASTM grain size number over 7) alloy
4) Nb + Ta

Sample coupons are prepared from tube materials which Foster Wheeler Energia Oy has provided. Test coupons are milled from tubes to the dimensions of 25 x 15 x 5 mm^3. After this, some of the coupons are ground with #1200 grit emery paper. Some of the coupons are left in their "as-machined" state in order to simulate the effect of cold-work (shot peening) to the oxidation resistance. After surface finishing, the coupons are washed in pure water and acetone, dried and weighed on a balance to an uncertainty of ± 10 µg. The coupons are exposed to supercritical steam at 650 °C and 250 bar in the

autoclave described in section 6.1. Since the test setup is isothermal, the test temperature chosen corresponds steam temperature of approximately 600 ºC in actual boiler, depending on the heat transfer between steam and inner tube surface. The test durations varied between 24 – 600 hours in the 2009 test campaign and between 600 – 2000 hours in the 2010 test campaign. For both test campaigns, three sample coupons of each tested material and surface finish combination were prepared. Samples were removed for evaluation after 24, 168 and 600 hours of exposure in the 2009 campaign, and after 600, 1000 and 2000 hours of exposure in the 2010 campaign.

Table 6.2. Targeted and measured values for the test environment.

Variable	Unit	2009		2010	
		Target	**Measured**	**Target**	**Measured**
Temperature	ºC	650		650	649 ± 1
Pressure	bar	250		250	250 ± 0,9
Inlet conductivity	µS/cm	0,5 – 2,0	0,5 – 2,0	0,1 – 0,5	0,053 ± 0,001
Outlet conductivity	µS/cm	1,0 – 3,0	1,0 – 3,0	1,0 – 3,0	0,29 ± 0,11
Inlet dissolved O_2	ppb	150	149 ± 13	150	150 ± 0,5 ppb
Inlet water pH	pH	8,2 – 8,5	8,4 ± 0,1	7,0	(Pure water)
Flow rate	ml/min	2 – 3		~1	

The properties of circulating water/steam were monitored, and the measured values are reported together with the target values in Table 6.2. As can be seen, properties of the test environment were slightly changed between the two testing campaigns. The values in 2009 tests correspond roughly the actual feed water properties in once-through supercritical steam boilers. In 2010 tests, pure water was used to generate the steam. The reason for this change was that in 2010 tests nuclear power plant materials were also tested in the same autoclave, and the properties of the steam were set according to their requirements. Effect of lower pH is expected to be negligible, since the European standard for feed water quality (SFS-EN 12952-12) states that the pH level in once-through boilers should be 7 – 10. This may also be confirmed by comparing the behavior of the reference material (Alloy G) used in laboratory tests.

After removing the sample coupons from autoclave chamber, they were weighed in order to determine the weight gain per unit area. After this, oxide scale thicknesses were determined from sample coupon cross-sections by using scanning electron microscope (SEM). The compositions of the oxide scales were determined by energy dispersive spectroscopy (EDS) during the SEM-analysis. However, these analysis methods proved to be inadequate for very thin (~ 1 µm) oxide scales. In order to get better understanding on the scale structure and composition of very thin oxide scales,

the cross-section samples were further analyzed with high-resolution Zeiss ULTRAplus SEM at Tampere University of Technology. Additionally, glow discharge optical emission spectrometry (GDOES) was used to get more accurate compositional profile analysis from thin oxide scales. GDOES was applied on surface area of about 5 mm^2.

7. EVALUATION OF TEST RESULTS

7.1. Test results

7.1.1. Weight gain data

Mass gains of sample coupons were calculated by weighing the sample coupons after exposure. Based on this, the mass gain per unit area was calculated for each sample coupon. The results are summarized in Figure 7.1, which plots the logarithmic mass gain per unit area as a function of time. All tested alloys showed nearly parabolic oxidation rate, as it could be expected. Based on Figure 7.1, the materials may be ranked in following order, from worst to the best: Alloy G, Alloy D, Alloy E, Alloy F, Alloy A, Alloy C and Alloy B. Accordingly, a relation between chromium content and oxidation resistance of the tested alloys is evident, and there seems to be a gap between the performance of 16-18% Cr alloys (D, E, F and G) and 25% Cr alloys (A, B and C). Moreover, it can be observed that cold working ("machined" samples in Figure 7.1) considerably increased the oxidation resistance of material. Cold-working does not seem to change the ranking of the materials, although the differences between the alloys decrease considerably. Also the better performance of fine-grained 18% Cr alloys E and F in their ground state is verified.

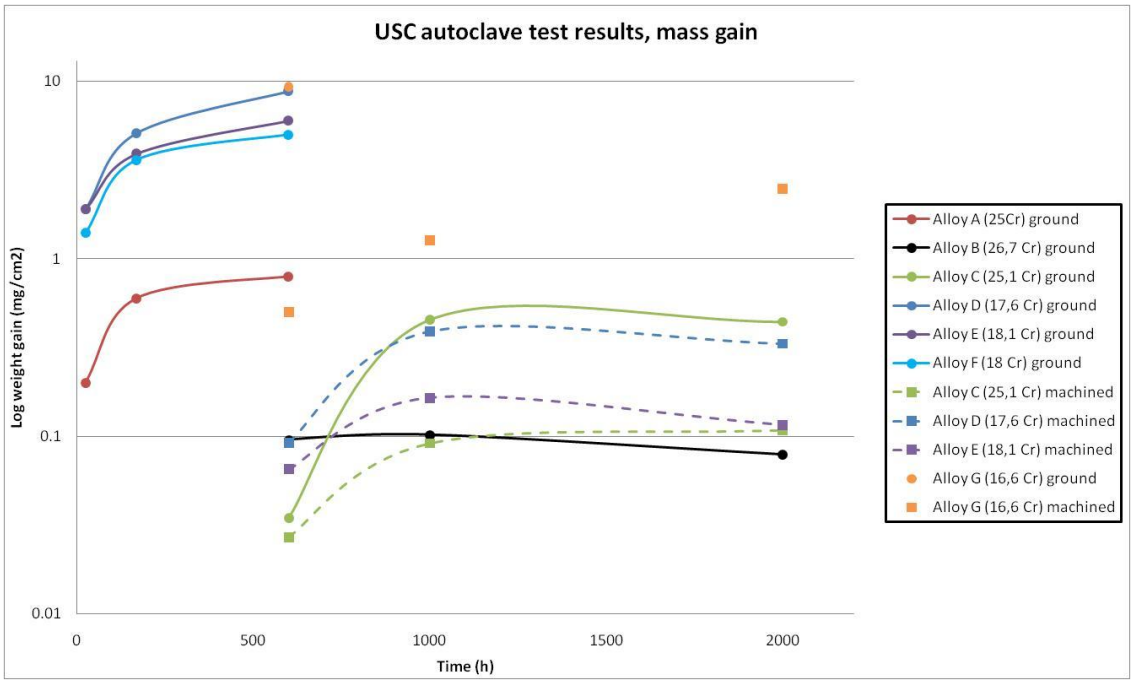

Figure 7.1. Mass gain per unit area of each sample coupon exposed to supercritical steam in autoclave.

Even though reporting oxidation rate as mass gain per unit area is a common method to evaluate oxidation and corrosion behavior of materials, it does not tell the whole truth from the oxidation process. As can be seen from figure, some materials actually experience mass loss during the tests. This may, of course, be due to uncertainty in weighing of the samples or local spallation of the oxide layer, but another explanation is that some alloying elements have formed evaporating species, like chromium oxy-hydroxide $CrO_2(OH)_2$. Another fact which cannot be indicated by the weight gain data is the structure and actual thicknesses of oxide layers formed. Both of these factors are crucial regarding the adherence and protectivity of the oxide scale.

The mass gain data is well in line with the experimental data found in literature. If the oxidation parameters introduced in Table 5.3 are applied, the theoretical mass gain assuming parabolic oxidation kinetics are very close to the values what was measured from samples. After 600 hours at 650 °C for alloys with nominally 18wt-% the theoretical mass gain is 7,68 mg / cm^2. For advanced austenitic alloys after 2000 hours, the theoretical mass gain is 0,09 mg / cm^2.

7.1.2. Scale thickness data

Minimum and maximum oxide scale thicknesses for samples tested in 2010 were determined from cross-sectioned sample pieces with SEM. For 2009 test campaign, only maximum oxide thickness was determined from samples exposed for 600 hours. The results are summarized in Table 7.1.

Table 7.1. Summary of scale thickness data measured from cross-sectioned sample coupons. Results are reported in micrometers.

	2009	2010		
Alloy and surface finish [1)]	600h	600h	1000h	2000h
Alloy A, ground	0,9	-	-	-
Alloy B, ground	-	0,15-0,3	0,4-0,8	0,3
Alloy C, ground	-	0,7-19	0,8-23	3-11
Alloy C, machined	-	0,5-1,6	0,3-1,0	0,4-2,9
Alloy D, ground	84	-	-	-
Alloy D, machined	-	0,4-1,0	0,4-0,8	0,5-48
Alloy E (FG), ground	65	-	-	-
Alloy E (FG), machined	-	0,6-1,1	0,4-0,6	0,4-4,4
Alloy F (FG), ground	58	-	-	-
Alloy G, ground	92	-	-	-
Alloy G, machined	0,6-1,0	-	0,4-0,5	0,5-75

1) FG stands for fine grained (ASTM grain size number over 7) alloy

Cold-working the surface layer seems to considerably improve the performance of all tested alloys, but some localized oxide growth on alloys D and G was observed after 2000 hours. This suggests that cold-working does not improve the long-term

performance of these alloys. The alloys with higher Cr content (A, B and C) perform well even in ground state, and cold-working the surface improved the performance considerably.

7.1.3. SEM analyzes

The alloys exposed for 2000 hours were further analyzed with SEM with better resolution in order to determine the scale structure from samples with very thin oxide scales. Images of ground alloys B and C are shown in Figure 7.2. Even though there is relatively small difference in chromium content between the two alloys (26,7 % Cr in B and 25,1% Cr in C), the oxide scale structure appears completely different: alloy B has thin, uniform oxide layer with submicron thickness (200-300nm), whereas alloy C has thin oxide layer with locally thicker oxide islands which have double layered structure. Alloy B has also a discontinuous secondary phase under the oxide layer. This may be a more thermodynamically stable oxide phase, e.g. SiO_2 which has formed under the Cr_2O_3 layer.

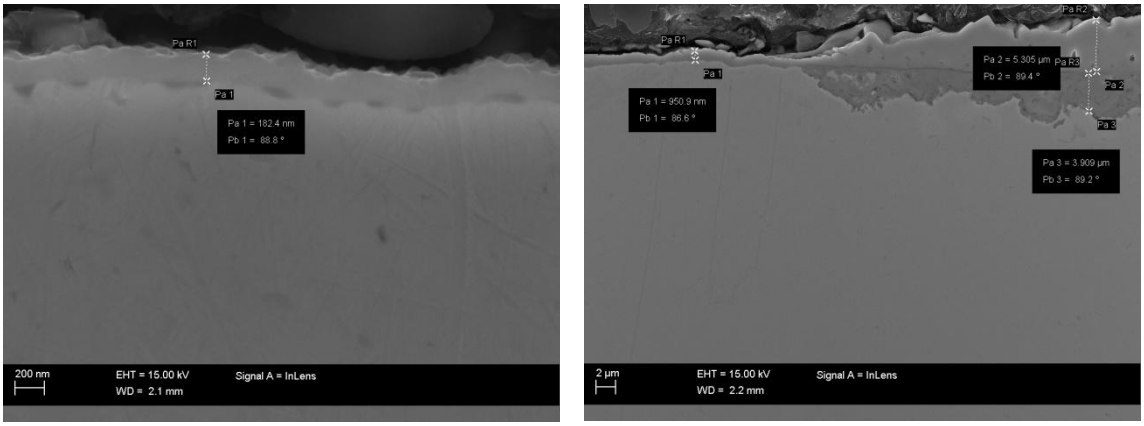

a) Alloy B, ground b) Alloy C, ground

Figure 7.2. Steam-side oxide scales formed after 2000 hours on ground alloys B and C.

Figure 7.3 shows the double-layered structure of oxide scale formed on alloy C in more detail. EDS analysis was also performed, Figure 7.4, and it confirmed that the outer porous oxide layer is iron oxide (most probably Fe_3O_4) and the inner oxide is Fe-Cr-Mn spinel type oxide. Chromium depletion just beneath the oxide-metal interface can also be detected, but no clear signs on thin Cr_2O_3 scale can be seen. Nickel seems to have enriched on the oxide-metal interface. There is also a strip enriched in Ni in the middle of the oxide scale, highlighted with red circle in Figure 7.4. This could be a location where the oxide-metal interface was previously located.

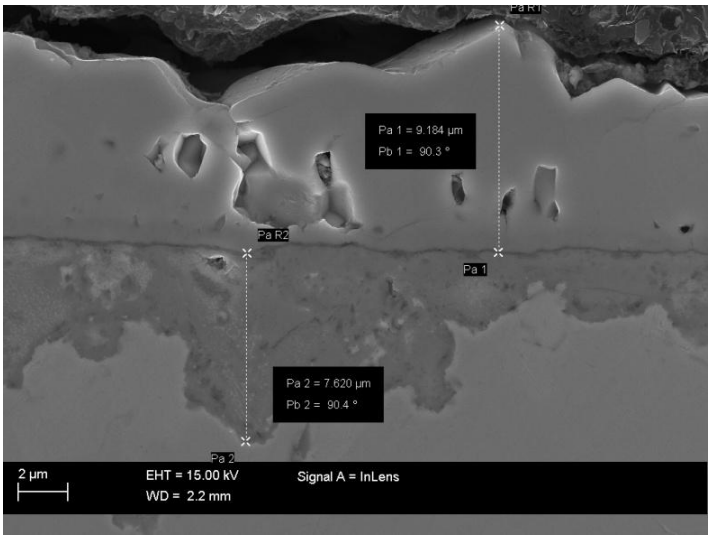

Figure 7.3. Double layered oxide scale formed on ground alloy C after 2000 hours.

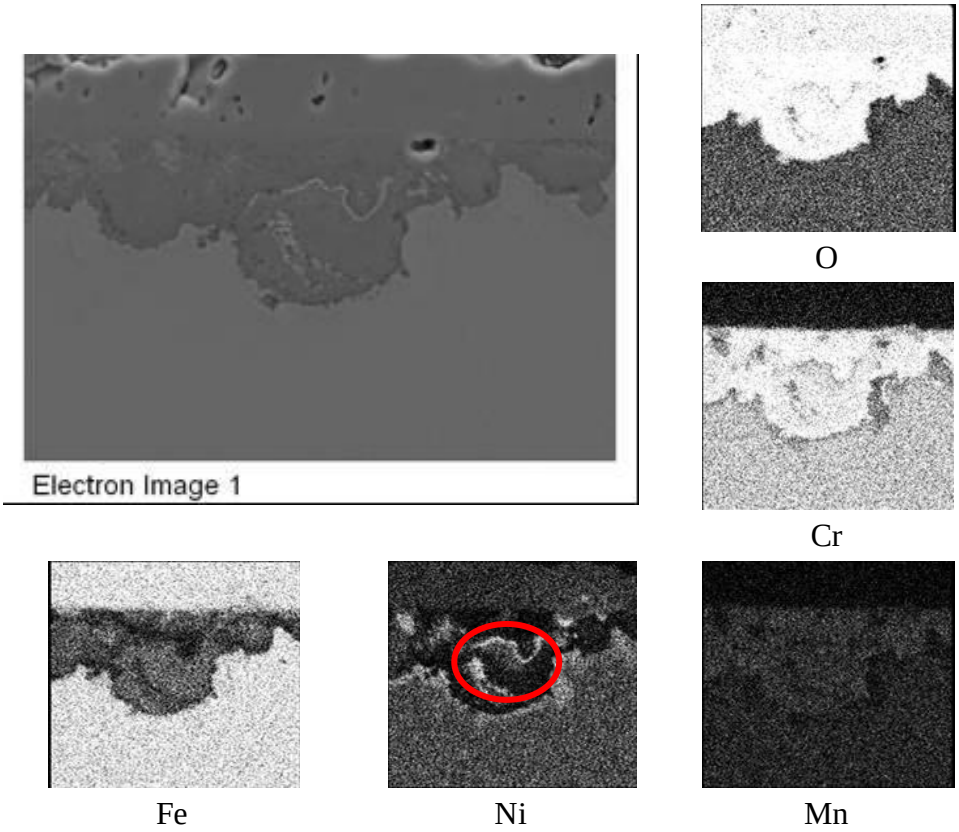

Figure 7.4. EDS mapping from oxide layer formed on ground alloy C after 2000 hours.

Samples with machined surfaces had generally very thin oxide layers. According to scale thickness measurements performed by VTT, alloys D and G had locally thicker oxide islands. However, these thicker oxide islands could not be detected when the samples were investigated at TUT, suggesting that the outer scale has been spalled off during transportation or re-polishing of the samples. The inner scales were still attached, although it also seems to exfoliate as seen in Figure 7.5. The thin oxide scale has laminated structure, which suggests that these alloys will not have acceptable long-term performance even if the inner surface is cold-worked.

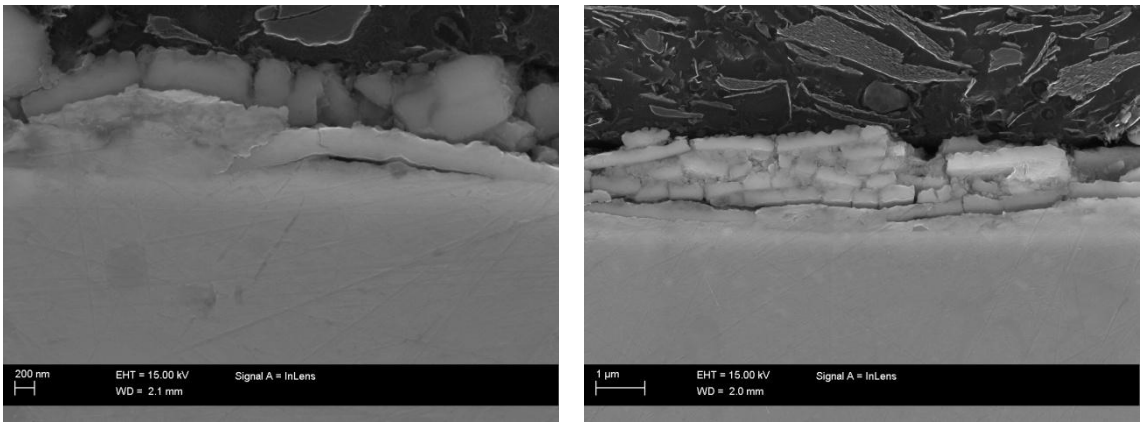

a) Alloy D, machined b) Alloy G, machined

Figure 7.5. Steam-side oxide scales formed after 2000 hours on machined alloys D and G. Images are from locations where only thin oxide scale was formed.

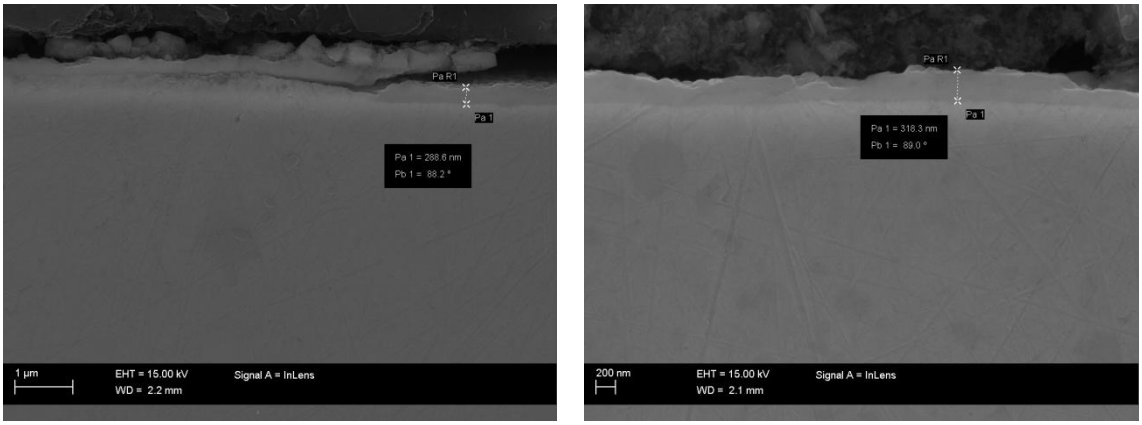

a) alloy E, machined b) alloy C, machined

Figure 7.6. Steam-side oxide scale formed after 2000 hours on machined alloys E and C. Images are from locations where only thin scale was formed

The machined fine-grained alloy E had similar scale structure than alloys D and G. The outer scale was partially detached during transportation or re-polishing also from this sample. Some scale lamination was also detected as can be seen from Figure 7.6 a). Alloy C had thin, uniform oxide scale, Figure 7.6 b) which showed no clear marks of scale detachment or lamination.

7.1.4. GDOES analyzes

Since EDS analyzes of thin scales were impossible to perform, VTT ordered also GDOES analyzes in order to determine the oxide scale composition. The GDOES analyzes are represented in Appendix 3. The GDOES analyzes performed for ground sample coupon B and machined sample coupons C, D and E suggest that the thin oxide scales contain mainly oxides of Cr and Mn. Enrichment of minor alloying elements, e.g. Ti, Al and Si can also be detected from the oxide scale. Alloy B has a clear spike in Si content just beneath the Cr-Mn rich oxide, which suggests that the secondary phase detected under the oxide scale in SEM analyzes contains SiO_2.

Based on the GDOES analyzes, it can be concluded that thin oxide scales formed in steam consist of oxides of Cr and Mn. Oxides of Fe can be found on the outer part of oxide scale. Nickel seems not to participate in oxidation reaction.

7.2. Discussion

The steam-side oxidation resistance of various austenitic stainless steels for supercritical boilers can be evaluated based on the performed laboratory tests. Advanced austenitic alloys A, B and C had very low mass gains, which would suggest that these alloys are applicable to over 600 ºC live steam temperature. Austenitic stainless steels with nominally 18 wt-% Cr (Alloys D, E and F) had considerably higher mass gains if cold work was not applied on the surface layer. The mass gain and scale thickness data suggest that these alloys are not applicable when the live steam temperature exceeds 600 ºC.

While the weight gain data suggests that the oxidation resistance of alloys containing 18 wt-% Cr can be improved to the same level than alloys with ~25 wt-% Cr by introducing cold work to the surface layer, the scale thickness data and SEM analyzes show the difference between the two alloy class. Thicker oxide islands were detected from sample coupon cross-sections of Alloys D, E and G with machined surface finish after 2000 hours of exposure. This suggests that the long-term performance of these alloys will not be adequate when the live steam temperature is over 600 ºC. The laminated scale structure detected from these samples also supports this assumption. Advanced austenitic alloy C was tested with both ground and machined surface finish. Machining improved the performance slightly, but the difference was not very dramatic at test temperature.

The cold-work was introduced to the surface of sample coupons simply by machining, while the actual shot-peening that some tube suppliers use to improve oxidation resistance of their materials is a more complex process. Shot-peening is made with metallic bids which are blown to the inner tube surface with special shot-peening equipment. The structure and depth of the surface layer modified by this process is probably different from the structure introduced by machining. Some test material which is shot-peened by tube supplier should be tested and compared to a machined sample coupon in order to determine if machining has the same effect than shot-peening.

The importance of chromium regarding steam-side oxidation resistance of an alloy is evident, but the EDS and GDOES analyzes suggest that also other alloying elements have a certain role in the oxide scale formation and growth. The thin scales formed on advanced austenitic alloy B coupon and all the machined sample coupons consist of oxides of chromium and manganese. In some cases, patches of Si-rich oxide are detected beneath the Cr-Mn oxide. Contrary to what was expected according to literature, nickel was not detected from the oxide scale, but it seemed to be enriched on the scale-metal interface. However, when the steam temperature is increased, the risk

for chromium evaporation from the metal surface also increases. This may lead to a conclusion that the alloys which rely their oxidation resistance on formation of Cr_2O_3 scale will have shorter life-time than would be expected when the steam temperature is increased towards 700 °C.

One ambition of this work was to determine the temperature limits for austenitic boiler steels. However, such ambition could not be fulfilled based on the tests that could be conducted within the given timeframe. More tests at different temperatures are necessary to determine actual temperature limits. Also field testing should be considered, since laboratory conditions are typically isothermal, which is not the case in actual superheater tubes. Another option would be to arrange a laboratory equipment where the sample coupons can be heated to the actual metal temperature, while supercritical steam is flown through the autoclave, thus creating a realistic temperature gradient.

8. CONCLUSIONS

Steam-side oxidation of materials for supercritical boilers was researched in this thesis. The focus was on austenitic stainless steels, which will be used in the hottest components of a steam boiler, i.e. final superheaters and reheaters. In these components, the steam temperature exceeds 600 ºC in today's advanced steam boilers which are in operation. Lot of effort has been put in increasing the live steam temperature even further, but this sets very demanding requirements for materials. Biggest concern is often the corrosion on the flue gas side or the high-temperature strength and creep resistance, but when the steam temperatures are increased, also the steam-side oxidation must be considered, and it may become a limiting factor in material selection. If the oxide scales formed on the inner surface of heat exchanging tube become increasingly thick, the risk for oxide scale exfoliation increases. The exfoliated oxide scales may cause tube blockages especially on bends. Also, if the exfoliated particles reach the steam turbine, they will cause erosion of turbine blades.

Literature survey on steam boiler technology and different material degradation mechanisms was the starting point of this study. Also the basics of CFB technology were briefly reviewed. The steam-side oxidation was researched in more detail. The literature available was very extensive, and the theory is well known. Also some extensive field test campaigns have been executed. Based on the literature survey, some austenitic stainless steels are applicable for over 600 ºC live steam temperatures. Nickel based alloys perform even better, but they are also considerably more expensive than stainless steel alloys.

The exfoliation tendency of an oxide scale formed in steam was approximated by using the Armitt diagram, which estimates the exfoliation tendency if scale thickness and elastic strain acting in the oxide scale can be approximated. A very rough estimate for austenitic stainless steels is that the oxide scale should be less than 50 µm thick, if only strain generated during cooling is taken into account. In reality, the value could be considerably smaller, since there may be also other strains and stresses acting in the scale. Also the oxide scale contains always voids and pores, which weaken the scale integrity.

The available literature suggests that the formation of thin, dense and adherent chromium oxide layer is crucial for steam-side oxidation resistance of an alloy. To form a Cr_2O_3 film there must be sufficient amount of Cr in the alloy. Also the chromium mobility in the alloy has an important role on the formation of thin Cr_2O_3 film. Increasing the diffusion rate increases the migration of chromium to the surface, where it may form protective oxide scale. The diffusion rate may be increased by increasing

the amount of grain boundaries (i.e. having fine-grained material) or by introducing cold work to surface layer. Both strategies are commonly used by tube suppliers. The effect of cold work was also observed in the experimental work here reported, most notably on the performance of nominally 18 wt-% Cr alloys. However, the improvement in long term performance of these alloys was not so evident, and locally thicker oxide islands were detected from sample coupon cross sections. An advanced austenitic alloy with 25,1 wt-% Cr (Alloy C) was tested in ground and machined surface finish, and also it showed slightly increased performance when the surface was cold worked. However, the degree of improvement was probably insufficient to justify the additional costs for cold-working, at least at the temperature where tests were performed. Besides chromium, some other alloying elements, namely Mn, Si, Al and Ti, were also detected in the oxide scales. This suggests that also these elements participate in steam-side oxidation reaction.

The test results and literature suggest that advanced austenitic stainless steels with ~25 wt-% Cr are applicable in steam temperatures exceeding 600 ºC. While by cold working the surface considerably improved the performance of nominally 18 wt-% alloys, their long term performance still be inadequate if steam temperature exceeds 600 ºC. The determination of actual temperature limits for tested materials regarding steam-side oxidation requires further testing in different temperatures. Also, to validate the steam-side oxidation resistance of shot-peened tubes, actual shot-peened tube pieces should be tested in autoclave and compared to the already tested machined sample coupons.

REFERENCES

1. Huhtinen, M., et al. Höyrykattilatekniikka. 2nd - 4th Edition. Helsinki 1999, Edita. ISBN 951-37-1327-X.
2. International Energy Agency. IEA Energy Statistics - Electricity for World in 2007. International Energy Agency (IEA). [Online] [Cited: June 3, 2010.] http://www.iea.org/stats/electricitydata.asp?COUNTRY_CODE=29.
3. Teir, S. Steam Boiler Technology. Helsinki 2003, Helsinki University of Technology.
4. Sarver, J.M. and Tanzosh, J.M. Steam Oxidation Testing of Candidate Ultrasupercritical Boiler Materials. 28th International Technical Conference on Coal Utilization and Fuel Systems, Clearwater. 2003.
5. Kiameh, P. Power Generation Handbook. 2004, McGraw-Hill.
6. Raiko, R. Ener-8200 Höyrytekniikka. Lecture notes. 2006. Tampereen teknillinen yliopisto.
7. Aittomäki, A. Teknillinen termodynamiikka. Prosessit ja energian muutokset. 2010. Tampereen teknillinen yliopisto.
8. Engel, C.A. and Boles, M.A. Thermodynamics: An Engineering Approach. 5th Edition. 2006, McGraw-Hill.
9. Budabest University of Technology and Economics. Supercritical Fluid Extraction. Supercritical Fluid Extraction research group. [Online] [Cited: 10. June 2010.] http://sfe.vemt.bme.hu/angol/supercritical.html.
10. Mogk, D. Teaching Phase Equilibria. SERC. [Online] [Cited: June 8, 2010.] http://serc.carleton.edu/research_education/equilibria/phaserule.html.
11. Beér, J. Higher Efficiency Power Generation Reduces Emissions. 2009, National Coal Council.
12. Slotte, M. Large scale co-firing of REF and biofuels in a CFB with advanced steam parameters and very high plant efficiency. 34th International Technical Conference of Coal Utilization & Fuel Systems. Clearwater, 2008.
13. Coda Zabetta, E., et al. Foster Wheeler Experience With Biomass and Waste in CFBs. 34th International Technical Conference of Coal Utilization & Fuel Systems. Clearwater, 2008.
14. Oka, S.N. Fluidized Bed Combustion. New York 2004, Marcer Dekker, Inc. ISBN 0-8247-4699-6.
15. Basu, P. Combustion and Gasification in Fluidized Beds. Boca Raton. 2006, CRC Press, Taylor & Francis Group. ISBN 0-8493-3396-2.
16. Foster Wheeler Energia Oy. BFB Boilers, Power Point presentation. 2009.
17. Foster Wheeler Energia Oy. CFB Boilers, Power Point presentation. 2010.

18. Viswanathan, R., Sarver, J. and Tanzosh, J.M. Boiler Materials for Ultra-Supercritical Coal Power Plants - Steamside Oxidation. Journal of Materials Engineering and Performance, Vol. 15(2006)3, pp. 255-274. ISSN 1544-1024.
19. Raiko, R., et al. Poltto ja palaminen. 2nd Edition. Jyväskylä 2002, International Flame Research Foundation - Suomen kansallinen osasto. ISBN 951-666-604-3.
20. Kunnossapitoyhdistys ry. Korroosiokäsikirja. Hamina 2004, Oy Kotkan kirjapaino Ab. ISBN 951-97101-7-5.
21. Grabke, H.J., Spiegel, M. and Zahs, A. Role of Alloying Elements and Carbides in the Chlorine-Induced Corrosion of Steels and Alloys. Materials Research 7(2004)1, pp. 89-95.
22. Energy Research Centre of Netherlands (ECN). Phyllis: The Composition of Biomass and Waste. [Online] [Cited 16th. July 2010.] http://www.ecn.nl/phyllis/.
23. Mohammed, S. and Sarver, J. Steamside Oxidation Resistance of Materials for Use in Ultra-supercritical Coal Power Plants (a Literature Review). Ohio 2002, McDermott Technology, Inc.
24. ASM International. ASM Handbook Volume 6, Welding, Brazing and Soldering. 1993, ASM. ISBN 0-87170-382-3.
25. Bhadeshia, H.K.D.H. and Honeycombe, R.W.K. Steels Microstructure and Properties. 3rd Edition. Oxford 2006,: Elsevier Ltd. ISBN 0-7506-8084-9.
26. Wright, I.G. and Dooley, R.B. A Review of the Oxidation Behavior of Structural Alloys in Steam. 2010.
27. Haarmann, K., et al. The T91/P91 Book. 2002, Vallourec & Mannesmann Tubes.
28. Richardot, D., et al. The T92/P92 Book. 2000, Vallourec & Mannesmann Tubes.
29. ASM International. ASM Handbook Volume 1, Properties and Selection: Irons, Steels, and High Performance Alloys. 1990, ASM. ISBN 0-87170-377-7.
30. Viswanathan, R., Purgert, R. and Rao, U. Materials Technology for Advanced Coal Power Plants. 2005.
31. ASM International. ASM Handbook Volume 2, Properties and Selection: Nonferrous Alloys and Special Purpose Materials. 1991, ASM. ISBN 0-87170-378-5.
32. Birks, N. and Meier, G.H. Introduction to High Temperature Oxidation of Metals. London 1983, Edward Arnold Ltd. ISBN 0-7131-3464-X.
33. Callister, W.D.Jr. Materials Science and Engineering - an Introduction. Hoboken, 2003. John Wiley & Sons, Inc. ISBN 0-471-22471-5.
34. Otsuka, N., Shida, Y. and Fujikawa, H. Internal-External Transition for the Oxidation of Fe-Cr-Ni Austenitic Stainless Steels in Steam. Oxidation of Metals 120(1989)1/2.
35. Matsuo, H., Nishiyama, Y. and Yamadera, Y. Steam oxidation property of Fine-grain Steels. Proceedings from the Fourth International Conference on Advances in Materials Technology. Hilton Head Island, South Carolina 2005, ASM International. pp. 441-450.
36. Haruyama, H., et al.Effect of shot peening and pre-oxidation treatment in air on steam oxidation resistance of Mod.9Cr-1Mo steel. Proceedings from the Fourth

International Conference on Advances in Materials Technology. Hilton Head Island, South Carolina 2005, ASM International. pp. 412-419.
37. SFS-EN 12952-12. Vesiputkikattilat ja niihin liittyvät laitteistot. Osa 12: Laatuvaatimukset syöttö- ja kattilavedelle. Helsinki : Suomen Standardoimisliitto, 2003. p. 32.
38. VGB Powertech. Guidelines for Feed Water, Boiler Water and Steam Quality for Power Plants / Industrial Plants. Essen 2004, VGB Powertech.
39. Importance of Good Boiler Feedwater Treatment, Technical Bulletin. Babcock Power Inc. [Online]. [Cited: April 23, 2010.] http://www.babcockpower.com/pdf/vpi-07.pdf.
40. Young, D.J. and Pint, B.A. Chromium Volatilization Rates from Cr2O3 Scales into Flowing Gases Containing Water Vapor. Oxidation of Metals 66(2006)3, pp. 137-153.
41. Mehrer, H. Diffusion in solids: fundamentals, methods, materials, diffusion-controlled processes. 2007, Springer.
42. Wright, I.G., Tortorelli, P.F. and Schütze, M. Program on Technology Innovation: Oxide Growth and Exfoliation on Alloys Exposed to Steam. Palo Alto 2007, EPRI. Report no. 1013666.
43. Armitt, J., et al. The Spalling of Steam-Grown Oxide from Superheater and Reheater Tube Steels. Palo Alto 1978, EPRI. Report no. 686.
44. Meyer, H., et al. KOMET 650 - Coal-fired Power Stations with Steam Temperatures up to 650 °C. VGB PowerTech - International Journal for Electricity and Heat Generation (2008)3.
45. Uerlings, R., Bruch, U. and Meyer, H. KOMET 650 - Investigations of the Operating Behaviour of Boiler Materials and their Welded Joints at Temperatures up to 650 °C. VGB PowerTech - International Journal for Electricity and Heat Generation (2008)3.
46. Henry, J.;Zhou, G. and Ward, T. Lessons from the past: materials-related issues in an ultra-supercritical boiler at Eddystone plant. Materials at High Temperatures 24(2007)4, pp. 249-258.
47. Komai, N., et al. Field test results of newly developed austenitic steels in the Eddystone no.1 boiler. Proceedings of CREEP8 - Eighth International Conference on Creep and Fatigue at Elevated Temperatures. San Antonio 2007, ASME.
48. Toivonen, A., Penttilä, S. and Heikinheimo, L. VTT HPLWR corrosion test results at 400 – 650 ºC. 2007. Presentation at HPLWR InformationExchange Meetingat CEA, Cadarache, France, September4, 2007. [Online] [Cited February 10, 2011] http://www.iket.fzk.de/hplwr/public/Conferences/CEA_Sep_2007/IEM-VTT-Corrosion_Test_Results2-Toivonen.pdf

APPENDIX 1: TYPES OF OXIDE SCALES FORMED ON COARSE-GRAINED STEELS

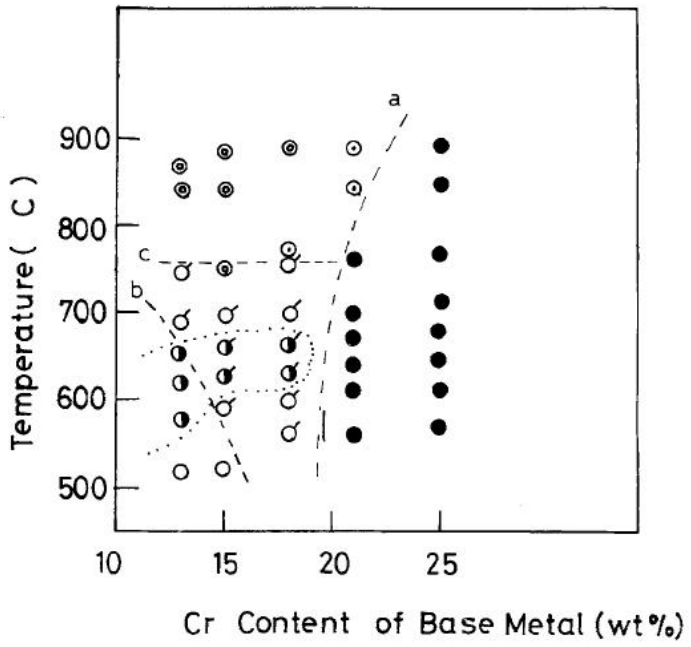

Fig. 2. Types of oxide scale in terms of the chromium concentration of the base metal and the oxidation temperature for the coarse-grain 13–25 wt.% Cr 15 wt.% Ni stainless steels (grain size 110 μm) reacted with steam for 1000 hr. (●) Type I. (Ø) Type II. (◎) Type III. (◑) Type IV. (○) Type V. (◑) Type II. Type IV. See Fig. 3.

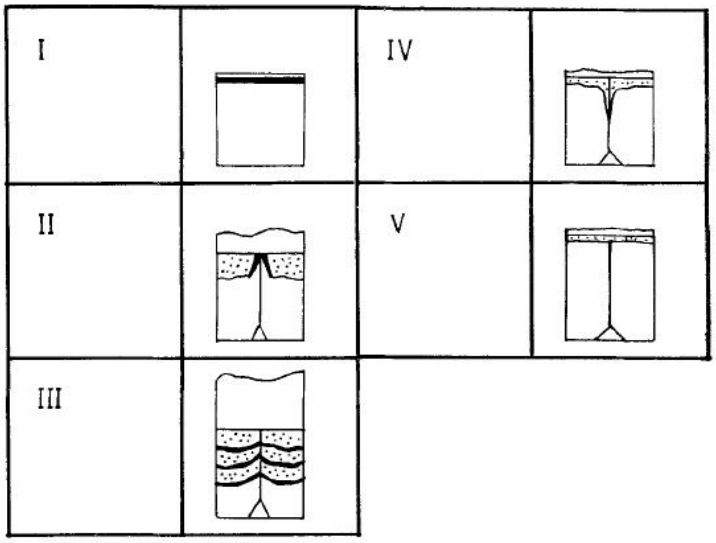

Fig. 3. Schematic representation for the types of oxide scale observed on the coarse-grain 13–25 wt.% Cr–15 wt.% Ni stainless steel reacted with steam for 1000 hr (grain size 110 μm).

APPENDIX 2: TYPES OF OXIDE SCALES FORMED ON FINE-GRAINED STEELS

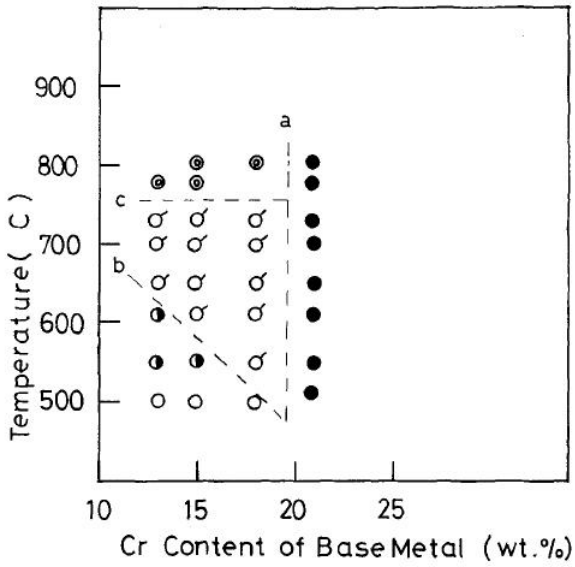

Fig. 10. Types of oxide scale in terms of the chromium concentration of the base metal and the oxidation temperature for the fine-grain 13–21 wt.% Cr–15 wt.% Ni stainless steels (grain size 20 μm) reacted with steam for 1000 hr. (●) Type I. (◑) Type IV. (○) Type V. (Ó) Type VI. (◎) Type VII. See Figure 11.

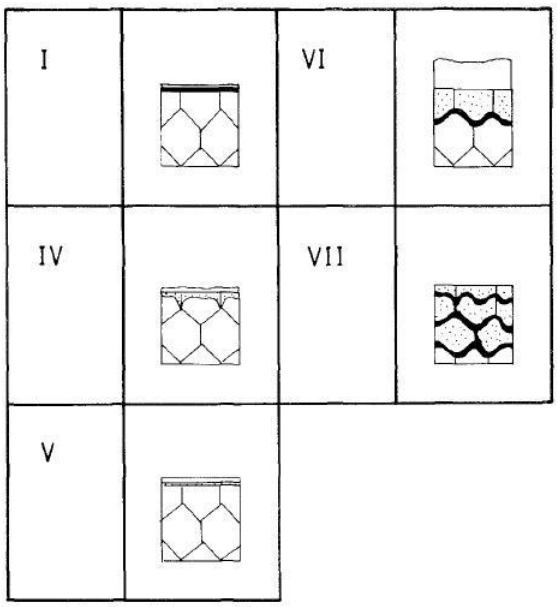

Fig. 11. Schematic representation for the types of oxide scale observed on the fine-grain 13–21 wt.% Cr–15 wt.% Ni stainless steels reacted with steam for 1000 hr (grain size 20 μm).

APPENDIX 3: GDOES ANALYZES 1/2

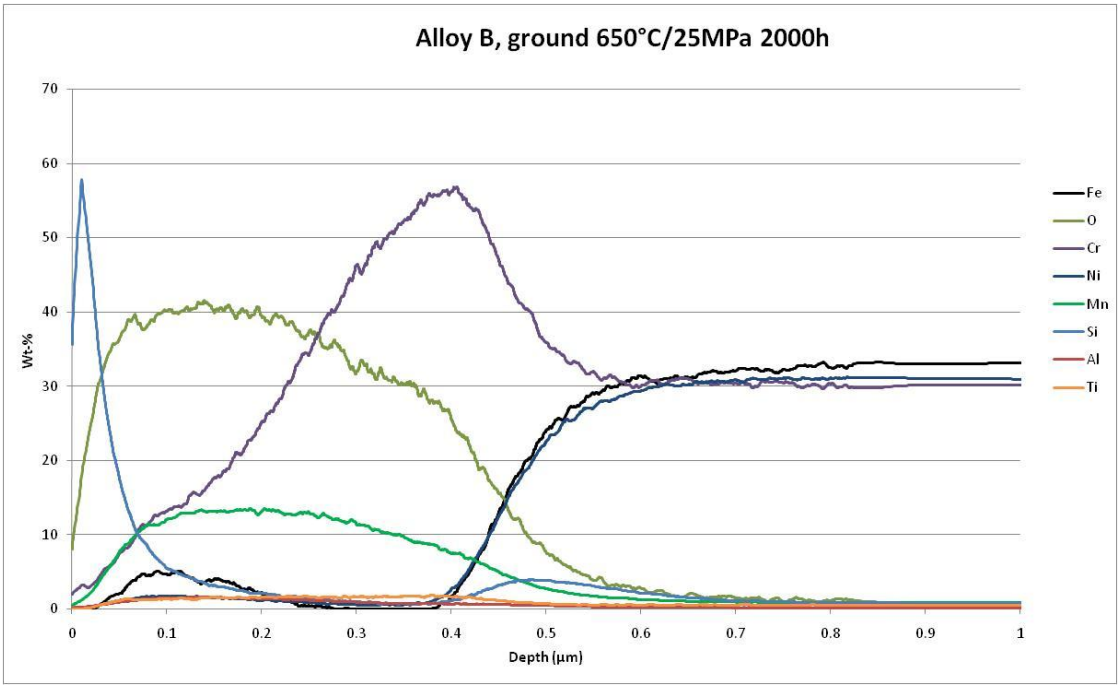

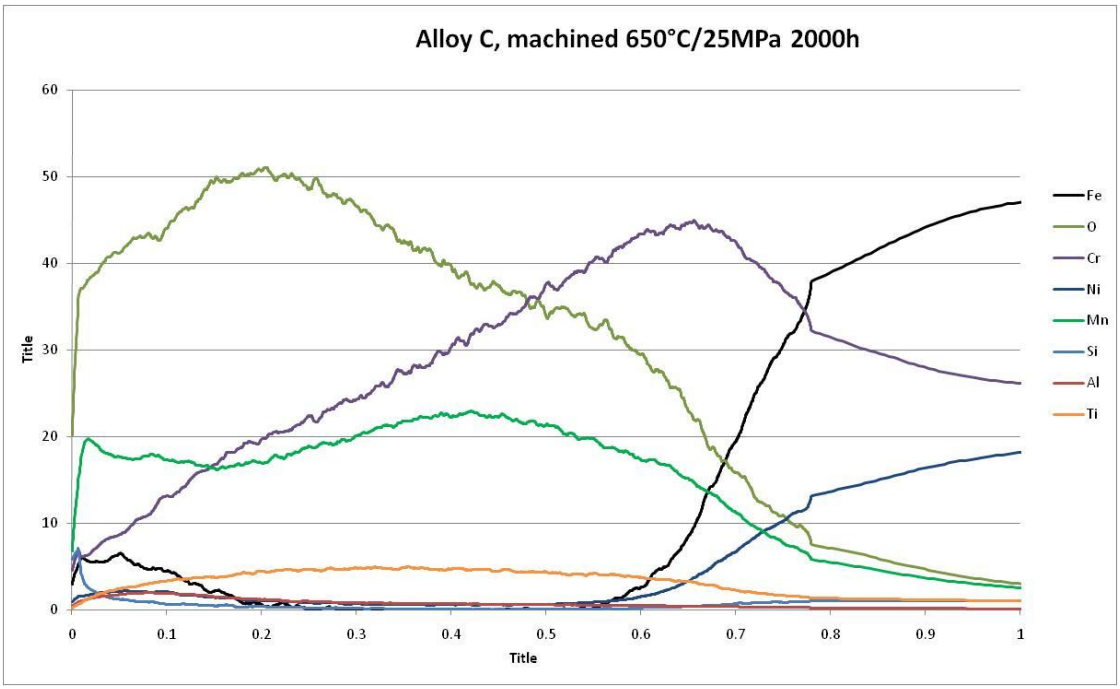

APPENDIX 3: GDOES ANALYZES 2/2